Alma Mater Studiorum - Università di Bologna

DOTTORATO DI RICERCA IN

INGEGNERIA CIVILE, CHIMICA, AMBIENTALE E DEI MATERIALI

Ciclo 35

Settore Concorsuale: 09/D3 - IMPIANTI E PROCESSI INDUSTRIALI CHIMICI

Settore Scientifico Disciplinare: ING-IND/25 - IMPIANTI CHIMICI

CHARACTERIZATION OF PYROLYSIS AND OXIDATION PROCESSES OF BIOMATERIALS, BIOMASSES AND BIOFUELS

Presentata da: Fekadu Mosisa Wako

Coordinatore Dottorato

Alessandro Tugnoli

Supervisore

Ernesto Salzano

Co-supervisore

Gianmaria Pio

Esame finale anno 2023

"Climate Change isn't something people get to choose to believe or not: it's happening"

Matt Gaetz

Dedication

This thesis is dedicated to my late mom **Aberash Lebeta** (Aayyookoo) and my late dad **Mosisa Wako** (Aabbookoo) who sent me to school without being themselves schooled. I'm pretty much sure that if my mom got this opportunity, she would have achieved something way far better than this. I'm thankful and grateful for having such a strong and gentle soul who paid the ultimate price for me being achieved this today.

Aayyookoo nagaa naaf ta'i bakkuma jirtutti!

Acknowledgement

First of all, I would like to thank the **almighty God** for his mercy, grace, care and blessing throughout my life. Foremost, I would like to express my sincere gratitude to **Prof. Ernesto Salzano** for the guidance, motivation, enthusiasm and immense support provided as my supervisor during the research work. I would also like to express a special thanks to **Dr. Gianmaria Pio** for his exceptional dedication, excellent assistance, kind follow-up and unreserved support throughout the research work, manuscript preparations and thesis writing. My special thanks would go to **Partnership for Knowledge (PFK)** the higher education initiative of the Italian Agency for Development Corporation (AICS)**,** the funding agency who supported my study from beginning to the end, without their funding this wouldn't happened. I am really grateful for them. I would also thank **Marco Polo Scholarship** of university of Bologna for supporting my research abroad to university of Calgary, Canada and led me to work on diverse research projects under multi-cultural research environment. I thank **Prof. Nader Mahinpey** and **Dr. Ashraf Amin** for the opportunity and close supervision during my stay at University of Calgary, Canada. I would also like to thank **Prof. Alessandro Tugnoli,** a coordinator of the PhD program for his efforts in delivering necessary information, courses and for being there for any relevant activities required. And also, I would like to thank all my PhD examiners. I express gratitude to Haramaya University, where my academic career started for giving me the study leave. I would also like to thank my colleagues from DICAM research group who are being very special for me, who made me always to feel as home, the group which is hard to leave and forget. They're just special. A very deep appreciation is sent out to my families who are always there for me and encourage me from far. Particularly, my wife **Mrs. Ebise Efrem,** and **my late mother Aberash Lebeta** who hold an irreplaceable place in my heart deserve my utmost gratitude. I would also like to thank **Gadise Efrem, Etana Chewaka, Birhanu Mekonta, Zerfe Tsegaye, Nimona Fekadu, Ayantu Gizaw and Tujuba Etana**, who incredibly took care of me during my stay in Canada. Finally, thanks to my good friends **Dr. Eric Awere, Ali Salii and Bereket Arsicha** for being there for me when I needed them.

Table of Contents

Abstract

The urgent need for alternative solutions mitigating the impacts of human activities on the environment has strongly opened new challenges and opportunities for the energy supply chain, in view of the energy transition. Indeed, the automotive industry is going through a revolutionary moment in its quest to reduce its carbon footprint, with biofuels being one of the viable alternatives. The use of different classes of oxygenated biofuels, such as alcohols, carboxylic acids, aldehydes, and esters as fuel additives or standalone fuel components has attracted the attention of many researchers worldwide. Despite their beneficial effects, biofuel's combustion can also result in the production of undesirable pollutants such as aldehydes and organic acids. Hence, the use of these fuels requires a complete characterization of the phenomena that occur during their production and consumption. Industrial scale-up of biomass conversion is challenging owing to the complexity of its chemistry and transport phenomena involved in the process, thereby affecting yield distributions and product compositions. In this view, the role of solid-phase and gas-phase chemistry is paramount for a complete understanding of energy recovery processes, undesired pollutants formation and consumption, and in general for several industrial sectors. Thus, this study is devoted to a detailed analysis of physical-chemical phenomena characterizing biomass pyrolysis and biofuel oxidation aiming at the realization and implementation in real systems of a kinetic mechanism. The solid-phase kinetics is dedicated to how the pyrolysis kinetic mechanism is constructed and implemented in process simulation software (i.e. Aspen Plus) to be able to simulate pyrolysis process. The pyrolysis mechanism has been represented by 20 first order decomposition reactions. In the gas-phase, predictive chemical kinetic models have been constructed following two approaches; manually upgrading the existing mechanism (i.e. KiBo_MU) and automatically generating a new mechanism using RMG (i.e. KiBo_AG). The former comprises 141 species and 453 reactions, while the latter contains 631 species and 28329 reactions. The accuracy of the pyrolysis kinetic mechanism has been tested against the experimental pyrolyzed product distributions from different biomass sources while, the combustion kinetic models have been evaluated through the investigation of fundamental combustion parameters (i.e. laminar burning velocity, species profile and ignition delay times) under wide range of reaction conditions and fuel compositions. Formic acid, acetic acid, acetaldehyde, methanol and ethanol were considered for validation of the combustion mechanisms. Under the investigated conditions, the kinetic mechanisms captured the experimental trends well and in

particular, KiBo_MU and KiBo_AG showed better accuracy when compared to the well-validated existing kinetic models. The overall agreement between experimental measurements and numerical estimations allowed for the use of KiBo_MU and KiBo_AG kinetic models to unravel the chemistry of the investigated species.

Although the development and validation of detailed kinetic mechanisms suitable for the evaluation of the chemistry of biomass-based fuels represent the main deliverable of this project, the realized procedure integrating schematic classifications with methodologies for the identification of common decomposition pathways and intermediates represents an additional source of novelty in this study. Besides, the fundamental-oriented nature of the adopted approach has allowed for the identification of the most relevant reactions and species under operative conditions of interest in different industrial applications, paving the way for the reduction of the kinetic mechanism. Eventually, the resulting skeletal version of a detailed kinetic mechanism can be intended for its integration with more complex models accounting for the fluid dynamics to accurately reproduce the behaviour of real systems and reactors.

Chapter 1: Introduction

Fossil fuels are still the main feedstock for global energy production [1, 2]. These petroleum derivatives are inherently expensive, declining with time and upon combustion, they release large amounts of greenhouse gas emissions (GHG) and other pollutants (i.e., both regulated and unregulated). With the advent of the industrial revolution, the levels of greenhouse gases in the atmosphere began to rise. Over the last century, global temperatures have increased due to greenhouse gas emissions [3]. Coal-based power plants account for approximately 40% of the total amount of greenhouse gases entrapping heat in the atmosphere [4]. To alleviate these problems, rapid decarbonization of the power supply chain is required to achieve the target of 2 °C warming, in line with the goals discussed in the Paris Agreement [5, 6]. To go along with this plan, the use of renewable energy such as biomass, wind, solar, hydrothermal, geothermal etc., is critical.

Biomass is one of the most promising feedstocks to meet the growing demand for clean energy while satisfying strict environmental regulations [7]. It is a carbon-neutral energy source that can be converted into various energy forms such as heat, electricity, transportation fuels etc. [8], which can be used in current applications from small-scale (i.e., cooking, lighting) to large-scale (i.e., transportation, industry). Depending on the processing method and feedstock used, biomass-derived fuels can be solid fuels (biochar), liquid fuels (bioethanol, biodiesel and bio-oil) and gaseous fuels (biohydrogen, biogas, syngas) [9]. For instance, gaseous or liquid fuels can be obtained via gasification or pyrolysis, respectively [10]. Pyrolysis is one of the main thermochemical conversion pathways for converting biomass into different chemical components [11]. Biomass fuels account for 10–14% of the world's energy use, with approximately 90% of the energy generated using biomass fuels in rural areas and 40% in urban areas [12]. Overall, biomass accounts for more than one-third of all primary energy use and

thus, the world's energy needs can be met using biomass and other clean, renewable energy sources [13, 14]. Bio-fuels, which are typically known as oxy-biofuels are one of the bioenergy components predominantly derived from biomass and widely used in different sectors more specifically, the application of these fuels in the transportation sector is attracting attention at both national and international levels because this sector is significantly contributing to the global warming [15].

1.1 Oxy-biofuels for transportation

As we all know, internal combustion engines (ICEs) have been the target of a heated debate about the future of clean transportation, and in general, two routes stand out. Some affirm that ICEs are primarily responsible for environmental pollution and argue that the transition to fully electric vehicles (so-called "zero" emission vehicles - ZEVs) is a matter of time [16, 17]. Conversely, some defend the persistence of ICEs in the market, claiming that their development is the fastest way to reduce the carbon footprint of cars [18, 19]. In this perspective, research on advanced vehicle technologies such as fuel cells, hybrid vehicles, solar technology, and pure electric vehicles has accelerated in the past three decades [20-24]. However, most of them are still in the development process, and due to several issues, it seems impossible to find a broad field of use in the short to medium term. Therefore, the power demand of the vehicle will be provided by the internal combustion engine for a long time. This necessitates the use of cleaner fuels in internal combustion engines. Oxygenated fuels are the most popular alternative fuels because their oxygen content improves combustion in the cylinder and reduces emissions at the source [25-27]. Another attractive aspect of this oxyfuel is, most of them are produced from renewable bio-based resources [28-34] thus, they are considered CO_2-free as the CO_2 get absorbed back by the plants for photosynthesis.

These types of fuels can be used in ICEs either in full or in combination with petroleum fuels [35, 36]. Ethanol and biodiesel were among the first motor fuels in use in recent years [37]. A small amount of alcohol fuel can be used in gasoline engines, and a small amount of biodiesel can be added to diesel fuel. Several studies have considered the use of alcohol in compression ignition (CI) engines, although alcohol presents challenges compared to diesel due to lower cetane number, lubrication and viscosity, and higher auto-ignition temperature [38]. In this view, dual-fuel combustion, using a small amount of diesel fuel combined with alcohol, seems to be a viable alternative to alter exhaust emissions and operating costs, particularly when low-cost local fuels are used [39, 40]. For instance, from the study conducted by the California Energy Commission on buses using diesel and methanol dual-fuel engines, similar road performance and cleaner exhaust emissions than using diesel alone are observed [41]. In the same way, from the study reported by Costal et al. [40] on the investigation of two biofuels (i.e., biogas, ethanol) in dual-fuel spark ignition engines, it has been observed that biofuels can potentially be used in internal combustion engines to achieve net-zero pollutant emissions.

In this regard, the use of different classes of oxygenated biofuels, such as alcohols, esters, acids, aldehydes, and furans, as fuel additives or standalone fuel components has attracted the attention of many researchers worldwide [42-46]. Alcohols are biofuel products that are obtained from second and third-generation biomass and have become increasingly in use with the growing energy demands [47]. They are alternative transportation fuels because of their properties that allow them to be used in existing engines with minor modifications to the hardware. Alcohols have a higher-octane rating than gasoline. Fuels with a higher-octane number can tolerate a higher compression ratio before the engine starts to knock, allowing the engine to deliver more power efficiently and economically [48]. Alcohol burns cleaner than regular gasoline and produces less carbon monoxide, HC, and nitrogen oxides [49, 50]. They

have a higher heat of vaporization; have a lower peak temperature in the combustion chamber, which reduces NOx emissions and increases engine power. However, aldehyde emissions, which are a precursor for photochemical smog increase significantly.

The ignition propensity (i.e. knock resistance, octane rating) of alcohols is perhaps their most attractive feature for internal combustion engine applications [51]. This feature of them boosted applications in ICEs and the adoption of higher volumetric compression ratios [52], resulting in improved fuel conversion efficiency and performance parameters. They can be used in spark-ignition engines (SI) in pure form and/or in blends with only minor modifications to the engine and fuel system [53]. Undoubtedly, of the other alcohol types, ethanol is widely in use in transportation sectors, especially in passenger cars as an alternative to petroleum-based fuels in minimizing CO_2 emissions worldwide [54, 55]. It has a high H/C ratio, high flame propagation speed, high research octane number, safe storage, low volatility and transportation features also make it a reliable fuel, especially for spark-ignition engines [56-61]. It can easily be blended with conventional fuels such as gasoline or diesel or can be employed as a 100% renewable transportation fuel [55]. For instance, the U.S. Environmental Protection Agency reported a reduction in greenhouse gas emissions by an average of 57 – 86% compared to conventional diesel fuel [62]. Stump et al. [63] studied tailpipe and evaporative emissions from three passenger motor vehicles using ethanol (9% v/v) and non-oxidative fuel. A general reduction in hydrocarbon, carbon monoxide, benzene and 1,3-butadiene emissions were observed when ethanol fuel was used. However, both formaldehyde and acetaldehyde emissions from ethanol mixtures increased (almost doubled) [63].

Moreover, following the 1973 oil crisis, methanol was extensively studied by automakers such as Volkswagen and Ford, either in pure form or blended with gasoline [64], the most common ratios being M10 (10% methanol and 90% gasoline) and M85 (85% methanol and 15%

gasoline) [65]. Methanol offers higher engine efficiency and is less flammable than gasoline, but because of its lower energy density and calorific value, methanol-fueled vehicles have half the mileage, requiring a larger fuel tank [66]. The organic emissions (ozone precursors) from the combustion of methanol are less reactive than gasoline fuels and therefore less likely to form ozone. Very low benzene and PAH emissions have been reported when pure methanol is used [67]. Besides, methanol fuel is a carrier for H_2, which can be easily converted into other fuels, fuel additives and fuel production feedstocks [68]. Overall, according to Europe's transport sector report, by 2030, alcohol fuels are one of the top listed renewable fuels to be used due to their carbon emission-reducing tendency [69].

1.2 Chemistry of oxy-biofuels oxidation

1.2.1 Alcohols

Alcohols with various molecular structures (i.e., carbon number and substitution) can be used in today's SI and CI engines with only minor modifications to the engine design. However, the details of the combustion chemistry of alcohol fuels, including pathways of potential contaminants, are less well understood than the hydrocarbons that make up today's petroleum-derived transportation fuels [70]. Some aspects of concern regarding their perceived "cleaner combustion" image are the emissions of carbonyls such as formaldehyde (CH_2O), acetaldehyde (C_2H_4O), acetone (C_3H_6O), acrolein (acrolein, C_3H_4O). These compounds present air quality problems because they are toxic and irritating, and are precursors of urban smog (e.g. free radicals, ozone, and peroxyacetyl nitrates) [71-73]. Pang et al. [74] studied carbonyl emissions from ethanol-gasoline and ethanol-biodiesel-diesel mixtures in CI and SI engines. Ethanol blending reduced tailpipe emissions of CO and PM, but increased total tailpipe carbonyl emissions particularly, acetaldehyde. Besides, from the study performed by He et al. [75] the use of the increased amount of n-butanol in gasoline fuel in HCCI engines was seen to

significantly influence formaldehyde and acetaldehyde emissions. The emission of acetaldehyde was nearly independent of engine speed under the investigated conditions. The authors suggest that aldehyde emission levels are the result of different reaction mechanisms that may contribute to their formation, in addition to the type of engine used, load and combustion mode. Furthermore, the oxygenated nature of primary alcohols can result in additional chemical reaction pathways as compared to the well-studied alkane fuels [76], eventually, the importance and nature of alcohol-specific reactions may vary from one alcohol to another which suggests the need for studying combustion properties of different primary alcohols that lies a foundation for the larger alcohols fuels. In this regard, the combustion chemistry study of alcohols is the area that requires great attention and insight into the kinetic study of alcohols can help to determine the importance of oxygenated emissions by elucidating the role of fuel-bound oxygen during combustion.

1.2.2 Organic acids

Organic acids, in particular, acetic acid [77-79] and formic acid are widely produced through molecular dehydrogenation reactions during the pyrolysis and partial oxidation of alcohols [80], ethers [81], esters [82], and other oxygenated biofuels. They are not common constituents of conventional fossil fuels but can be present as intermediates in biodiesel production and thermochemically processed biomass (i.e., bio-oil/bio-crude). They are one of the main pollutants in the atmosphere that leads to the formation of acid rain [83, 84]. Currently, this class of compounds can be derived from the emission of exhaust gas from internal combustion engines [85, 86] or wildfire [87], thus involving both urban and rural atmospheres [83]. Among organic acids, formic acid and acetic acids have been largely detected within exhaust gas [86, 88, 89]. Formic acid is an intermediate product during the oxidation of oxygenated biofuels [90] such as methanol [91], ethyl acetate [92] and dimethyl ether [93]. In addition, it is mainly

obtained from cellulose pyrolysis through ring opening and fragmentation reactions of levoglucosan (i.e. the main intermediate product of cellulose pyrolysis) and 1,6-anhydroglucofuranone in the temperature range of 400 – 500 °C and 300 – 400 °C, respectively [94]. As a result, the chemistry of formic acid plays a determining role in the sustainable production of energy from several oxygenated species being included in several kinetic models [43, 78, 95, 96]. From a chemical kinetic perspective, the interest in industrial processes directly producing formic acid from carbon dioxide has been largely increased as they can be considered for the carbon capture utilization and storage (CCUS) as well as for the production of hydrogen carrier components through the reaction $CO_2 + H_2 \leftrightharpoons HOCHO$ [97, 98]. One litre of formic acid can have the same amount of hydrogen as in a compressed hydrogen storage tank at 700 bar [99]. On the other hand, it contains 53 g l^{-1} hydrogen at room temperature and atmospheric pressure, which is twice as much as compressed hydrogen gas can attain at typical storage conditions [100]. Thermodynamically, dehydrogenation of formic acid has low reaction enthalpy which leads to hydrogen production at a lower temperature (lower than 100 °C) [100]. Since number of C – C bonds in a fuel structure is related to soot formation tendency [101], the lack of C – C bonds in the chemical structure of formic acid, coupled with its high energy density, can favour its application within fuel blends in advanced engine technology [101].

On the other hand, acetic acid is an abundantly available substance in the environment [84] and the main acidic component of bio-oils [102] and one of the major volatile primary pyrolysis products from cellulose degradation [103]. It is the reference substance representing the carboxylic acid components in the conversion of biomass residues to heat by fast pyrolysis of bio-oils [103]. For instance, in the flames of hydrocarbon fuels and oxygenated fuels [104] and low-temperature oxidations [105], very high concentrations of carboxylic acids are formed,

most of which is acetic acid. The C−CO bonds of acetic acid split into methyl and carboxyl radicals, whereas the carboxyl radical decomposes to CO_2 and H radical through β-scission and to CO and hydroxyl radical through α-scission [106]. Overall, given their poor low-temperature performance, as well as their high solubility in water, high relative oxygen content, and acidity (which can lead to corrosion of materials used in engines), carboxylic acids may have a more detrimental effect on overall fuel performance. However, some problems can be alleviated by esterification [107].

1.2.3 Light aldehydes

Aldehydes are hydrocarbons with additional embedded oxygen atoms. They are present in bio-oil vapors and can be obtained from the chemical transformation of bio-derived molecules. Besides, aldehydes such as acetaldehydes can also be sustainably produced from fast pyrolysis of bio-oil, especially from the lignin component of the biomass [108], xylan, cellulose and further decomposition of intermediate pyrolyzed products (e.g. 3,4-altrosan, levoglucosan and levoglucosenone) [94]. These O−H−C compounds are mainly produced during the combustion of fuels with high oxygen content, such as alcohol [109]. Under cold-start conditions, alcohols crack to produce aldehydes, principally formaldehyde in the case of methanol and acetaldehyde in the case of ethanol. Among the most important, acetaldehyde has an unusually weaker C−C bond in the acetyl (CH_3CO) group [110], which makes it readily decompose to methyl (CH_3) and carbon monoxide (CO), thus indicating the strong relation between acetaldehyde chemistry and methyl chemistry. Overall, due to the hierarchical nature of combustion modelling [111, 112], all reactions associated with lower carbon chain fuels shall be included to investigate larger carbon chain fuels. Notably, in high-temperature combustion of fuels, reactions leading to C_1 and C_2 fragments are too fast to limit the overall combustion rate, and it is the oxidation rate of these smaller hydrocarbons that control the most observed combustion properties [111,

113, 114]. Similarly, in the low-temperature oxidation process of alkanes, aldehydes are the key components in the pre-ignition stage of hydrocarbon combustion [115]. From the recent studies reported on diethyl ether (DEE) and dimethyl ether (DME) mixtures with ethanol [116], it has been concluded that the formation of acetaldehyde is the leading intermediate step for the improved reactivity of these blends. Therefore, from the pure chemical kinetics perspective, aldehydes are the main stable intermediate products of biofuel oxidation and pyrolysis, which affect the reaction pathway and important combustion characteristics, thus cannot be ignored for the design of more efficient and environmentally friendly combustion systems [117].

Overall, due to the presence of oxygen in the molecular structure of oxygenated fuels, oxy-biofuel combustion reduces the emission of CO, which is mostly formed by the incomplete combustion of fuels most readily from petroleum fuels, which contain no oxygen in their molecular structure. Studies have shown a 30% reduction in CO emissions depending on the type and age of the engine/vehicle, the emission control system used, and the atmospheric conditions in which the vehicle is operating when using one of the widely used oxygenated fuels, ethanol. Due to health concerns about CO, the U.S. Clean Air Act Amendments of 1990 required the use of oxygenated gasoline in major urban centers during the winter months (when atmospheric CO levels are at their highest) to reduce this pollution [118, 119]. Thus, biofuels can safely be part of a diverse energy portfolio that can potentially replace fossil fuel consumption.

1.3 Combustion model

Combustion in an internal combustion engine is a complex process involving fuel atomization, vaporization, fuel-air mixing, ignition, and combustion. In the field of combustion, three distinct states are commonly observed for most fuels, namely low temperature, intermediate temperature and high temperature [120]. As reported by Dec [121] on the phenomenological

description of the diesel combustion model, the low-temperature reaction spontaneously ignites part of the premixed fuel and air within fuel-rich conditions, resulting in a rapid release of heat. The remaining fuel spray is then consumed in a high-temperature diffusion flame. This unstable, heterogeneous, three-dimensional process is challenging to model, and it is difficult to separate the physical mixing process from the chemical kinetic process. To accurately describe this phenomenon, an investigation into the thousands of elementary reactions and their rate parameters governing the complete combustion of a given fuel is indispensable. In this regard, computer simulations can combine fluid dynamics, spray dynamics, chemical kinetics, and heat and mass transfer to reproduce ignition behavior, flame propagation, pollutant formation, energy release, and other characteristics of engine operation. This simulation is widely used in the automotive industry to improve fuel economy and reduce emissions. Westbrook et al. [122] conducted a comprehensive review of computational combustion methods and their application in SI, CI, and HCCI engine combustion simulations. From the later study reported by Westbrook et al. [123, 124], an understanding of engine-relevant phenomena can be obtained using detailed chemical kinetic models in simpler reactive flow simulations, under defined boundary conditions.

Developing a detailed chemical kinetic model follows the hierarchical nature of combustion modelling [111, 112], which should include all reactions associated with lower carbon chain fuels to study larger carbon chain fuels. To this aim, the chemical kinetic mechanisms study of lower carbon chains from each class of oxygenated fuel category (e.g. methanol and ethanol from primary alcohols, formic acid and acetic acid from organic acids, acetaldehyde from aldehydes) are considered. Due to the lack of properly guided theoretical or experimental studies, key reaction classes affecting the oxidation of these fuels are not well studied in detail, and some main pathways remain unknown. Besides, the inherent uncertainties corresponding

to the input parameters (i.e. thermodynamics and rate coefficients) and their complex temperature, pressure and fuel composition dependencies remain challenging [125, 126].

Combustion chemistry of a given fuel component can be studied through the evaluation of the fundamental combustion parameters such as laminar burning velocity, ignition delay time, reaction paths, species profile from jet-stirred reactor, etc. These properties can be analysed as a function of time *t*, temperature *T*, pressure *P*, or composition [127]. Ignition delay time (IDT) is an important macro information about the reactivity of fuels (i.e. in intermediate and high temperatures) and can be correlated with fuels octane rating [128, 129]. It defines the time that a specific fuel mixture takes to oxidize and release heat when exposed to specific thermodynamic conditions of pressure and temperature, thus, it is a critical parameter for engine design and operation. It has been noted that octane ratings are primarily determined by chemical kinetics rather than physical fuel effects (e.g. latent heat of vaporization, density, viscosity, physical mixing effects, etc.) [130]. Furthermore, premixed laminar burning velocity is a fundamental indicator of fuel reactivity (i.e. especially in low-temperature combustion) and a critical parameter for determining complex combustion phenomena occurring in engines, such as the turbulent flame speed, flame stabilization, flame structure and extinction [127, 131]. It is a measure of how a flame propagates into a quiescent unburned mixture at a specific temperature, pressure and fuel composition. In general, the emissions formed upon fuel oxidation and/or pyrolysis in ideal reactors are indicative of the species formed in engines under similar temperature, pressure, and equivalence ratio conditions. Thus, understanding combustion in idealized systems can offer insights into a fuel's performance in practical engines.

1.4. Research Questions

The growing interest in biofuels from biomass pyrolysis has motivated systematic investigations of different chemical families such as alcohols [44, 132], aldehydes [133, 134], acids [43], and oxygenated aromatics [135, 136] to elucidate the effects of the oxygen functional groups on their combustion chemistry. In addition, the incomplete combustion of biofuels produces a small amount of harmful chemical components for the environment and human health (e.g., acetic acid, aldehydes, and ketones) [1, 2, 137]. The O atom present in biofuels is bound in the form of alcohol (hydroxyl, −OH), ether (−O−), aldehydes and ketones (C=O), acids, furans and ester (−COO−) groups. The existence of oxygen functional groups in the molecular arrangement of biofuels changes the electronic structure of the fuel, thus limiting the production of aromatic compounds and carbon soot. This difference in the structural characteristics of biofuels will lead to differences in chemical reactivities, reaction pathways, intermediates and unwanted by-products. In this regard, the accurate evaluation of the fuel decomposition and oxidation kinetic mechanisms of alcohols, carboxylic acids, esters, furans and aldehydes classes of oxygenated fuels is a valuable step toward the awareness of the reaction paths ruling the formation of relevant intermediates [70]. The variations in the chemical structure of biofuels will certainly affect the reaction pathways and eventually dictate the combustion characteristics, such as autoignition and flame propagation.

A complete evaluation of fuel molecules requires a detailed analysis of their combustion characteristics, which also requires an understanding of how these intermediates are produced during biomass pyrolysis. The heat transfer and reaction rates during biomass conversion are strongly influenced by biomass composition (i.e., cellulose, hemicellulose, and lignin) and reactor configuration, thereby affecting yield profiles and product properties. Thus, understanding how these chemical components decompose during biomass pyrolysis requires

extensive studies, especially considering different compositions of cellulose, hemicellulose and lignin.

Besides, experimental combustion studies are hindered by technical difficulties related to the different functions of oxygen-enriched biomass, intermediates, and products; temperature sensitivity to products, short lifetimes to intermediates; and product dependence on volatile residence time. In this framework, the design and optimization of any combustion process based on oxy-biofuels need the understanding of fundamental biomass pyrolysis and biofuel oxidation kinetics through the definition of detailed chemical kinetic models.

For clarification, the current research aims at developing a chemical-physical model for the quantification of the most relevant phenomena ruling the energy production from bio-based fuels. However, the project can be also intended as a combination of different work packages dedicated to the characterization of the behaviour of the biomass and possible lighter intermediates, as discussed below.

Biomass pyrolysis: Being the first step in biofuel production and energy recovery, biomass pyrolysis requires careful characterization and processing methods. Hence, the fate of the successive biofuel processing methods relies on understanding how biomass decomposes, intermediate species consumed, and desired species are produced with the help of robust kinetic mechanisms. Due to the multi-phase nature of biomass, and the multi-step and multi-scale nature of processing methods, developing an accurate kinetic model is however a challenging step since the main efforts in biomass pyrolysis simulation lie in accurately capturing the molecular conversion kinetics. Understanding fast pyrolysis for scale-up is then reported to be a challenge, requiring careful examination of specific rate-determining steps and addressing the question of whether the heat transfer mechanism is efficient and whether the residence time of the two phases is sufficient. This needs to be reported along with the biomass properties and

their sub-components. Thus, this work is devoted to the realization of a numerical characterization of biomass pyrolysis which included a newly developed kinetic model considering the recent improvements and updated kinetic schemes.

Formic acid combustion: monocarboxylic acids have been reported to be one of the main pollutants detected from IC engines and an intermediate product of oxygenated biofuel oxidation, including methanol and dimethyl ether. Formic acid is also considered one of the most promising hydrogen carrier components through the $HOCHO \leftrightarrow CO_2 + H_2$ reaction and can be used as a platform for chemical energy storage. Being an intermediate product of the oxidation of different oxygenated components, rising concerns as hydrogen and CO storage, and energy provision via combustion, the kinetic mechanism study of formic acid deserves in-depth analysis, which obviously contributes to the understanding of the combustion kinetics of other intermediates and larger carboxylic acid components. In this regard, the gas-phase kinetic mechanism study of formic acid oxidation is very crucial in environmental chemistry, hydrogen production and modern engine technology. To the level of its importance, the combustion chemistry of formic acid is poorly understood, and the study of formic acid oxidation has been very limited. Apart from Glarborg and updated Aramco 2.0 kinetic models, there are no comprehensive chemical kinetic mechanisms developed for formic acid combustion. For these reasons, the current study is devoted to the development of detailed kinetic mechanisms for formic acid combustion and provides insights into the chemistry ruling the decomposition of formic acid in an oxidative environment.

Acetic acid combustion: As a major bio-oil component and one of the main volatile products of cellulose pyrolysis, acetic acid can be considered as a reference component representing the chemical family of carboxylic acids in biomass conversion and combustion of hydrocarbon and oxyfuel flames. It is found in large concentrations in the troposphere and considerably

affects the environment. Therefore, to understand how acetic acid is formed in flames and envision reducing the emissions of this pollutant, it is important to study the pathways involved in its formation and consumption through a comprehensive chemical kinetic model. In this regard, a semi-lumped kinetic model and a detailed kinetic model have been developed and the combustion chemistry of acetic acid has been studied through the evaluation of its combustion parameters.

Acetaldehyde combustion: It is the main stable intermediate product of biomass pyrolysis and biofuel oxidation, and is the key component in the pre-ignition stage of hydrocarbon combustion, especially the low-temperature oxidation of alkanes. Under combustion-related conditions, acetaldehyde cannot withstand high temperatures and reacts chemically to produce single-carbon species, and as a result, it is present in high concentrations in exhaust gases (i.e. especially when ethanol is considered). On the other hand, it is also a major unregulated pollutant from the combustion of biofuels, especially alcohol. The oxidative behavior of acetaldehyde is the key to hypothesising higher-order aldehyde reaction patterns. In this view, understanding the kinetics of acetaldehyde formation and consumption in flames requires the definition of chemical kinetic mechanisms, in which existing kinetic models have difficulty accurately capturing the chemical properties of acetaldehyde in an oxidative environment. To this end, two kinetic models (i.e. a simplified kinetic model and a detailed kinetic model) were developed and used to evaluate the combustion chemistry of acetaldehyde under different reaction conditions.

Methanol combustion: High octane number, low flame temperature and high oxygen content (i.e., reduced risk of explosion, NOx and soot formation) make methanol one of the important alternative fuels. It is also a major source of formaldehyde, one of the main pollutants in the oxidation of biofuels, and a central intermediate in the combustion of biofuels and hydrocarbon

fuels. Methanol lies on the main oxidation pathway of methane and methyl radicals and plays a key role in the conversion of carbon to CO. CO and formaldehyde are important in low-temperature fuel chemistry. Therefore, as an important model fuel component and a major source of formaldehyde, the combustion kinetics study of methanol is very crucial to understand its combustion kinetics, which obviously helps to realize the chemistry of CH_2O formation, and larger alcohols. Thus, a simplified kinetic model has been developed and used for the investigation of methanol chemistry.

Ethanol combustion: Ethanol burns cleaner and more completely than gasoline and diesel, and its proportion in gasoline is expected to increase in the future. Similarly, the utilization of pure ethanol has also received attention from the transportation sector. Therefore, the use of ethanol as part of the near-term energy transition to low-carbon intensity fuels requires a more fundamental understanding of its combustion properties. During combustion, ethanol favors the OH-terminated pathway to form acetaldehyde and hydroperoxy radicals rather than low-temperature chain branching reactions. Therefore, as an essential alcohol and commercial fuel component, the study of the combustion kinetics of ethanol is crucial for understanding its kinetics chemistry, intermediates, higher alcohols and, of course, for the continuous improvement of oxyfuels in the transportation sector. In this view, a kinetic model is developed and the chemistry of ethanol in an oxidative environment was evaluated under a range of reaction conditions (i.e., covering low-temperature and high-temperature combustions).

Chapter 2: State of the Art

The current understanding of the chemical and physical aspects characterizing the conversion of solid and gaseous environmentally friendly alternative fuels is summarized in this chapter. A specific focus on the detailed kinetic mechanisms of biomass and the most common intermediate species is provided in the following. Either numerical or experimental studies have been included in this aim, providing a general perspective on the available strategies and data, as well as on the current gap of knowledge in the investigated fields. Before going into the details of the physical-chemical phenomena happening during biofuel production and combustion, an overview of the current biofuel global production, research metrics, perspectives and policy directives towards its share in the global energy distribution has been provided.

2.1 Oxy-biofuels as a potential energy source

As reported by the International Energy Agency (IEA), the worldwide biofuel production has increased from 9.84×10^6 tons to 1.5×10^8 tons between the years 2018 to 2020. Based on this trend, IEA forecasted a consistent increase of biofuels up to 25% for the coming years, reaching 1.87×10^8 tons by 2024. In addition, from the recent review paper published as part of this work, the scientific studies and patents on biofuels have been consistently increasing for the last ten years [138]. Figure 1 shows data collected from the most important scientific and patent databases over the past decade (2009-2020). The figure below contains information on the number of publications devoted to the production or consumption of liquid and solid biofuels (Figure 1a), differentiated by chemical category (Figure 1b) and author affiliation (Figure 1c). The number of scientific articles each year has remained largely unchanged in recent years. Similarly, scientific research on oxygenated biofuels (such as alcohols, furans, aldehydes, esters, phenols, and acids) is increasing [42, 43, 46, 139]. Indeed, most of the biofuel research is devoted to the investigation of these chemical classes, as shown in Figure 1(c), which reports data referring to 2020. Additional information can be gained by the comparison of the share of published articles for countries, as shown in Figure 1c. It is worth noting that Europe, the United States of America, and China lead the innovation in this field, followed by India and Brazil, confirming the relevance of local policies.

Overall, global biofuel demand has been growing since 2000, and strong growth is expected in the future due to favorable government policies in Europe, North America and China aligned

with the zero-emissions agenda. For instance, the European Union set two new policy directives in 2003 on biofuel [140]. The first policy is aimed at making 20% of their automobile fuel; biofuel, hydrogen, natural gas, and other renewable fuels by 2020, as per the agreement by all EU member states in the Renewable energy Directives (RED) 2009/28/EC. Secondly, the union agreed to put a tax deduction on biofuels. Besides, under the climate and energy framework of 2030, the EU member countries have agreed to reduce greenhouse gas emissions by 40% by 2030 (compared to 1990), make 27% of their energy from renewable sources, and increase energy efficiency by at least 27% [140]. In light of such concerns among EU member states, the U.S. Energy Independence and Security Act (EISA) of 2007 defined a Renewable Fuels Standard Scheme, known as RFS2.1 [141]. EISA guides the use of biofuels and established a 50% reduction in greenhouse gas emissions by 2022. Biofuels offer many economic, technological, and environmental advantages due to the significant reduction of particulate matter, soot formation, unburned hydrocarbon, and NOx emissions [48]. To achieve this and realize the bio-based economy, it is important to focus on unresolved issues that hinder the wider application of biofuels, which requires extensive studies of pyrolysis and combustion mechanisms, highlighting existing knowledge gaps.

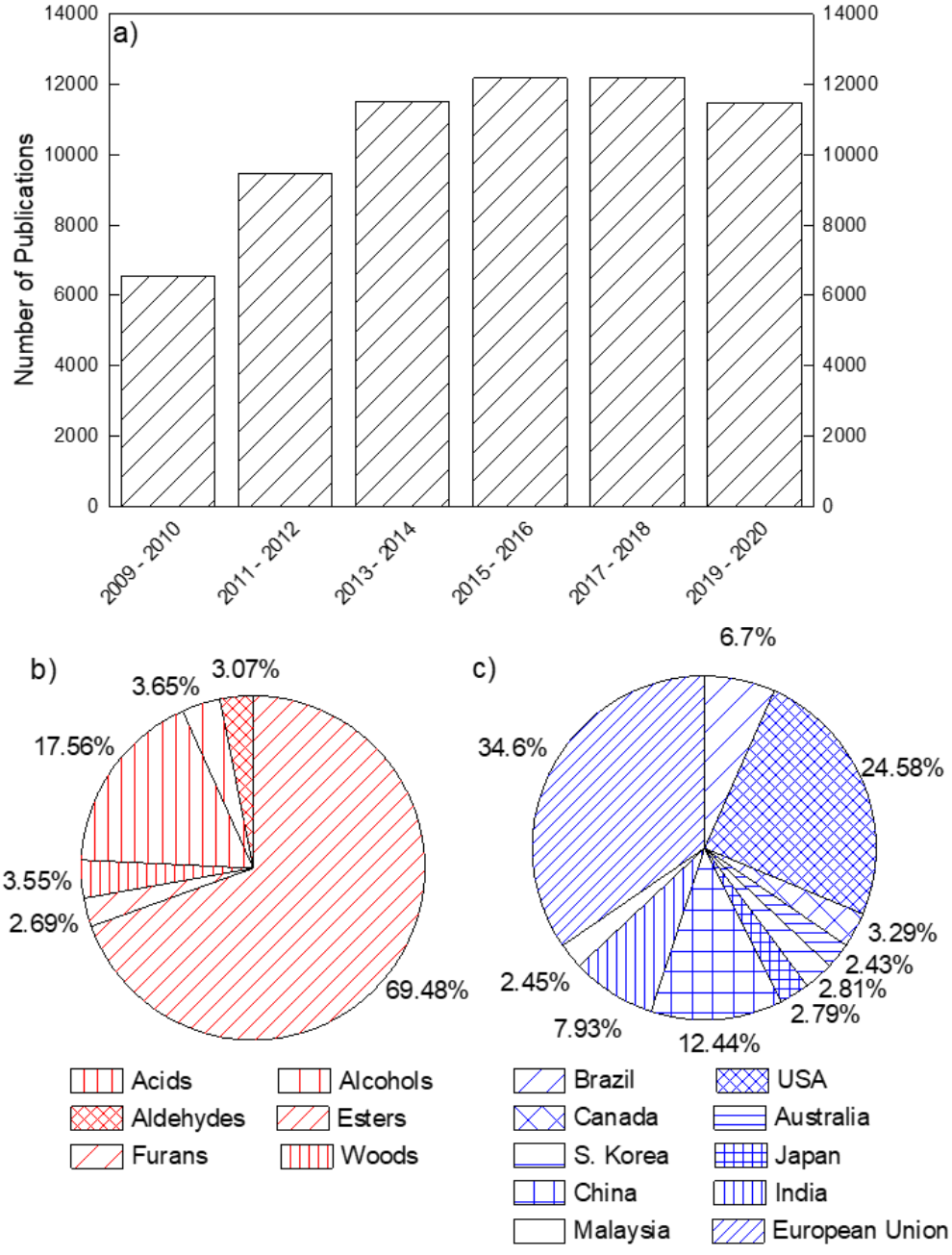

Figure 1: Global research trends of oxy-biofuels for the last ten years (a), for chemical classes (b), and countries (c) [138].

2.2 Kinetics of Biomass Pyrolysis

The kinetic study of biomass degradation is very crucial for understanding how the building blocks in biomass feedstock decompose and intermediate products are produced during pyrolysis. To this view, the kinetic modelling study of biomass pyrolysis typically considers the decomposition and multi-step devolatilization of the three independent components: cellulose, hemicellulose, and lignin [142]. Several kinetic schemes have been developed in the

literature ranging from simple single-step kinetic models to complex reaction models containing hundreds of reactions [143-149]. In this light, simplified reaction schemes are reported to be suitable [150] given the complexity of the feedstocks and plenty of intermediate products. Several studies have been reported on biomass pyrolysis kinetics including the first global kinetic scheme developed by Bradbury et al. [151] where cellulose decomposition is represented by three parallel reactions forming active cellulose, gases, and char. Active cellulose further depolymerizes forming volatile species as reported by Shafizadeh et al. [152] and of which levoglucosan (LVG) is the main fraction [153]. Extensive studies on cellulose pyrolysis and its dependence on temperature [154-158] support the assumption that hydroxy acetaldehyde (HAA) is the primary decomposition product, especially through a ring scission reaction that becomes increasingly crucial at elevated temperatures. In this regard, Piskorz et al. [159] proposed the modified version of the Bradbury et al. [151] mechanism taking into account the formation of both HAA and LVG during cellulose pyrolysis. The initial stage of the mechanism considered the competitive formation of char and activated cellulose, followed by ring cleavage producing HAA and depolymerization leading to LVG [159]. Later studies [160-162] largely confirm the mechanistic findings of Piskorz et al. [159]. Given the heterogeneity of hemicellulose, xylan has been widely considered as a surrogate for understanding the kinetics of hemicellulose pyrolysis [163-165]. Insights between pyrolysis product distribution and structural features of xylose-based hemicelluloses have been reported [166, 167]. As described in Ranzi et al. [145] pyrolysis model, xylose degrades forming two hemicellulose intermediate species (HCE1 and HCE2), followed by successive decomposition routes leading to the formation of xylan, light oxygenates, gases and char. However, their model does not include several major products, such as acetic acid, furfural, formic acid, hydroxy acetone, anhydroxylose, dianhydroxylose and other smaller molecules which have been experimentally measured in large yields [168, 169]. Similarly, due to its complex chemical structure, lignin also requires the adoption of different reference components as named by Faravelli et al. [170] as LIG-C (lignin rich in carbon), LIG-H (lignin rich in hydrogen), and LIG-O (lignin rich in oxygen), respectively. These reference components decompose releasing gases and intermediate components which further degrade forming lighter species and lignin intermediate derivatives [171]. For a better illustration of biomass degradation, a reaction path diagram showing biomass decomposition is shown in Figure 2.

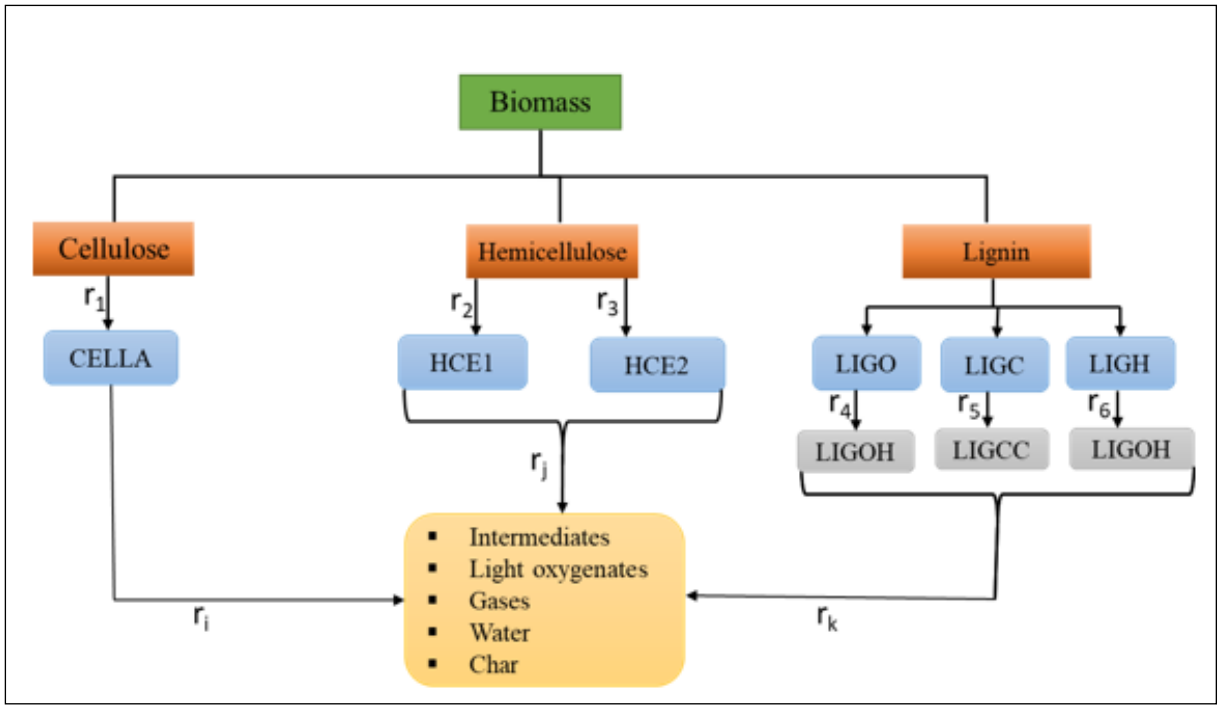

Figure 2. A simplified reaction pathway for biomass pyrolysis for the production of oxy-biofuels

2.3 Combustion kinetics of oxy-biofuels

Oxygenated species as a potential replacement to petroleum fuels need to be understood from different practical points of view (i.e., combustion). Because, in addition to the sustainability of the source, knowledge of the compatibility of the fuel within transportation sectors and combustion machinery is very important and needs to be analyzed [70] considering engine-relevant conditions. In this view, predictive chemical kinetic models provide a better understanding of the combustion performance and emissions characteristics of biofuel compositions. Chemical kinetic models can be constructed in two ways; first, by manually collecting rate coefficients and thermodynamic data for relevant species and reactions from the literature. In this approach, the mechanism involves a series of refining reactions and, relatively, comprises a low number of species and reactions. Second, automated algorithms are used by defining initial conditions (i.e., temperature, pressure, composition), reaction library (i.e., kinetics and heat) and fuel structure. Given the conditions, the tool uses reaction families to define templates that manipulate matching functional groups when converting molecules from reactants to products. The chemical kinetic model developed in this way contains more species and reactions than the previous one. In this regard, the combustion studies of

oxygenated biofuels such as light alcohols, organic acids, and aldehydes with the help of chemical kinetic models are reviewed from the recent literature as follows.

2.3.1 Light Alcohols

The energy production via alcohols is primarily satisfied by using them as alternative fuels or additives in blends [7,25]. However, in the kinetic field, alcohols are commonly adopted as per the definition of a surrogate to mimic the combustion behaviour of more complex mixtures characterized by flexible compositions (e.g. biodiesels) [77]. Among them, the primary alcohols (such as methanol, ethanol, and butanol) are ideal for engine combustion [78]. These fuels have no negative temperature coefficient (NTC) behaviours and are all water-soluble [78]. Besides, their moderate tendency to form soot and elevated octane rating makes the light alcohols (i.e., ≤ C5) good aspirants for lean to rich stratified combustion [79] and low-temperature combustion [7,80]. Moreover, in homogeneous charge compression ignition, methanol and ethanol have limited sensitivity to the equivalent ratio but high sensitivity to the temperature, while n-butanol has similar reactivity to equivalent ratios and temperatures like that of gasoline [81,82]. The average bond dissociation energies of alcohol fuels are around 105 kcal mol^{-1}. Due to the good electron-losing ability of the hydroxyl functional group, the bond dissociation energies of the secondary C−H bond in the α-position largely decreases to ∼95 kcal mol^{-1} and that of β- position to ∼100 kcal mol^{-1} [7]. In addition, the location of the hydroxyl group (–OH) attached to the carbon atom in alcohol plays a crucial role in the physical-chemical properties. Further, this functional group acts as a radical chain terminating group following H-abstraction, which ends up hindering the cool flame reactivity [83,84]. The presence of the –OH functional group also helps them to suppress the NTC bearing of other fuels [78]. In this view, recent reports on the chemistry of methanol and ethanol are reviewed and presented below.

The high H/C ratio, the lack of C–C bonds, and the high latent heat of methanol help to reduce the peak temperature and, ultimately, result in low NOx emissions. Besides, the low molecular weight and high oxygen content of methanol result in a high combustion speed and high-octane number, thereby providing an elevated thermal efficiency [47]. From this point of view, several experimental and numerical studies have been reported. For instance, Bowman [172] conducted both experimental and numerical studies of methanol–air mixture behind reflected shockwaves over the temperature range of 1545–2180 K and pressures of 1.5–4.2 atm. The times required to obtain the maximum concentrations of CO and O-atom were taken as ignition

delay times. The self-ignition of various fuel species including stoichiometric methanol-air mixtures at pressures of 13 and 40 bar and a temperature range of 800–1200 K has been reported by Fieweger et al. [173]. The period at which the CH band emission and maximum change in the rate of pressure occurred was defined as the ignition delay time. Moreover, the high-temperature ignition delay time of C_1–C_4 primary alcohols under pressures of 2, 10, and 12 atm were studied by Noorani et al. [54], and CH emissions were considered as a measure of the ignition delay time. Methanol oxidation under a rapid compression machine (RCM) was hardly reported in the literature, and the most commonly used data was reported by Kumar and Sung [174] and was performed at an equivalence ratio of 0.25–1.00, a pressure of 7–30 bar, and temperature range of 850–1100 K. The maximum rate of the pressure increase was used to define the ignition delay time. Cathonnet et al. [175] performed pyrolysis experiments of methanol using a static reactor at a pressure of 0.3–0.5 atm and a temperature range of 875–975 K. Additionally, methanol oxidation in a stirred reactor at nearly atmospheric pressure and temperature range of 650–700 K was studied by Aniolek and Wilk [176]. Recently, a comprehensive study on the ignition phenomena of a stoichiometric methanol/oxygen/argon mixtures was reported at the pressure range of 12–24 bar and temperature range of 840–1000 K under a rapid com- pression machine (RCM) by Wang et al. [177].

Westbrook and Dryer [178] reported one of the early detailed methanol chemical kinetic models comprising 26 species and 84 elementary reactions. The model fairly captured the experimental combustion data for a temperature range of 1000 – 2180 K, a pressure of 1 – 5 atm and an equivalence ratio range of 0.05 – 3. Burke et al. [179] reported an experimental study of methanol oxidation under a shock tube and compression machine (RCM) coupled with a detailed chemical kinetic model under a wide range of reaction conditions; pressure (2 – 50 atm), temperature (820 – 1650 K) and at all fuel flames (lean, stochiometric and rich). The kinetic model has been used for the evaluation of ignition delay time and jet-stirred reactor data of methanol. Later, to improve detailed chemical kinetic models, Pinzòn et al. [180] studied methanol oxidation behind reflected shock waves in shock tubes over the course of wide reaction conditions. The authors have compared with results with chemical kinetic models available in the literature, namely Li et al. [181] (Princeton), Konnov [182] (Lund university) and AramcoMech 3.0 [183] models. More specifically, good agreement has been obtained with AramcoMech 3.0 kinetic model. Aranda et al. [184] developed a detailed kinetic model for methanol oxidation and validated it with experimental data reported at high pressure (20–100

bar) and intermediate temperatures (600–900 K). The authors found that at high pressure, the onset reactions were particularly sensitive to H-abstraction by a hydroperoxyl radical (i.e., $CH_3OH + HO_2 \rightleftarrows CH_2OH + H_2O_2$). Recently, an experimental and computational study of methanol under shock wave tubes over ranges of reaction conditions has been reported [185]. The authors reported pre-ignition in shock tubes as a significant factor impacting the accuracy of ignition delay time data.

On the other hand, the low-temperature combustion chemistry of methanol has been studied through the evaluation and investigation of methanol flames. In this view, Akrich et al. [186] reported flame profiles and combustion mechanisms of methanol-air flames under low pressure. From the study, several species such as CH_3OH, O_2, H_2O, H_2, CO, and CO_2 were measured as a function of the distance from the burner, and H, OH, and HO_2 were found to be responsible species for H-abstraction during methanol oxidation. An experimental and numerical study on the laminar burning velocity study of methanol at atmospheric pressure and a temperature range of 298–368 K using a counter-flow twin flame method was reported [187]. A decade later, Liao et al. [188] studied the laminar burning velocity of methanol–air mixtures at 358 K using the spherical combustion bomb technique. The influence of fuel/air ratio and initial temperature on the laminar burning velocity of methanol-air flames has been investigated. A comparative experimental and numerical study of methanol, ethanol and n-butanol flames using the counter-flow configuration technique at atmospheric pressure and reaction temperature of 343 K has been reported by Veloo et al. [45]. From the study, CH_2O, HCO, and H were reported to be the dominating radical species. Moreover, the temperature dependency of laminar burning velocity at atmospheric pressure and temperature range of 298 – 358 K was reported using the heat flux method [189]. The oxidation chemistry of methanol in a laminar premixed flame of methanol-air mixtures at an initial temperature of 423 K and a wide range of pressure (1 – 10 atm) in a spherical combustion vessel has been reported [190]. Formaldehyde (CH_2O) and formic acid (HOCHO) were identified as the abundantly produced intermediates in methanol flames. Recently, Raida et al. [191] reported an experimental study on methanol-air flames over ranges of conditions including temperature (318 – 338 K), pressure (1 – 5 bar) and equivalence ratio (0.8 – 1.3) using the heat flux method. The authors also performed a kinetic modelling study using the available detailed kinetic models from Politecnico di Milano [131] (Polimi mech), the University of California at San Diego [192] (San Diego mech) and the University of Ireland Galway [179] (NUI Galway mech). A quite

reasonable agreement has been observed between the models and experimental results at atmospheric pressure however, the models over-predicted the burning velocity at relatively higher pressures.

Having robust experimental data, the need for detailed kinetic models has been growing. Among the previous kinetic model, the widely used methanol model of Li et al. [181] can fairly predict the laminar burning velocity in lean flames. However, recent measurements posed challenges to the Li model [181] under stoichiometric and rich conditions [45, 193]. Based on this, Konnov et al. [194] emphasized that the performance of the Li model could be significantly improved by updating the branching ratios for reactions of methanol with O_2, HO_2, OH, and H, using the recent calculation results [195-197]. A year later, Christensen et al. [198] developed a kinetic model for CH_2O and CH_3OH using revised rate coefficients from the literature and validated the model over a wide range of experimental conditions and equipment. However, the model predicted maximum burning velocities with richer equivalence ratios than experimental results [55, 193, 194, 199], which occurs in all conditions and leads to underpredictions in lean conditions, while overprediction in rich conditions. Later on, Zhang et al. [190] studied the chemistry of methanol oxidation in a laminar premixed flame both experimentally and numerically. The detailed kinetic model has been developed by extensively retrieving experimental and theoretical literature data. The model has been validated with laminar burning velocity data from a spherical combustion vessel at temperature of 423 K, pressure of 1 – 10 atm and equivalence ratio of lean, stoichiometric and rich conditions. Deviations between the model and experimental results has been observed at stoichiometric and rich conditions. To better illustrate the works being reported, the most relevant steps involved in the oxidation of methanol is shown in Figure 3.

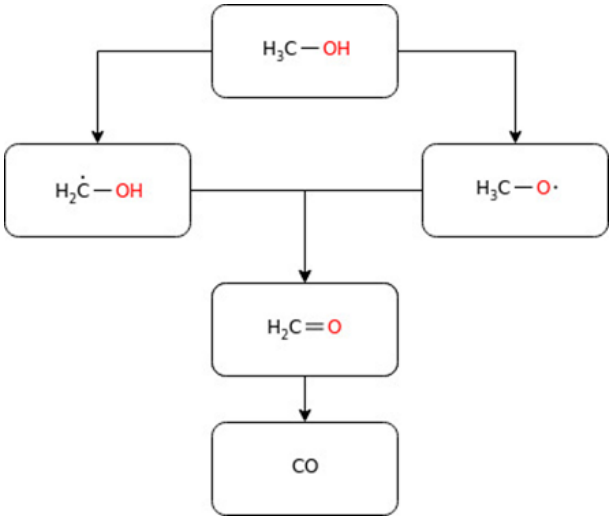

Figure 3. Simplified reaction pathway for methanol oxidation [138].

Table 1. Summary of detailed methanol kinetic models with their validation ranges as reported by the authors. NA: not available.

Mechanism	Species	Reactions	T(K)	P(atm)	φ	Year	Ref.
Marinov*	58	383	NA	NA	NA	1999	[95]
Dryer	55	290	633–2050	0.26–20	0.05–2.6	1998	[91]
Li	21	93	850–950	1.5–6	0.5–2	2007	[181]
San diego*	58	270	NA	NA	NA	2016	[200]
Mech15.34	170	900	800–1200	1–20	0.2–2	2016	[179]
Zhang	32	197	423	1–10	0.7–2.1	2017	[190]

Due to its high demand in the gasoline engine, ethanol combustion has been widely studied using different experimental systems (e.g., shock tubes [201-203], rapid compression machines [204-206], plate burner [207, 208], counter-flow twin flames [209, 210], and constant volume chambers [211, 212]. In addition, the oxidation of ethanol under several conditions has been experimentally investigated over temperature ranges of 800 – 950 K, pressure of 3 – 12 atm and equivalence ratio range of 0.3 – 1.4 in flow reactors as well [213]. Parallel to their experimental work, the authors developed a detailed kinetic model for ethanol combustion and validated their model using their experimental results (i.e., species profile) and experimental data from the literature (i.e., shock tubes, premixed flames). Barraza-Bo-tet et al. [204] reported new experimental data on ethanol ignition and species profile in a rapid compression machine.

The study revealed H-abstraction by HO_2 via $C_2H_5OH + HO_2 \rightleftarrows sC_2H_5OH + H_2O_2$ reaction as significantly affecting the overall reactivity of ethanol in ethanol oxidation. Mathieu et al. [214] studied the oxidation of ethanol under shock tubes by measuring the ignition delay time and water time history curves of this species at temperatures 944–1580 K; pressures ranging from 1.3–53 atm; and equivalence ratios of 0.5, 1, and 2. AramcoMech3.0 and CRECK kinetic models have been used to model the species profiles. From the study, it has been revealed that most of the models used were not accurately reproduced the experimental data at temperatures < 1300 K. Nevertheless, for temperatures (>1350 K), better consistency with AramcoMech 3.0 in terms of reactivity and water profile shape was observed. Similarly, Laich et al. [215] studied the oxidation of ethanol by measuring CO time histories and ignition delay times behind reflected shockwaves under elevated pressures. Good agreement between experimental and numerical data of the CO time history measured at elevated temperatures was obtained, while deviations are observed at lower temperatures. Bimolecular methyl radical and hydroperoxide radical reaction ($CH_3 + HO_2 \rightarrow CH_3O + OH$), and H-abstraction reaction at α position of ethanol ($C_2H_5OH + HO_2 \rightarrow sC_2H_4OH + H_2O_2$) were observed as low-temperature sensitivity reactions from sensitivity analysis.

On the other hand, the low-temperature chemistry of ethanol oxidation has been investigated through the study of ethanol flames. In this regard, Veloo et al. [45] experimentally reported the laminar burning velocity of ethanol using the counter-flow configuration technique at 1 atm and a temperature of 343 K. From the study, C_2H_4, CH_3CHO, CH_2O, CH_4, and CH_3, have been revealed as a major intermediate species from ethanol oxidation. Besides, three H-abstraction sites (at CH_3, CH_2 or OH) have been observed where abstraction from CH_3 leads to C_2H_4 and OH production, from the CH_2 site leads to the production of CH_3CHO and H, and finally, abstraction from the OH portion leads to the formation of CH_3CH_2O. Xu et al.[216] conducted an experimental study of the laminar combustion behaviour of ethanol-air premixed mixtures with laser-induced spark ignition (LISI) and electric spark ignition (SI) at a temperature of 358 K and pressure of 1 atm. Faster laminar burning velocity was observed for LISI at lean conditions, while lower values were noticed at stoichiometric and rich conditions. Katoch et al. [217] performed an experimental study of laminar burning velocities of ethanol-air mixtures. The power-law correlation was used to evaluate the influence of mixture temperature on laminar burning velocity, and the change of temperature index α and equivalent ratio shows the minimum value for a slightly richer mixture. Moreover, laminar burning velocities of

ethanol-water-air mixtures studied using the heat flux method under adiabatic conditions has been reported [218]. At a constant H_2O mole fraction, the chemical and thermal effects on the burning velocity were found to vary with variation in equivalence ratio.

With the extensive experimental data present in the literature; the demand for the relevant detailed kinetic model for the prediction of the combustion parameters is growing and attracting attention. Given this, earlier, Dunphy et al. [219] developed a kinetic model for ethanol comprising 30 species and 97 reactions. The author used the detailed mechanism previously reported for methanol, assembled with additional reactions that accounted for ethanol combustion. The model is in good agreement with shock tube experimental data at high temperatures and pressure of 2 − 3.4 bar. Marinov [95] developed a kinetic model for ethanol oxidation by assembling the sub-mechanisms reported in the literature for methane, hydrogen, ethane, ethylene, and propane oxidation. The model was validated using numerous experimental data of ignition delay times (from a reflected shock wave), laminar burning velocities (from constant volume bomb and counter flow twin-flame) and species profiles (from a jet-stirred and turbulent flow reactors) in the temperature range of 1000 − 1700 K and the pressure of 1−4.5 atm and is in an excellent agreement with experimental data. It has been found that, at elevated temperatures, ethanol oxidation is highly sensitive to the fall-off kinetics of ethanol decomposition, $C_2H_5OH + OH \leftrightarrow$ Products, and reactions involving the HO_2 radical. Marinov's kinetic model was found to underestimate the fuel consumption rates and concentrations of stable species from ethanol decompositions such as H_2O, C_2H_4, CH_3CHO, CH_4 and species related to abstraction channels, thus, using the Marinov mechanism as a base, Li et al. [220, 221] updated the kinetic model. A decade later, a new mechanism model called AramcoMech1.3 was developed [222] for the combustion of C_1−C_2 hydrocarbons (methane, ethane, ethylene, acetylene, acetaldehyde) and oxygenated species such as methanol and ethanol. The authors underlined the importance of the reactivity study of small fuels and intermediates for understanding and accurately describing the combustion characteristics of practical fuels. Mittal et al. [206] developed a chemical kinetic model for autoignition characteristics of ethanol at high pressures and low temperatures and validated the model with experimental ignition delay time data from a compression machine under ranges of reaction conditions, temperatures (825 – 985 K), pressures (10 – 50 bar) and equivalence ratio 0.3 – 1.0.

A detailed kinetic mechanism developed by the University of San Diego [200] is comparatively small, yet detailed and widely used in research works. During the same time, Hashemi et al.

[223] published a mechanism on ethanol pyrolysis where they addressed high-pressure conditions. Besides, a new detailed mechanism was recently developed by Zyada et al. [224] using a reaction mechanism generator (RMG). Several chemical kinetic mechanisms are reported in the literature [81] at different operating conditions for ethanol. Through the improvement in computational methods, numerically generated mechanisms are becoming more powerful. It is very difficult to meet all operating ranges with a single kinetic mechanism with the information available in the literature from previous studies [95, 225]. More recently, Roy and Askari [226] developed a new ethanol-detailed kinetic mechanism called PCRL-Mech1 (with 67 species and 1016 reactions) at engine-relevant conditions based on RMG. The important reactions were selected by sensitivity and path flux analysis, and the rate parameters of these reactions were adjusted during the development of the new mechanism. The model showed an excellent agreement with experimental results of laminar burning speed (obtained at temperature (300−600 K), pressure (1−10 atm), equivalence ratio (0.6−1.4) and ignition delay time (at a temperature within the range 820−1450 K, pressures included in 3.3−80 atm, and equivalence ratio ranging from 0.3−2). Besides, H, OH, O_2, and HO_2 were reported to be the radicals responsible for H-abstraction during ethanol oxidation. Summary of chemical kinetic models and the main reaction pathways for ethanol oxidation are shown in Figure 4 and Table 2, respectively.

Table 2. Summary of kinetic models of ethanol oxidation with their validation ranges as reported by the authors. NA: not available.

Mechanism	Species	Reactions	T (K)	P (atm)	φ	Year	Ref.
Dunphy	30	97	1080–1660	1.8–4.6	0.25–2	1991	[219]
Marinov	56	351	1000–1700	1–4.5	0.5–2	1999	[95]
Saxena*	57	288	NA	NA	NA	2007	[227]
Leplat	36	252	890–1250	1, 10	0.25–2	2011	[228]
CRECK	451	17848	300–450	1–20	0.6–1.2	2012	[131]
Aramco 2.0	164	2716	295–2500	0.03–60	0.06–6	2016	[179]
Sandiego	54	268	NA	NA	NA	2016	[200]
Merino	31	66	300–600	1–10	0.5–2	2018	[225]
Zyada	107	1795	850–1450	NA	NA	2019	[224]
PCRL-Mech1	67	1016	300–600	1–10	0.6–1.4	2020	[226]

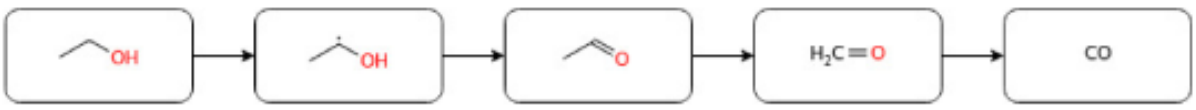

Figure 4. Simplified reaction path for ethanol oxidation [138].

2.3.2 Carboxylic Acids

Oxygenated fuels with carboxylic acid functionality, especially acetic acid and formic acid, are the dominant fractions in the tar released from biomass pyrolysis [102, 229, 230], and an accurate description of biofuel combustion must take into account the formation of these relevant intermediates. In this regard, recent studies reported in the literature on the oxidation of formic acid and acetic acid are reviewed as follows.

From a chemical perspective, the interest in industrial processes directly producing formic acid from carbon dioxide has been largely increased as they can be considered for the carbon capture utilization and storage (CCUS) as well as for the production of hydrogen carrier components through the reaction $CO_2 + H_2 \leftrightharpoons HOCHO$ [97, 98]. Besides, formic acid is an intermediate product from biomass pyrolysis [94] and oxidation of oxygenated biofuels [90] such as methanol [91], ethyl acetate [92] and dimethyl ether [93]. In this regard, the chemistry of formic acid has been investigated either experimentally in terms of laminar premixed flames [231] or numerically by kinetic models [96]. Yin et al. [232] reported experimental and kinetic studies of formic acid laminar burning velocities over a wide equivalence ratio range and temperature range of 423 – 453 K. The authors used the Glarborg and Updated AramcoMech 2.0 kinetic models to validate their experimental data, the former well agreed with the experimental results, whereas the latter overestimated the laminar burning velocity data. More recently, Osipova et al. [233] conducted an experimental and numerical study on the laminar burning velocity of pure formic acid and formic acid/hydrogen mixtures at temperatures of 368, 373 and 423 K, and equivalence ratio ranging from 0.5–1.5. From the comparison of the model and experimental data, the model overestimated the laminar burning velocity and the authors strongly suggest the importance of improving the existing chemical kinetic models or generating new detailed kinetic model. On the other hand, formic acid oxidation in a static thermal reactor within temperature range of 613 – 743 K has been reported by Bone and Gardner [234]. From the study, the pressure increase after formic acid oxidation is relatively slow, indicating low reactivity. Several studies [93, 95, 96] have reported detailed subsets of formic acid formation and oxidation, among which the study reported by Battin-Leclerc et al. [96] revealed the formation of formic acid in hydrocarbon flames to be primarily by the addition of OH radicals to formaldehyde followed by elimination of a hydrogen atom [96] through reactions; $CH_2O + OH (+ M) \leftrightarrow HOCH_2O (+ M)$, $HOCH_2O (+ M) \leftrightarrow HOCHO + H$

(+ M). Similarly, the study reported by Taylor et al. [235] on the formation of formic acid revealed the formation of formic acid by the reaction between OH and acetylene.

Since formic acid is an intermediate product during the combustion of many oxy-biofuels [90-93], its chemistry is included as a sub-mechanism in several kinetic models [43, 78, 95, 96]. In addition, the theoretical kinetic study of the unimolecular decomposition of formic acid via high-level quantum chemistry calculation has been reported by Chang et al. [236]. The gas phase reaction between HOCHO and hydroxyl radical with the high-level quantum mechanical theory has been studied by Anglada et al.[237]. In the same way, the reaction of intermediate radical HOCO with HO_2 has been studied by Yu et al. [238] employing quadratic configuration interaction with single and double excitations (QCISD (T)) method with a large basis set on the singlet and triplet potential energy surfaces. Later on, Marshall and Glarborg [239] developed the first detailed chemical kinetic model for formic acid oxidation. The model has shown a good agreement with a Bunsen burner laminar burning velocity data from de Wilde and van Tiggelen [240] for equivalence ratios ranging from 0.4 – 1.3. Rate coefficients for reactions; HOCHO + H, HOCHO + O and HOCHO + HO_2 were obtained from *ab initio* calculations. The study also indicated HOCHO + OH ↔ OCHO + H_2O reaction as the main consumption pathway for formic acid where OCHO further dissociates producing CO_2 + H and HOCO. Recently, Sarathy et al. [99] reported a detailed chemical kinetic mechanism called Updated Aramco2.0 using AramcoMech2.0 kinetic model [179, 222, 241] as a base mechanism. The authors validated the updated mechanism with the experimental laminar burning velocity data of pure formic acid and its mixtures with H_2 and CO_2. The reaction path diagram and comprehensive detailed chemical kinetic models of formic acid available in the literature are listed below in Figure 5 and Table 3, respectively.

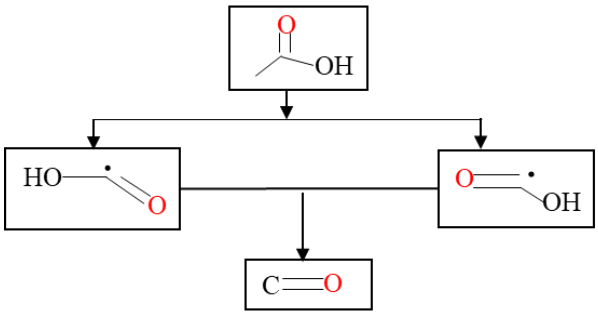

Figure 5. Simplified reaction path for formic acid oxidation.

Table 3. Detailed chemical kinetic models for formic acid oxidations

No	Mechanisms	No. of species	No. of reactions	Ref.
1	Glarborg et al.	27	75	[239]
2	Updated AramcoMech2.0	305	1761	[99]

The detection of organic acids emissions have been measured and reported the emission of a significant amount of acetic acid in the exhaust gas from spark-ignition engines [242] and rapid compression engines [243]. The studies indicated that, out of the total hydrocarbon emissions from combustion engines, organic acid emissions measured in spark-ignition engines are 4–27%, with acetic acid being the most important. In this regard, numerical and experimental studies of acetic acid combustion in laminar premixed flames were reported by Leplat and Vandooren [244]. The study reported ketene as a key intermediate species from the oxidation of acetic acid. Besides, ketene plays an important role in the consumption of acetylene, and C_2H_2 and to balance the formation of C_1 and C_2 species in C_2H_2 flames [245, 246]. Earlier, the thermal decomposition kinetics of acetic acid and its products in a single pulse shock tube within the temperature range of 1300–1950 K have been reported by Mackie and Doolan [247]. As part of this, decomposition kinetics having 21 species and 46 reactions were modelled and simulated using experimental data. From the decomposition kinetics, decarboxylation and dehydration were confirmed to be the two key decomposition reactions producing methane and carbon dioxide, on the one hand, through (Equation (1)) and ketene and water, on the other, through (Equation (2)), respectively. Ketene further decomposed to a methyl radical and CO_2, followed by a further reaction of the methyl radical with CH to form C_2H_4 and CO. In addition, methyl radicals were revealed to play an important role in determining the main products.

$$CH_3COOH \rightarrow CH_4 + CO_2 \quad (1)$$

$$CH_3COOH \rightarrow CH_2CO + H_2O \quad (2)$$

Similarly, Wagner and Zabel [248] studied the further decomposition kinetics of ketene (CH_2CO) behind reflected shocks at low pressure and reported the degradation rate constant-coefficient $K = 3.6 \times 10^{15} \exp(-248\ \text{kJ mol}^{-1}\ \text{K}^{-1})\ \text{cm}^3\ \text{mol}^{-1}\ \text{s}^{-1}$. Recently, the gas-phase reactivity analysis of acetic acid, rate constant estimation, and kinetic simulations were studied by Cavallotti et al. [249] using high-level quantum chemistry theory. The 1D master equation was also integrated on the potential energy surface (PES) to determine the rate coefficient of acetic acid degradation under a wide range of temperatures (700–2100 K) and pressures (0.1–

100 atm). The simulation showed a gradual decrease in the reaction rate at a temperature above 1200 K and a pressure of smaller than 10 atm. Besides, H-abstraction by H, OH, OOH, O_2, and CH_3 was reported to be the responsible radicals in the decomposition of acetic acid [249]. Lately, the laminar flame propagation and kinetic modelling of acetic acid at a low initial temperature and atmospheric pressure was studied by Zhang et al. [250]. The authors indicated the pathway related to ketene consumption (Equation (3)) as the main reaction governing flame propagation during acetic acid oxidation.

$$CH_2CO + H \rightarrow CH_3 + CO \quad (3)$$

In addition, the study revealed that, under rich conditions, ketene is mostly converted to CH_3 through reaction (i.e., $CH_2CO + H \rightarrow CH_3 + CO$), and the chain termination reaction of $CH_3 + H (+M) \rightarrow CH_4 (+M)$ is enhanced, which strongly inhibits the propagation of acetic acid in rich flames. Later on, the experimental laminar burning velocity of acetic acid using the heat flux method under three different initial temperatures (i.e., 338, 348 and 358 K), equivalence ratio range of 0.8–1.2 and a pressure of 1 bar has been reported by Christensen et al. [78]. The authors developed a detailed kinetic mechanism and compared their experimental results with the model. Their model over-predicted the laminar burning velocity by about 3 cm/s. Uncertainty in the laminar burning velocities was relatively high up to ±2 cm/s due to experimental problems related to the corrosiveness of acetic acid towards the burner material. Similar to formic acid, there are limited modelling studies available for acetic acid and the available chemical kinetic models are summarized in Table 4.

Table 4. Detailed kinetic models for acetic acid oxidation with their validation ranges as reported by the authors

Mechanism	Species	Reactions	T(K)	P(atm)	φ	Year	Ref.
Leplat*	45	270	-	0.05	0.7–1.05	2012	[244]
CRECK*	339	9781	-	-	-	2015	[251]
Konnov	100	1140	338–358	1	0.8–1.2	2016	[78]

Based on the reported observations, a simplified reaction pathway representative of the oxidation of acetic acid as reported in the recent review as part of this research work is shown in Figure 6.

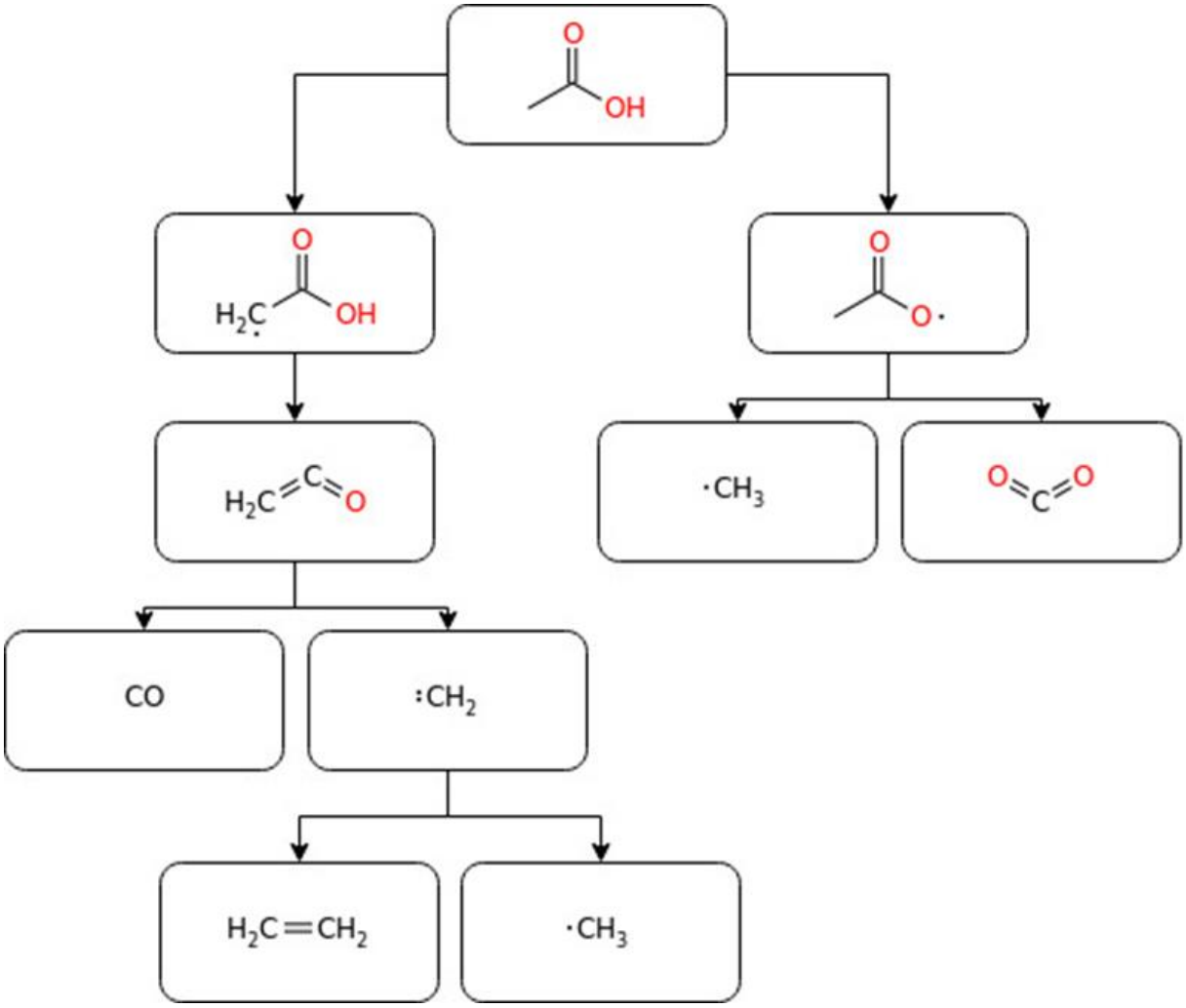

Figure 6. A simplified reaction pathway for acetic acid oxidation [138]

2.3.3 Light Aldehydes

The governing H-abstraction route at the aldehydic site was found to form a carbonyl radical (R_n-CO), which quickly further decomposes to an alkyl radical (R_n) and CO. Based on that there is a general implication that the low-temperature oxidation of the generic C_n aldehyde degraded to C_{n-1} alkyl radicals [133]. Acetaldehyde is a key intermediate in the oxidation of hydrocarbons and alcohols, especially ethanol, which is increasingly used as a motor fuel. However, it is one of the most abundant toxic oxidative emissions from biofuel combustion [127, 252] and its atmospheric reaction generates several secondary pollutants [253, 254]. Thus, the pyrolysis mechanism study of this intermediate at various reaction conditions can help to understand the overall combustion mechanism of hydrocarbons and alcohol-based fuels [255]. In this regard, the combustion kinetic study of acetaldehyde from both experimental and theoretical points of view is reviewed. Ernst et al. [256] conducted acetaldehyde pyrolysis

behind reflected shock waves under the temperature range 1350–1650K. The result revealed the decomposition as a first order reaction with rate constant expression of $K = 1.2 \times 10^{16} \exp(-81.74\ \text{kcal/RT})\ S^{-1}$. Hidaka et al. [257] studied the pyrolysis of acetaldehyde oxidation behind reflected shock wave tubes using single-pulse methods. The study considered different fuel concentrations (2.0% CH_3CHO, 4.0% CH_3CHO, 5.0 % CH_3CHO) diluted with argon under the temperature range of 1002–1700 K and pressure of 1.2 and 3.0 atm. Unimolecular decomposition reactions; $CH_3CHO \rightarrow CH_3 + CHO$, $CH_3CHO \rightarrow CH_4 + CO$, $CH_3CHO \rightarrow CH_2CO + H_2$, were mentioned to be the most important initiation reactions and $CH_3CHO + H \rightarrow CH_2CHO + H_2$, $CH_3CHO + CH_3 \rightarrow CH_2CHO + CH_4$ as the most crucial reactions responsible for acetaldehyde pyrolysis. In the same way, the pyrolysis and oxidation of acetaldehyde pyrolysis behind reflected shock waves under temperature range of 1000 – 1700 K, average pressure of 1.2 and 2.8 atm has been reported by Yasunaga et al. [53]. In the same year, Bentz et al. [258] studied the shock tube thermal decomposition of CH_3CHO and $CH_3CHO + H$ at a temperature within 1250 – 1650 K and a pressure range of 1–5 bar. Combining their results and low-temperature data from other studies, the authors reported acetaldehyde rate constant expression as $K = 6.6 \times 10^{-18} \exp(-800\ \text{K/T})\ cm^3\ S^{-1}$ for the temperature range of 300 – 2000 K. To better understand the combustion parameters, the ignition delay time of acetaldehyde behind shock tube waves under a range of reaction conditions was reported by Mével et al. [259]. The emission profile of OH, CH and CO_2 radicals were used to measure the ignition delay time. Besides, sensitivity analysis, energy release, and rate of production are reported, showing four important elementary reactions: R1: $CH_3CHO \rightarrow CH_3 + HCO$; R2: $CH_3CHO + CH_3 \rightarrow CH_3CO + CH_4$; R3: $CH_3CHO + H \rightarrow CH_3CO + H_2$; and R4: $CH_3CHO + CH_3 \rightarrow CH_2HCO + CH_4$ taking place during acetaldehyde pyrolysis and oxidation. As well, previously reported rate constants of the aforementioned reactions were collected and compared. Due to the huge differences observed during the research, the authors recommended the need for new experimental and detailed numerical studies [259]. Later on, the same author [260] updated the chemical kinetic model based on new ignition delay time measurements obtained from the shock tube and data from the literature, the revised kinetic model fairly reproduces most experimental trends. Zhang et al.[261], studied the oxidation of acetaldehyde under a wide range of conditions and revealed CH_3OO, CH_3OOH, and HOOCOCHO as the main oxidation products. Besides, H-abstracting agents were found to be by H, OH, HO_2, CH_3, O_2, CH_3COOO, CH_3OO and CH_3O. At lean condition, OH was found to be the most important H-abstracting agent. It has been concluded

that CH_3COOOH and CH_3OOH are the main decomposition pathway of acetaldehyde oxidation via chain-branching reaction and reactions related to methyl oxidation was reported to be very sensitive to CH_3OO and CH_3OOH under the studied conditions [261].

On the other hand, experimental and computational study on $CH_3CHO/O_2/Ar$ flames has been reported at an equivalence ratio of 0.75, 1, 1.25, and a pressure of 50 mbar [262]. The authors used the kinetic model developed by Yasunaga et al. [255] for the numerical study part. Under the studied condition, a good fit between the experimental results and model predictions was observed. Christensen et al. [263] studied the laminar burning velocities of acetaldehyde/air mixture at atmospheric pressure and different initial temperatures. Similarly, Christensen and Konnov [264] recently reported the laminar burning velocity of diacetyl and the updated sub-mechanism model of acetaldehyde and CH_3CO in their model. On the other hand, Tao et al. [265] conducted a study on the investigation of the chemical structures of laminar premixed flames of acetaldehyde for an equivalence ratio of 1 and 1.7 using mol.-beam mass spectrometry with synchrotron vacuum UV light for ionization. The study reported nearly 40 flame species.

In the same way, a kinetic study of acetaldehyde oxidation has been reported. For instance, Halstead et al. [266] studied the kinetic development of acetaldehyde for a better understanding of the cool flame feature of the intermediate and suggested 14-step mathematical models. From the study, acetyl was found to play a significant role in the chain-branching process through $CH_3CO \rightarrow CH_3CO_3 \rightarrow CH_3CO_3H \rightarrow CH_3CO_2 + OH$. The theoretical work reported by Felton et al. [267] and the detailed kinetic model developed by Cavanagh et al. [268] supported the result of Halstead et al.[266]. Nevertheless, Gibson et al. [269] have reported cool flame phenomena of acetaldehyde to be by CH_3OOH ($CH_3 \rightarrow CH_3OO \rightarrow CH_3OOH \rightarrow CH_3O + OH$). Moreover, the oxidation of acetaldehyde in the NTC regime has been numerically reported by Kaiser et al. [14]. The model has been validated against data from a static reactor from the same group under temperature range of 553 – 713 K and low pressure. The study revealed the radical decomposition reaction of the acetyl (i.e., $CH_3CO \rightarrow CH_3 + CO$) and O_2 addition to acetyl (i.e., $CH_3CO + O_2 \rightarrow CH_3CO_3$) as the main determining step of the chain-branching process. Besides, Sivaramakrishnan et al. [270] conducted a study on the theoretical calculations of acetaldehyde (C_2H_4O) and ethoxide (C_2H_5O) potential energy surfaces (PES) and updated the kinetic model of acetaldehyde pyrolysis. The study revealed C–C bond fission with a minor contribution from the roaming mechanism to form CH_4 and CO as the main

decomposition pathway of acetaldehyde during high-temperature processing. The model developed by the author incorporates a master equation for the analysis of H + CH_2CHOH as a primary reaction mechanism for the removal of CH_2CHOH.

Recently, Pelucchi et al. [134, 271] developed a kinetic model for low-temperature oxidation of acetaldehyde as well as C_3–C_4 aldehydes. By considering the two aforementioned chain branching reactions, the authors have validated their model with experimental data in a continuous stirred flow reactor [272]. An experimental and kinetic modelling study of acetaldehyde at low and intermediate temperatures has been reported [261]. Methyl peroxy, methyl hydroperoxide and keto hydroperoxide were reported to be the main reactive intermediates during acetaldehyde oxidation under low-temperature conditions detected using synchrotron vacuum ultraviolet photoionization mass spectrometry (SVUV-PIMS). The authors constructed the kinetic model by incorporating theoretical and modelling progress of acetaldehyde kinetics from literature and by calculating reaction coefficients associated with H-atom abstraction reactions of acetaldehyde by acetyl peroxy, methyl peroxy and methoxy. More recently, Hashemi et al. [273] developed a detailed chemical kinetic model for acetaldehyde oxidation at intermediate to high temperatures and high pressure. The model has shown good agreement with shock tube (i.e., ignition delay time) and jet-stirred (i.e., species profile) literature data, however, the model overpredicted onset reaction temperature at 100 bar. Similarly, detailed chemical kinetic model for acetaldehyde oxidation and its interaction with NOx has been developed by Shrestha et al. [274]. A quite fair agreement between model prediction and experimental data from shock tube, plug flow, jet-stirred, burner-stabilized premixed flames and freely propagating flames has been realized. For clarity, the main reaction pathway as published in the review part of this work and a simplified schematization of the oxidation pathway of acetaldehyde are shown in Figure 7 and Table 5, respectively.

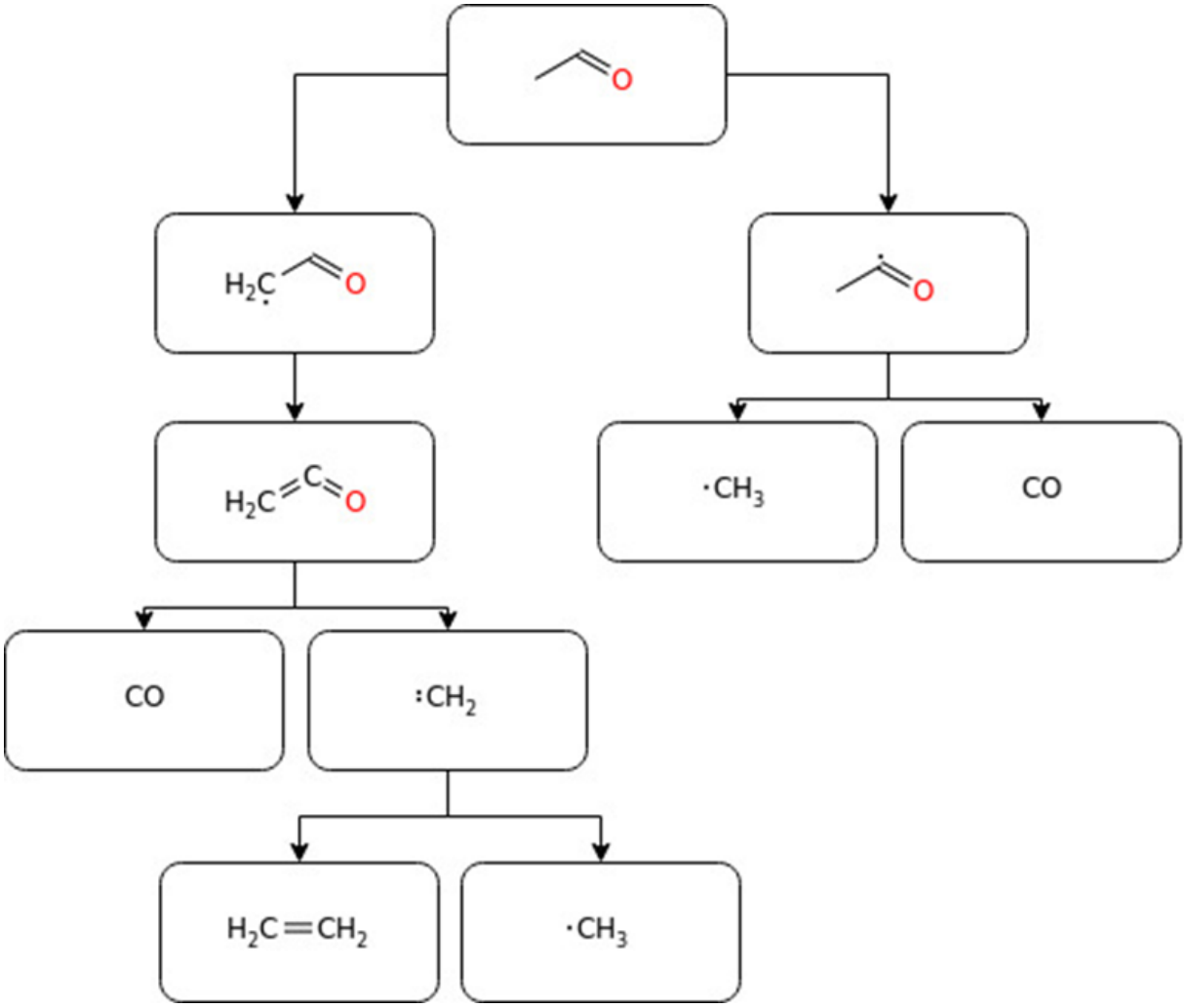

Figure 7. A simplified reaction pathway for acetaldehyde oxidation [138].

Table 5. List of available acetaldehyde chemical kinetic models and validation ranges.

Mechanism	Species	Reactions	T(K)	P(atm)	φ	Year	Ref.
Yasunaga	50	178	1000–1700	1.2–2.8	0.5–3.3	2007	[255]
Mevèl	132	994	1295–1580	3–4	0.5–1.5	2015	[275]
Tao	498	2770	700–1100	0.02–10	0.5–1.7	2018	[276]
Zhang	75	584	460–900	0.94	0.5–4	2018	[261]
Hashemi	683	71	600–900	25, 100	0.4–2.5	2021	[273]
Shrestha	139	3000	1149–1542	1.2	0.5–1	2021	[274]

A detailed discussion of recent studies on biofuel prospects and their combustion chemistry studies reported by recent researchers can be found in the review paper published by the author as part of this work as shown below.

FM Wako, G Pio, E Salzano, Laminar Burning Velocity and Ignition Delay Time of Oxygenated Biofuel. Energies, 2021.

There are different fundamental properties of a combustible mixture such as laminar burning velocity, species fraction, ignition delay times, etc, which are used for studying the combustion phenomena. These parameters are ideal for validating kinetic models and there are several experimental methods for obtaining these properties. Among the several experimental methods developed for the measurement of S_u, the opposed jet method, the closed vessel method, and the flat burner method are commonly used. The first method consists of two counter-flowing jets of fuel or oxidizer, creating stretched flame due to the flue gas flow to one side of the flame. The strain rate depends on the distance from the nozzle, which means that the unstretched burning rate can be estimated by repeating the experiment at different strain rates and extrapolating the data using the logarithmic correlation shown in Equation (4), as in Kelley and Law [277], or a linear dependence as shown in Equation (5) by Dowdy et al. [278], regarding Markstein length (L_b) and stretch ratio (k).

$$(S_b/S_b^0)^2 \ln (S_b/S_b^0)^2 = -2(L_b * k/S_b^0) \quad (4)$$

$$S_b = S_b^0 + L^b k \quad (5)$$

Where, S_b and S_b^0 are unstretched and stretched flame velocities, respectively.

In the case of the closed vessel method commonly referred to as combustion bombs, it produces rotationally symmetric, transient and stretched flames in a generally spherical closed vessel. In this method, the burning velocity is obtained by monitoring the time-dependent pressure distribution profile through extrapolation methods reported for the counterflow method. The last method (i.e., flat burner) consists of cylindrical perforated burner plates in which steady-state and unstretched flames can be produced, and the assumption of a one-dimensional flame is generally accepted due to the uniform inlet conditions provided [279]. This method can also be considered the heat flux method (HFM) when stabilization is performed using a heating/cooling fluid that controls the burner plate temperature. HFM, first introduced in 1993 by de Goey et al. [280] is based on the balance between the heat loss required for flame stabilization and the convective heat flux from the burner surface to the reaction front. In this case, Su is assumed as the velocity at which the burner plate showed constant temperature readings and was determined by measuring the temperature profile of the plate burner at different gas flow rates and given fuel/oxidant ratio, temperature and pressure conditions.

On the other hand, rapid compression machines and shock tubes are commonly used to evaluate IDT at intermediate and high temperatures, respectively [281]. The former represents a basic setup for evaluating the fuel-specific effects that occur at intermediate temperature combustion [282], which consists of a nearly adiabatic chamber in which the fuel-oxidant mixture is rapidly compressed by the motion of the piston, simulating the compression stroke of a single internal combustion engine. The later consists of a cylindrical tube separated by a diaphragm, one side is filled with high-pressure gas and the other side analyzes the mixture. Once the diaphragm ruptures, the shock wave propagates along the shock tube towards the closed-end wall of the tube, instantaneously heating the test gas and producing a reflected shock wave. The gas behind this plane is at rest, so it is analyzed for IDT measurements [283]. Considering the specificity of the system, zero-dimensional reactors with constant volume or constant pressure constraints can be employed, which can be measured by detecting the rate of pressure, temperature, or concentration of important radicals (i.e., OH and/or CH) during the combustion process) [284].

IDT represented by τ is strongly dependent on temperature and thus, described by Arrhenius expression of rate coefficients [285]. Besides, IDT also depends on pressure and fuel fraction as shown below by the modified Arrhenius expression [286-288].

$$\tau = A.\prod[X_i]^{\alpha i}.P^n.\exp(-Ea/RT) \quad (6)$$

where τ is the ignition delay time at temperature T and pressure P, [Xi] represents the concentration of various mixture species (oxygen, fuel, nitrogen, etc.), A is the pre-exponential parameter, ai is 6 the power dependence coefficient of species concentration, n is the power dependence coefficient of pressure, Ea is the activation energy and R is the gas constant.

Chapter 3: Modelling Biomass Pyrolysis Kinetics and Biofuels Combustion Chemistry

3.1 Kinetic modelling

Depending on the reaction phases and components involved during biomass pyrolysis and biofuel combustion reactions, the methodology part of the kinetic modelling is classified to describe the workflow adopted for the development of solid phase and gas phase kinetics, respectively. The solid-phase kinetics section describes how the pyrolysis kinetic mechanism was developed, and the gas-phase kinetics section describes how a detailed kinetic model was developed in an oxidative environment. The details of the procedures followed in constructing the kinetic mechanisms are discussed in detail as follows.

3.1.1 Kinetic modelling for solid phase

Kinetic modelling of biomass pyrolysis needs to describe different decomposition mechanisms. A common assumption and simplification is that each reference component decomposes independently through a multi-step branching mechanism of first-order reactions [145, 289, 290]. Therefore, the kinetic model developed in the current study follows the model approach proposed by Di Blasi et al. [291], where a linear interlinkage reaction process between the three biomass building blocks (i.e., cellulose, hemicellulose, lignin) has been assumed [292, 293]. The first step of the mechanism development was devoted to the identification of the main reaction schemes for biomass building blocks degradation followed by the collection of their rate parameters and thermophysical properties from the recent literature. The pyrolysis mechanism combines the kinetics of single-step reactions available in the current literature based on the works of several authors [145, 170, 294-298]. More specifically, this mechanism considers the recent improvements and updated kinetic schemes with additional components from Ranzi et al. [299] and revised reaction mechanisms from Humbird et al. [298] and Caudle et al. [297]. The multistep kinetic model presented here is based on the lumped reactions [145] and the kinetic parameter were derived from experimental findings and progressively extended and updated, based on new experimental data [299].

The kinetic mechanism can be intended as the sum of three sub-mechanisms, accounting for cellulose (CELL), hemicellulose (HCE), and lignin (LIGN) decomposition. More specially, two reactions in parallels were assumed for direct decomposition of CELL, leading to complete

conversion and one producing an activated species referred to as CELLA (activated cellulose), further transformed in a set of incompletely oxidized species. In the same way, a reaction is assumed for the conversion of HCE to produce hemicellulose intermediates (i.e., HCE1, HCE2) which are then further reacted to form pyrolysis end products (i.e., liquid, gas and char). In the end, lignin monomers (i.e., LIG-H (hydrogen-rich), LIG-O (oxygen-rich), LIG-C (carbon-rich)) decompose independently to produce the corresponding intermediates and pyrolysis end products, and subsequent reactions result in complete conversion of the intermediates. Overall, the current kinetic mechanism of biomass pyrolysis comprises 20 independent total reactions and 18 representative chemical components. A schematic representation of the procedures followed for developing the kinetic and process model is shown in Figure 7.

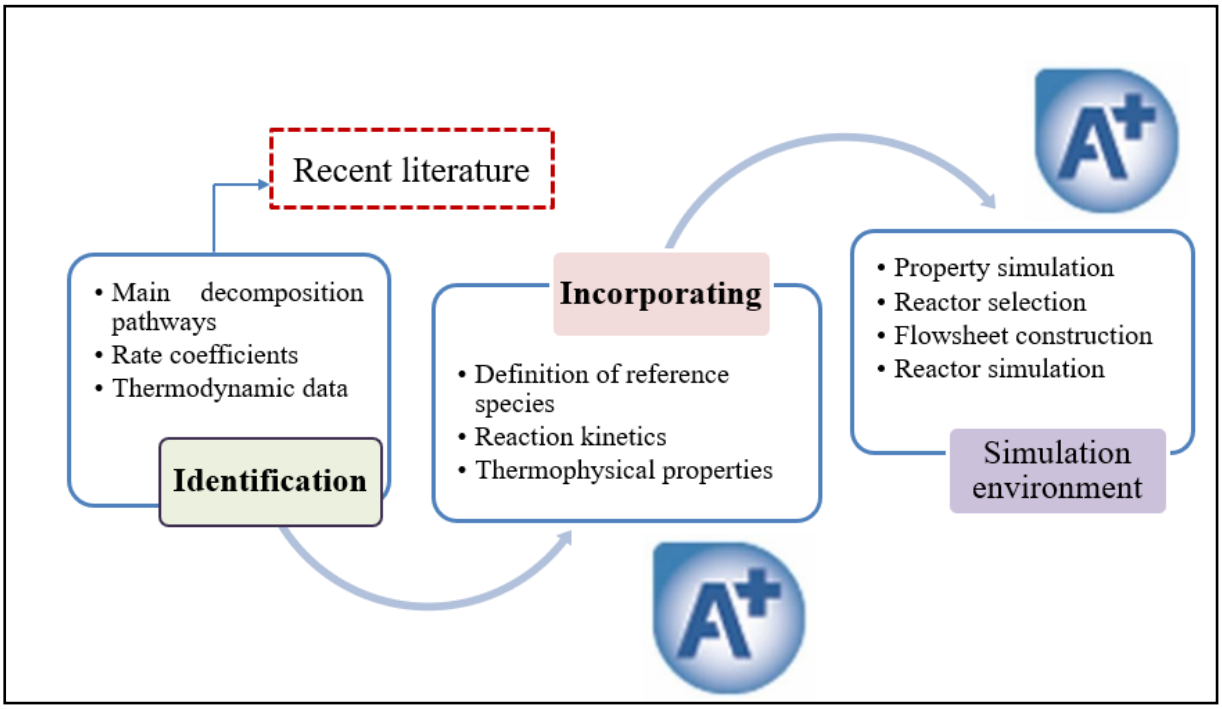

Figure 7. Schematic representation of developing pyrolysis kinetic model and process construction.

3.1.2 Modelling combustion chemistry

Optimizing engines burning liquid and gaseous fuels through repeated experiments is a routine but rather expensive and time-consuming process. Predictive numerical simulations with realistic chemistry are a promising option for reducing overall costs, especially if detailed mechanisms can be drastically reduced without significantly affecting the accuracy. Besides, the chemical kinetic model helps in understanding how intermediates are formed and consumed

in an oxidative environment which apparently helps in understanding the overall reactivity. Thus, this chapter describes how detailed chemistry for an oxidative environment is modeled as a predictive tool for mimicking an idealized combustion system chemistry so that the effect of molecular structure on combustion and emissions can be understood. Before proceeding to the kinetic modeling part, it is important to understand how a certain component is consumed and produced in a kinetically favorable process.

Many processes in an engine, including flame zone reactions that determine heat release, reactions controlling ignition, and air pollutant formation mechanisms, occur during rapid changes in temperature and pressure. These non-equilibrium processes depend on the rate of each individual chemical reaction (i.e., reaction kinetics), which is controlled by reaction temperature and reactant concentrations. The rate at which reactant species are consumed and product species are produced in a kinetically controlled process is governed by the law of mass action, which states that the rate of any chemical reaction is proportional to the product of the mass of the reacting species.

Therefore, for a given elementary chemical reaction, the rate at which reactants are consumed is proportional to the product concentration of each reactant to the power of its stoichiometric coefficient as shown in Equations (7) and (8).

$$aA + bB = cC + dD \tag{7}$$

$$-\frac{dA}{dt} = k_f[A]^a[B]^b \tag{8}$$

The rate constant (k) can be described in terms of the modified Arrhenius equation as shown in Equation (9). Where, A; is the pre-exponential factor, Ea; the activation energy, n; a constant representing the temperature dependence, T; the temperature and R; is the gas constant.

$$k = AT^n \exp\left(\frac{Ea}{RT}\right) \tag{9}$$

Understanding the conversion of reactants into products at the molecular level through a series of elementary reactions that can accurately describe the rate of energy release, ignition behavior, cold flame characteristics, pollutants and soot formations in the combustion of a given fuel through detailed chemical kinetic mechanisms involves the transfer of mass, energy, and momentum [300-302]. Thus, differential equations describing the mass, momentum,

energy, and species concentration in a chemical reaction are numerically integrated into the mechanism to generate concentration profiles for reactants, intermediates, and products [137]. The chemical kinetic mechanism couples chemical species concentrations with the energy equation via the enthalpy of the reaction [53].

Chemically reacting flow problems are mathematically formulated using equations for conservation of mass, momentum, energy, and concentration of chemical species, along with thermodynamic relationships [302-304]. The fundamental conservation equations governing the transfer of mass, energy, momentum and species in chemically reacting systems are provided as follows.

In a steady-state process, the rate at which mass enters the differential element is equal to the rate at which it leaves the element. The conservation of mass is expressed mathematically using the continuity equation, as shown in Equation (10).

$$\frac{\partial \rho}{\partial t} + \nabla.(\rho \bar{v}) \tag{10}$$

Where, ρ; stands for fluid density, $\bar{v}$; velocity vector, t; is time, and ∇; divergence operator.

The equation indicates the sum of the rate of change of mass in a differential element and the net mass flow in and out of that differential element is equal to zero as shown in Equation (11).

$$(\frac{\partial \rho}{\partial t}) + \nabla(\rho V) = 0 \tag{11}$$

States that the sum of the change in momentum with respect to time in a differential element and the contribution of convection on momentum ($\rho \bar{V}.\nabla \bar{v}$) is equal to the contribution of viscous stress on momentum ($\nabla.\bar{\bar{\tau}}$) minus pressure contribution on momentum plus the contribution of gravitational force on momentum ($\rho \bar{g}$). Mathematically, momentum conservation is shown below in Equation (12).

$$\rho \frac{\partial \bar{v} \partial t}{\partial t} \rho \bar{v}.\nabla \bar{v} = f_{surface} + f_{body} = \nabla \bar{\bar{\tau}} - \nabla p + \rho \bar{g} \tag{12}$$

Where ρ stands for fluid density; $\bar{v}$ for velocity vector; t for time; p for pressure representing a surface force $f_{surface}$; $\bar{\bar{\tau}}$ for stress tensor; and $\bar{g}$ for gravitational force representing body force, f_{body}.

In chemically reactive flow systems containing multi-component gas mixtures, the conservation of individual species is very important, and the mass fraction of individual species in the reaction component mixture can be expressed as shown in Equations (13) and (14).

$$Y_i = \frac{\rho_i}{\rho} \tag{13}$$

Where Y_i is mass fraction of ith species; ρ is total fluid density; ρ_i is the density of the ith species

$$\mathrm{P}\frac{\partial Y_i}{\partial t} + \rho\bar{v}.\nabla Y_i = \acute{\omega}_i W_i - \nabla J_i \tag{14}$$

Where ρ stands for fluid density; $\bar{v}$ for velocity vector; $\bar{J}_i$ for diffusive mass flux vector for ith species; $\acute{\omega}_i$ for the net molar production rate of ith species, and W_i for the molecular weight of the ith species.

Processes including chemical reaction, convection and molecular diffusion for instance, in a chemically reacting flow are affected by the temperature distribution in the system. The thermal energy equation shown in Equation (15) is derived from the first law of thermodynamics assuming an ideal gas and a low Mach number, and Fourier's law of heat conduction.

$$PC_p \frac{\partial T}{\partial t} + \rho C_p \bar{v}_i.\nabla = \nabla.(\lambda\nabla\mathrm{T}) - \rho\sum_{i=1}^{I} C_{p,i} Y_i \bar{v}_i.\nabla\mathrm{T} - \sum_{i=1}^{I} h_i \acute{\omega}_i W_i q_{rad} \tag{15}$$

Where $\mathrm{C_p}$ is heat capacity at a constant pressure of the ith species; λ is the thermal conductivity; $\mathrm{h_k}$ is enthalpy formation of ith species; and $\mathrm{q_{rad}}$ is the radiative heat transfer.

In a combustion system, ideal combustion occurs when an equilibrium is reached between the fuel and oxidant, allowing the complete conversion of the reactants to carbon dioxide (CO_2) and water (H_2O). Complete combustion is preferable as it results in maximum energy from the available fuel. However, in real-life combustion systems, this is not possible due to heat loss. So, when there is a balanced mixture of fuel and air in an ideal combustion system, the mixture is called stoichiometric composition. Commonly, the concentration of fuel and oxidizer can be related to the term called Equivalence ratio (φ). φ, is defined as the ratio of fuel-to-oxidizer in a mixture to the ratio of fuel-to-oxidizer at stoichiometric condition, as described in Equation (16).

$$\varphi = \frac{\left(\frac{fuel}{O_2}\right)mixt}{\left(\frac{fuel}{O_2}\right)stoich} \tag{16}$$

If the mixture contains an excess of oxygen, the mixture is called fuel-lean and φ<1. Similarly, if $\varphi = 1$, the mixture is in stoichiometric condition (i.e., a balance between fuel and air). Lastly, a mixture is called fuel-rich if it contains excess fuel and, in this case, φ>1.

Considering complete combustion, the general combustion equation is shown in Equation (17).

$$C_xH_yO_z + O_2 \rightarrow CO_2 + H_2O \quad (17)$$

The conversion of a fuel and oxidizer to carbon dioxide and water does not occur in one single reaction step. Instead, there can be hundreds or even thousands of reactions involved, where intermediate species are produced and consumed. Some of these species are called radicals which are highly reactive and play a central role in the combustion processes. Reactions that produce radicals from stable species are called chain initiation reactions, the radicals involved can proceed to react with other stable species resulting in one or two new radicals through reactions called chain propagation and chain branching, respectively. On the other hand, if the reacting free radical generates stable species, the reaction is called a chain-terminating reaction. Overall, the abstraction of H-atom in all these reactions occurs via different radicals such as hydrogen atom (H), hydroxyl radical (OH), oxygen (O, O_2), hydroperoxyl radical (HO_2), methyl radical (CH_3), formyl radical (HCO), etc.

3.1.3 Detailed kinetic modelling for gaseous phase

Following the solid phase kinetic study described earlier, the next step of the present study is devoted to the detailed kinetic modeling of light oxygenates obtained from biomass pyrolysis in the gaseous phase. In view of the procedures followed, the methodological section applied for developing the kinetic mechanisms for the gases phase accommodates the detailed description of the procedure implemented for the generation of a detailed kinetic mechanism; which are either by merging the existing models or using a dedicated algorithm for the selection of reactions and estimation of the corresponding coefficients.

In this methodology, the model update procedure was first devoted to the identification of reactions responsible for the combustion of the given fuel component followed by the collection of their rate coefficients from the literature. The existing detailed kinetic mechanism developed at the University of Bologna (KiBo) was used as a seed mechanism for C_0-C_3 chemistry, because of its high accuracy in predicting the chemistry of short-chain hydrocarbons [305]. As the existing mechanism only accounted for light hydrocarbons, it was updated to

include the chemistry of oxygenated species such as; formic acid, methanol, ethanol, acetic acid and acetaldehyde. All the reactions corresponding to these components' combustion have been newly added following the hierarchal nature of combustion mechanisms. Primarily, the rate coefficients of these reactions were taken from experimental data reported in the recent literature and/or high-level quantum chemistry calculations, when available. Alternatively, rate coefficients obtained by correlations and estimation procedures (e.g., reaction family approach) were also considered. For the species added during the implementation of the described procedure, thermodynamic data were taken from the following databases; PrimaryThermoLibrary [306], DFT_QCI_thermo [307], CHO [308], CBS_QB3_1dHR [309] generated through *ab initio* calculations at a high level of theory. The listing of the thermodynamic library was based on the accuracy of the methodology involved. The final kinetic mechanism is named as KiBo_MU (i.e., manually upgraded mechanism). The procedures followed for constructing the mechanism have been schematically shown in Fig.8.

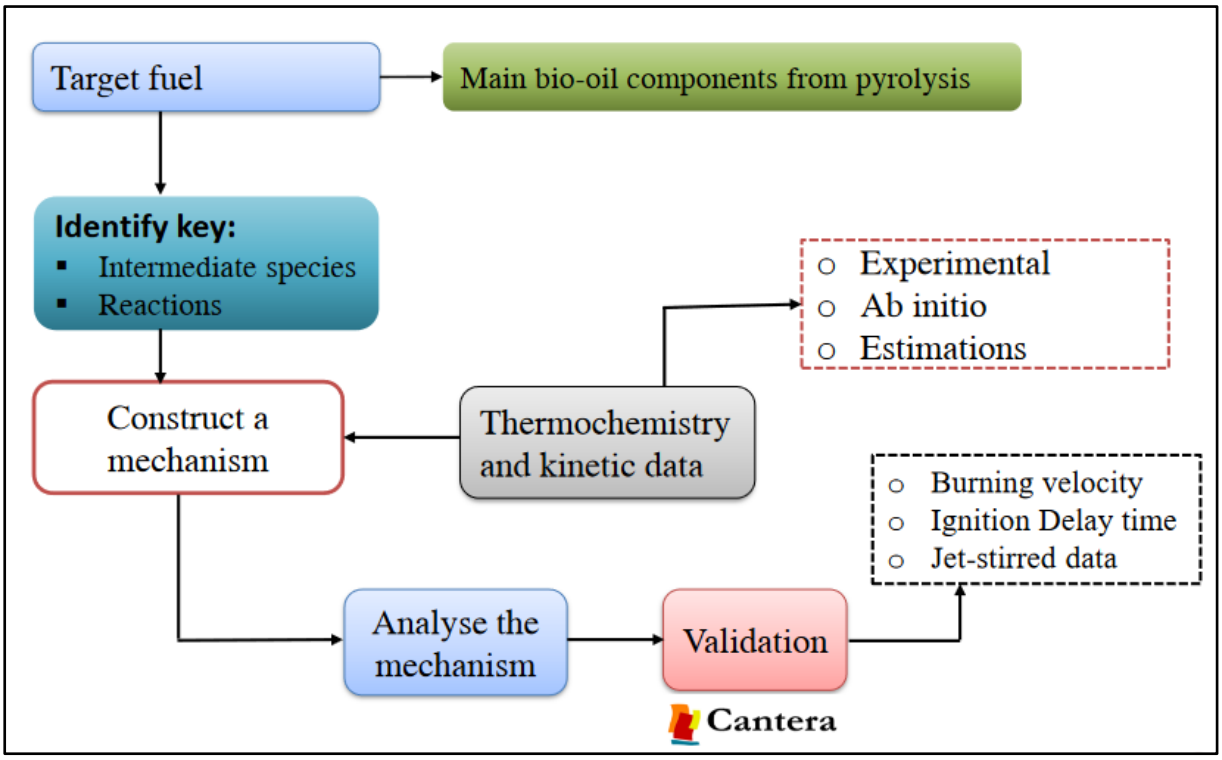

Figure 8. Schematic representation of developing the lumped kinetic model

The second methodology (i.e., the automated generation of a new detailed kinetic mechanism) was devoted to developing a new detailed kinetic mechanism with the help of the Reaction Mechanism Generator (RMG). RMG is an open-source rate-based automatic kinetic

mechanism generation software [310-312], which uses a known chemistry knowledge database stored in it for generating detailed chemical kinetic mechanisms. A detailed kinetic mechanism has been developed for formic acid, acetic acid and acetaldehyde. The construction of the mechanism begins by specifying initial conditions, such as temperature, and pressure, define fuel representations (i.e., 'adjacency lists or smiles notation), fuel composition, kinetic and thermodynamic libraries, and termination criteria. Then, an iterative procedure using a rate-based algorithm is used to select species and reactions to add to the generating core mechanism until termination criteria (e.g., time or conversion for a given reactant) are met [313]. RMG uses a functional group-based approach to deal with species and reactions [311]. In this approach, the tool uses reaction families to define the templates that manipulate matching functional groups in converting molecules from reactants to products.

During the mechanism generation course, the core and edge mechanisms are generated. Species were allocated in the appropriate mechanism according to their net rate of production and the defined tolerance criteria: *Move to Core* (= 0.012); *Keep in Edge* (= 0.01); *Interrupt Simulation* (= 0.02). Once the simulations converge, the resulting core mechanisms can be refined by identifying the most influential species and reactions through a so-called sensitivity analysis, followed by additional iterations in the RMG using the updated library. The reaction conditions used to generate the mechanism were temperature 650 – 2000 K, pressure 1 – 100 bar and stoichiometric composition of an equimolar mixture of acetaldehyde and acetic acid. The same conditions were applied for generating a detailed kinetic mechanism for formic acid. RMG considers several reaction families (e.g., hydrogen abstraction, β-cleavage, bond dissociation) in generating kinetic mechanisms. The required thermodynamic data were orderly taken from PrimaryThermoLibrary [306], DFT_QCI_thermo [307], thermo_DFT_CCSDTF12_BAC [314], CBS_QB3_1dHR [309], CHO [308], FFCM1(-) [315] whereas, BurkeH2O2inN2 [316] was the source for the kinetic data. In addition, Klippenstein_Glarborg2016 [223] and C2H4+O_Klipp2017 [317] were used as seed mechanisms. In all cases, sources were prioritized in the presented order, based on the accuracy of the theory of the quantum chemistry calculation involved. However, if thermochemical data for species do not exist in a given library, RMG estimates them using group additivity [318, 319], while the missing rate coefficients are estimated using a suitable database with known rate rules and reaction templates [311]. Nevertheless, these methods cannot accurately estimate oxygenated species data [320], suggesting the need to use more robust theories, such as ab initio calculations.

Quantum mechanical calculations are the most trusted thermochemistry calculation methods for species whose thermodynamic and kinetic data have not been reported experimentally. They use various mathematical transformations and approximation techniques to find optimal molecular geometry, vibrational frequencies and bond energies [321]. The mechanism generated is name as KiBo_AG (i.e., automatically generated mechanism). For better illustration of the procedures followed in generating the mechanism, the process followed has been schematically shown in Fig. 9.

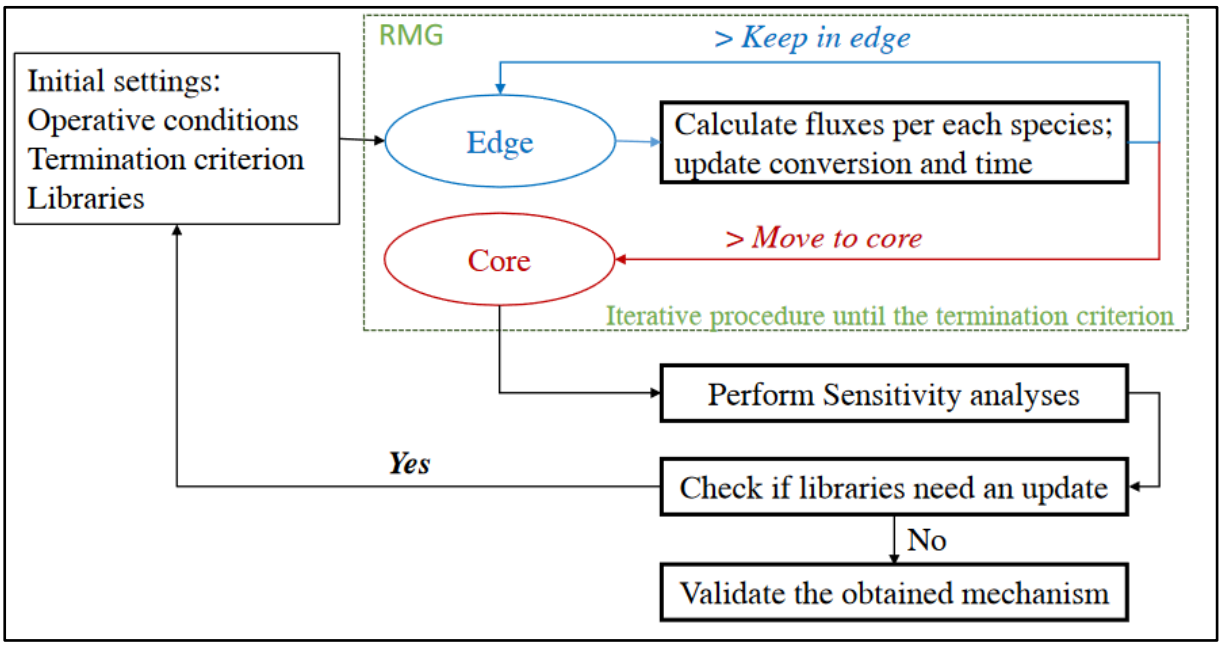

Figure 9. Schematic representation of the procedure adopted for developing the detailed chemical kinetic mechanism using RMG [322].

3.2 Mechanism Evaluation

The solid phase kinetic mechanism (i.e., pyrolysis kinetic mechanism) has been evaluated by its accuracy to predict pyrolysis product distributions, considering ranges of reaction conditions, number of biomass feedstocks, and a fraction of cellulose, hemicellulose and lignin in the feed. For the detailed gases phase mechanisms, particularly for the KiBo_MU, its accuracy has been evaluated by its ability to capture the combustion data (e.g., laminar burning velocity, ignition delay time, and species profile concentration) under engine-relevant conditions over wide ranges of reaction conditions. In case of large deviation between numerical and experimental data, a sensitivity analysis was performed at the particular conditions where the variations were observed. Furthermore, for the detailed RMG-generated kinetic mechanism (i.e., KiBo_AG), it is difficult to implement all species included in the

detailed mechanism due to the computational cost associated with this method. Hence, stepwise evaluation of the mechanisms has been performed by Flux Diagram and Sensitivity analysis at a wide range of reaction conditions (i.e., 650 K – 1250 K, atmospheric pressure and equimolar composition (i.e., in the case of acetaldehyde and acetic acid) after each model generation. The final mechanism used for the study is the one obtained after the 3rd iteration. Within these iterations, the thermodynamic data of the sensitive species were calculated when needed based on the electronic structures provided in the literature [323]. In this case, high-level *ab initio* quantum chemistry calculations were carried out for the important intermediate species. The B3LYP/6-311++G(d,p) method has been used as a basis set for optimizing molecular structures. Once a possible geometry has been determined, energies associated with each possible rotor scan have been calculated by applying an 8° rotation per simulation until the rotation is completed. Frequency calculations have been performed at the same level to obtain zero-point energy (ZPE) and determine whether each point is a local minimum or transition state (TS). Based on the electronic structure and related energies, the required thermodynamic properties were calculated by using the Gaussian 09 program [324] and the Automated Rate Calculator (ARC) [325]. The gathered properties were collected in newly generated libraries, namely OxyLibrary_1 and OxyLibrary_2, to be used for the second and third iterations, respectively. A summary of the input databases used for mechanism generation is provided in Table 6.

Table 6. Summary of input databases considered for the generation of the detailed mechanism.

Iteration	Kinetic library	Thermo library	Seed Mechanisms
I	BurkeH2O2inN2	PrimaryThermoLibrary, DFT_QCI_thermo, thermo_DFT_CCSDTF12_BAC, CBS_QB3_1dHR, CHO, FFCM1(-)	Klippenstein_Glarborg2016, C_2H_4+O_Klipp2017
II	BurkeH2O2inN2	PrimaryThermoLibrary, DFT_QCI_thermo, thermo_DFT_CCSDTF12_BAC, CBS_QB3_1dHR, CHO, FFCM1(-), OxyLibrary_1	Klippenstein_Glarborg2016, C_2H_4+O_Klipp2017
III	BurkeH2O2inN2	PrimaryThermoLibrary, DFT_QCI_thermo, thermo_DFT_CCSDTF12_BAC, CBS_QB3_1dHR, CHO, FFCM1(-), OxyLibrary_1, OxyLibrary_2	Klippenstein_Glarborg2016, C_2H_4+O_Klipp2017

3.2.1 Sensitivity analysis

Sensitivity analysis is a useful tool for the evaluation of kinetic models, as it shows the most impacting parameters in the model under given conditions. Hence, possible reasons for deviations from actual behaviour can be inferred and solved thanks to this approach. Besides, it is another way of reducing the size of the mechanism by ignoring the less important branches. The sensitivity coefficients associated with each entry of the kinetic mechanism can be defined as shown in Equation (18).

$$Si = \partial lnY_i \frac{\partial lnY_i}{\partial ln\alpha_i} = \frac{\alpha_i}{Y_i}\frac{\delta Y_i}{\delta \alpha_i} \quad (18)$$

Where, α_i represents the pre-exponential factor A in the Arrhenius expression, and Y_i the specific parameter of interest, such as the laminar burning velocity or species concentration. A reaction associated with a high degree of sensitivity indicates that the solution will be more strongly affected by changes in its rate constant, compared to reactions with low sensitivity.

3.3 Mechanism validation

Considering the nature of the processes for which the mechanisms were aimed, validation of kinetic models is described as discussed below.

3.3.1 Simulation of the pyrolysis process

The pyrolysis kinetic model produced in this work is tested using Aspen plus to simulate the biomass pyrolysis process and evaluate pyrolysis product distributions (i.e., bio-oil, gas and char). Aspen Plus is a process-oriented software that facilitates the calculation of physical, chemical, and biological parameters [326]. In the Aspen Plus, biomass was set as an unconventional component with the global simulation stream class set to be MIXCINC (i.e., comprising both conventional and non-conventional solids). Empirical correlations of coal enthalpy and density methods were used as described in the current literature [327] to calculate the enthalpy and density of the unconventional component. A decomposition reaction is implemented in Aspen Plus using an RYield-type reactor for converting biomass into conventional components (i.e., cellulose, hemicellulose, lignin, and ash). In the simulation, $(C_6H_{10}O_5)n$ and $(C_5H_8O_4)n$ represent cellulose and hemicellulose [327, 328], respectively, whereas LIG-C $(C_{15}H_4O_4)n$, LIG-H $(C_{22}H_{28}O_9)n$ and LIG-O $(C_{20}H_{22}O_{10})n$ represents lignin

components [170]. The thermophysical properties of the components involved in the present study were adopted from the detailed study reported by Gorensek et al. [329]. The ideal gas heat capacity, ideal gas heat of formation and critical properties were estimated from the Aly-Lee equation [330] whereas, vapor pressure is obtained based on Pitzer vapor pressure correlation fitted to the Aspen Plus PLXANT extended Antonie model [331]. Peng-Robinson's cubic equation of state with Boston−Mathias alpha function [332] was selected as a thermodynamic property method. This method, represented in Aspen Plus [333] as the PR-BM method and is the most commonly used property method in gas processing, refining, petrochemicals and biomass pyrolysis applications [296, 298, 334]. Aspen Plus performs material and energy balance based on the product distribution and the specified heat of the reaction of the components involved [335]. The simulation process involves two main parts; the first part is termed property simulation, which involves defining all species and incorporating their thermophysical properties in the Aspen Plus tool followed by running the properties. Once the property simulation is successful, the second part is called setting the simulation environment, which involves selection of reactor configuration and construction of process flow sheets (i.e., connecting different block units). This section involves, incorporation of reaction mechanisms, defining of the streams and setting reaction conditions (i.e., temperature, pressure, composition).

For the sake of representation, experimental results from Drop Tube Reactor (DTR) are considered for validation and presented here. Understanding fast pyrolysis in DTR for scale-up is then reported to be a challenge, requiring careful examination of specific rate-determining steps and addressing the question of whether the heat transfer mechanism is efficient and whether the residence time of the two phases is sufficient. This needs to be reported along with the biomass properties and their sub-components. In this regard, different biomass components having different fractions of cellulose, hemicellulose and lignin have been considered for validation. A plug flow reactor (RPLUG) was chosen from reactor models present in the Aspen Plus simulation environment to simulate the pyrolysis process. Because the radius of the DTR reactor is much smaller than the length the change in concentration and temperature of both the solid and the vapor phases in the radial direction is very small as compared to the axial direction. The kinetic reaction scheme was implemented as a power-law type kinetic expression, and the reaction rate was calculated in Aspen plus following the Arrhenius-like equation expressing the rate of reaction r as a function of the pre-exponential factor k, the

absolute temperature *T*, the temperature exponent n, the activation energy *Ea*, and the gas law constant *R*. Schematic representation of the simulation process has been shown in Figure 10.

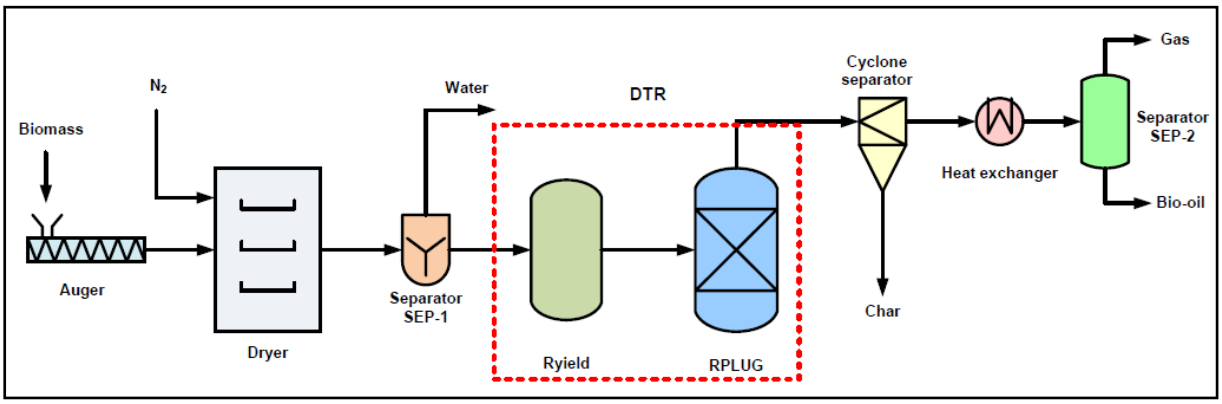

Figure 10. Schematic process model adopted for fast pyrolysis in a drop tube reactor.

The process starts with the feeding of the biomass. After the biomass is fed from the auger feeder, the particle starts to travel in the feeding tube leading to the heated zone. The particles get dried further leaving moisture which is reflected in the Dryer where the model removes the water content from the biomass. This was done as the biomass heats up above 100 ^{O}C. Then, the moisture is removed in the separator (SEP-1). A yield reactor (RYIELD) is used to convert the biomass into its polymeric components of cellulose, hemicellulose, lignin, and other extractives, and that led to a DTR reactor modeled as an RPLUG at pyrolysis temperature of 450 – 550 ^{O}C. The main pyrolysis process took place in the RPLUG producing pyrolyzed products (both condensable and non-condensable vapors) and char. A cyclone separator is used to separate the char from the vapors. The vapors pass through a heat exchanger that reduces the temperature of vapors below the boiling point of the condensable gases to change their phase and become liquid and non-condensable gases. Finally, condensed vapors (i.e., bio-oils) and non-condensable gases such as CO, CO_2, CH_4, H_2, etc. are separated in a separator (SEP-2). Product yields (i.e., bio-oil, gas and char) obtained from the simulation have been compared with the experimental results reported in the literature. Details of the yield distributions are presented in Chapter 4 of this thesis.

3.3.2 Validation of detailed kinetic mechanisms

Detailed combustion kinetic mechanisms developed in the present study have been validated against experimental combustion data available in the literature. To neglect chemical phenomena from turbulent and physical aspects, premixed and laminar flames are preferred in these studies. For this purpose, a characterization of the flame structure or a measurement of the overall reactivity can be carried out. Depending on the selected conditions, the total reactivity can be expressed in terms of laminar burn velocity (S_u) or ignition delay time (IDT). S_u is a representative of the low temperature chemistry [336], while IDT is suitable parameter for the evaluation of the oxidation phenomena occurring at intermediate and high temperature conditions [337].

All the simulations were performed using an open-source Cantera suite [338] with appropriate reactor modules using a transient condition as a first-attempt solution for the steady-state conditions. The following simulation criteria were used for solving steady-state problems (ss) and transient-state (ts) problems: absolute tolerance_ss = 1.0×10^{-8}, relative tolerance_ss 1.0×10^{-15}, absolute tolerance_ts = 1.0×10^{-4}, relative tolerance_ts 1.0×10^{-13}. An adaptive grid was determined by using the following criteria: maximum acceptable ratio among adjacent solutions (ratio) equal to 3, maximum first derivative for adjacent solutions (slope) equal to 0.06, and maximum acceptable second derivative for adjacent solutions (curve) equal to 0.12. Soret effect and multicomponent transport model were neglected, at first, to generate a first-guess result and subsequently accounted for the final solution. The laminar burning velocity was modelled using the premix flame code (PREMIX) [339]. The mixed average formula is used to calculate the multicomponent diffusion coefficient. Conservation equations as reported here [339, 340] with appropriate boundary conditions are discretized with non-uniform grid spacing. In the simulation of IDT, Cantera integrates the time-dependent governing equations for a network of reactors connected by various means, e.g. wall, mass flow reactor, valve, or pressure controllers. The inputs to each simulation include a detailed chemical kinetic reaction mechanism, a dataset of thermochemical properties, and a dataset of transport properties. These input files are available as supplemental material to the journal publication of this study. Comparison between the experimental and simulation results of laminar burning velocity and ignition delay times by the investigated kinetic mechanisms at different reaction conditions were performed, based on the availability of experimental data from the current literature.

Details of simulation results and its comparison with literature data are discussed in detail in Chapter 4 of the thesis.

Table 7. Kinetic mechanisms applied in the present study

No	Mechanisms	No. of species	No. of reactions	Ref.
1	Glarborg et al.	27	75	[239]
2	Aramco1.3	305	1761	[99]
3	CRECK	299	8028	[341]
4	Konnov	89	1419	[342]
5	Li et al.	21	93	[181]
6	San Diego	58	270	[343]
7	Dryer	55	290	[91]
8	Zhang	32	197	[190]
9	Marinov	58	383	[95]
10	KiBo_MU	142	440	Current work
11	KiBo_AG	90	1047	Current work
12	KiBo_AG	541	27282	Current work

For acetic acid, there is only laminar burning velocity data available, no intermediate and /or high-temperature data (IDT) available in the literature. Thus, only laminar burning velocity has been considered for validation. Fuel mixtures, reaction conditions and experimental sources of laminar burning velocity, species profile and ignition delay time considered for validating the models has been summarized and shown in Table 8 – 10, respectively. The operative conditions to conduct the numerical analysis were selected following the presented data to mimic the experimental database.

Table 8. Sources of experimental data of laminar burning velocity considered for validation.

Species	Diluent	Pressure (atm)	Temperature (K)	Equivalence ratio	Reference
HCOOH	Ar/N_2/air	1	368 – 453	0.5 – 1.6	[99, 232, 240, 344]
HCOOH/CH_4	Air	1	353	0.8 – 1.3	[345]
CH_3OH	Air	1	298 – 358	0.7 – 1.5	[45, 189, 193]
CH_3COOH	Air	1	338 – 348	0.7 – 1.4	[78]
C_2H_5OH	Air	1	298 – 358	0.65 – 1.55	[45, 55]
CH_3CHO	Air	1	298 – 338	0.7 – 1.6	[263]

Table 9. Sources of experimental data of jet-stirred reactor data considered for validation

Species	Diluent	Residence time (s)	Pressure (atm)	Temperature (K)	Equivalence ratio	Reference
HCOOH	Ar	2	1	500 – 1100	0.5 – 2.0	[346]

Table 10. Sources of experimental data of Ignition delay times data considered for validation.

Species	Diluent	Pressure (atm)	Temperature (K)	Equivalence ratio	Reference
CH_3OH	Ar	1.1 – 14	941 – 1763	0.5 – 2.0	[54, 180, 187]
C_2H_5OH	Ar	1 – 13.5	944 – 1589	0.5 – 2.0	[54, 214]
CH_3CHO	Ar	1.5 – 4.0	1276 – 1703	0.5 – 2.0	[255, 275]

Chapter 4: Results and Discussion

This section comprises the main findings from the present study, where the majority of the results have been published in peer-reviewed journals. A more detailed discussion of the results can be found in the authors' publications.

The main outcome of the current work can be intended as a validated and comprehensive kinetic mechanism accounting for heterogeneous as well as homogeneous reactions relevant to energy production from bio-resources. More specifically, the kinetics mechanisms developed in this study have been used to simulate their respective intended chemical processes (i.e., pyrolysis kinetics for biomass pyrolysis processes and detailed kinetics for combustion parameters) available in the current literature. To this aim, different combustion parameters have been selected and investigated for each target fuel component based on the availability of experimental data in the literature. Overall, simulations were performed under various reaction conditions including low, intermediate, and high-temperature combustion chemistries, and the results were compared with experimental data as well as with other well-validated kinetic models available in the literature. Due to the different mechanistic goals, the validation part is described as mechanism validation for solid-phase reaction (i.e., pyrolysis) and gas-phase reaction (i.e., combustion).

4.1 Validation for Pyrolysis Kinetic Mechanism

The set of 20 reactions selected as representative of the fast pyrolysis is shown in Table 11. At this stage, the main scope of the model was mimicking the behaviour of solid substances at different temperatures and conditions relevant to the investigated processes in terms of thermal and product distributions. The kinetic mechanism produced in this work can be intended as the sum of three sub-mechanisms, accounting for CELL, HCE, and lignin (LIG-O, LIG-H, LIG-C) decompositions. More particularly, two reactions in parallels were assumed for direct degradation of CELL leading to complete conversion, and one producing an activated intermediate species referred to as CELLA which further transformed in a set of incompletely oxidized species. In the same way, a reaction is assumed for the conversion of HCE to produce hemicellulose intermediate species known as HCE1 and HCE2, which are then further reacted to form pyrolysis end products (i.e., liquid, gas and char). In the end, lignin monomers decompose independently to produce different intermediates including respective lignin intermediates from lignin monomers (LIGOH, LIGCC, LIG) and pyrolysis end products,

followed by subsequent reactions resulting in the complete conversion of the intermediates to light oxygenates, phenolic intermediates, gases, water and char.

Table 11. Selected reactions representative of biomass pyrolysis and the corresponding kinetic parameters available in the current literature [145, 299]. Nomenclature is considered following the definition provided by Gorensek et al. [329]. Units, T (K)

#	Pyrolysis reactions	A [s^{-1}]	n	Ea/T
	Cellulose			
1	CELL → CELLA	4.10^{13}	0	22647.2
2	CELLA → 0.8 HAA + 0.2 GLYOX + 0.1 CH_3CHO + 0.25 HMFU + 0.3 C_3H_6O + 0.21 CO_2 + 0.1 H_2 + 0.4 CH_2O + 0.16 CO + 0.83 H_2O + 0.02 HCOOH + 0.61 Char	5.10^{8}	0	14594.8
3	CELLA → LVG	$1.8.10^{0}$	1	5032.7
4	CELL → 5 H_2O + 6 Char	4.10^{7}	1	19627.6
	Hemicellulose			
5	HCE → 0.4 HCE1 + 0.6 HCE2	$3.3.10^{9}$	0	15601.4
6	HCE1 → 0.025 H_2O + 0.775 CO_2 + 0.025 HCOOH + 0.5 CO + 0.8 CH_2O + 0.125 C_2H_5OH + 0.55 CH_3OH + 0.25 C_2H_4 + + 0.125 H_2 + 0.4 COH_2 + 0.325 CH_4 + 0.875 Char	1.10^{9}	0	16104.7
7	HCE1 → 0.25 H_2O + 0.75 CO_2 + 0.05 HCOOH + 0.45 CO + 0.375 C_2H_4 + 1.7 COH_2 + 0.625 CH_4 + 0.675 Char	5.10^{-02}	1	4026.2
8	HCE1 → 0.6 XYLAN + 0.2 $C_3H_6O_2$ + 0.12 GLYOX + 0.2 FURF + 0.4 H_2O + 0.08 H_2 + 0.16 CO	3.10^{0}	1	5536.0
9	HCE2 → 0.2 H_2O + CO + 0.575 CO_2 + 0.4 CH_2O + 0.1 C_2H_5OH + 0.05 HAA + 0.35 ACAC + 0.025 HCOOH + 0.25 CH_4 + 0.3 CH_3OH + 0.225 C_2H_4 + 0.725 H_2 + Char	$5.0.10^{9}$	0	15853.0
	Lignin			
10	LIGC → 0.35 LIGCC + 0.1 COUMARYL + 0.08 PHENOL + 0.41 C_2H_4 + H_2O + 0.3 CH_2O + 0.32 CO + 0.7 COH_2 + 0.495 CH_4 + 5.735 Char	$1.33.10^{1}$	0	24408.7
11	LIGH → LIGOH + C_3H_6O	$6.7.10^{12}$		18872.7
12	LIGO → LIGOH + CO_2	$3.3.10^{8}$	0	12833.4
13	LIGCC → 0.3 COUMARYL + 0.2 PHENOL + 0.35 HAA + 0.7 H_2O + 0.6 C_2H_4 + 0.8 CO + COH_2 + 0.65 CH_4 + 6.75 Char	$1.6.10^{6}$	0	15853.0
14	LIGOH → LIG + 0.15 H_2 + 0.9 H_2O + 0.45 CH_4 + CH_3OH + 0.05 CO_2 + 1.3 CO + 0.05 HCOOH + 0.2 C_2H_4 + 0.6 COH_2 + 4.15 Char	5.10^{7}	0	15098.1
15	LIGOH → 1.5 H_2O + 2.1 CO + 1.75 CH_4 + CH_3OH + 0.5 H2 + 3.9 COH_2 + 0.3 C_2H_4 + 0.5 CH_3OH + 10.15 Char	$3.3.10^{1}$	0	7549.07
16	LIG → 0.7 FE2MARC + 0.3 ANISOLE + 0.6 CO + 0.3 CH_3CHO	4.10^{0}	1	6039.3
17	LIG → 0.95 H_2O + 0.2 CH_2O + 0.4 CH_3OH + 1.45 CO + 0.6 CH_4 + 0.05 HCOOH + 0.5 COH_2 + 0.65 C_2H_4 + 0.2 CH_3CHO + 0.2 C_3H_6O + 5.5 Char	4.10^{8}	0	15098.1
18	LIG → 0.6 H_2O + 0.6 CO + 0.6 CH_4 + 0.4 CH_2O + 0.5 C_2H_4 + 0.4 CH_3OH + 2 COH_2 + 6 Char	$8.3.10^{-02}$	1	4026.2
	Water			
19	H_2O(L) → H_2O(V)	$5.13.10^{6}$	0	10583.8
	Metaplastic			
20	COH_2 → CO + H_2	5.10^{11}	0	35732.3

The pyrolysis mechanism has been used for prediction of pyrolysis products distribution at different pyrolysis temperatures for different feedstocks containing different fraction of cellulose, hemicellulose and lignin. Figure 11 – 13 depicts the yield of bio-oil, gas and char, respectively obtained from different biomasses. The effect of pyrolysis temperature on pyrolysis yield has been evaluated and discussed.

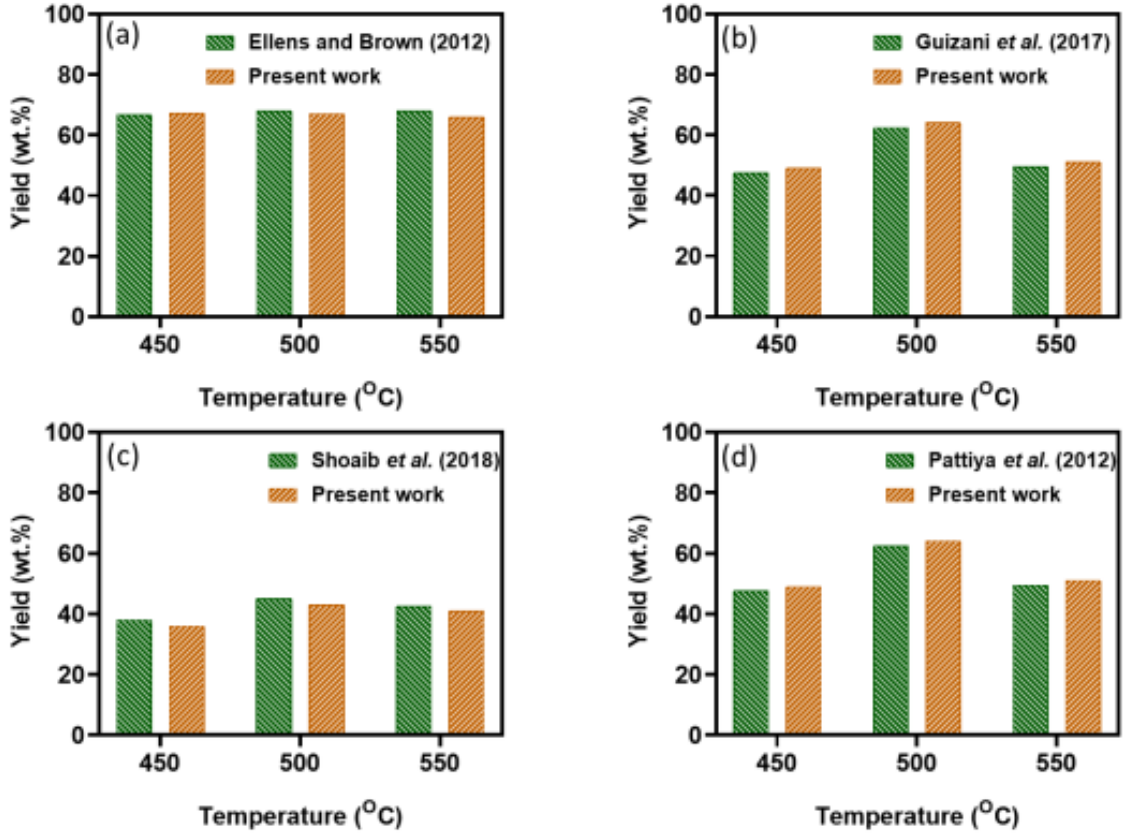

Figure 11. Bio-oil product distribution from different feedstocks; Oak (a), Beechwood (b), Rice straw (c) and Cassava stalk (d).

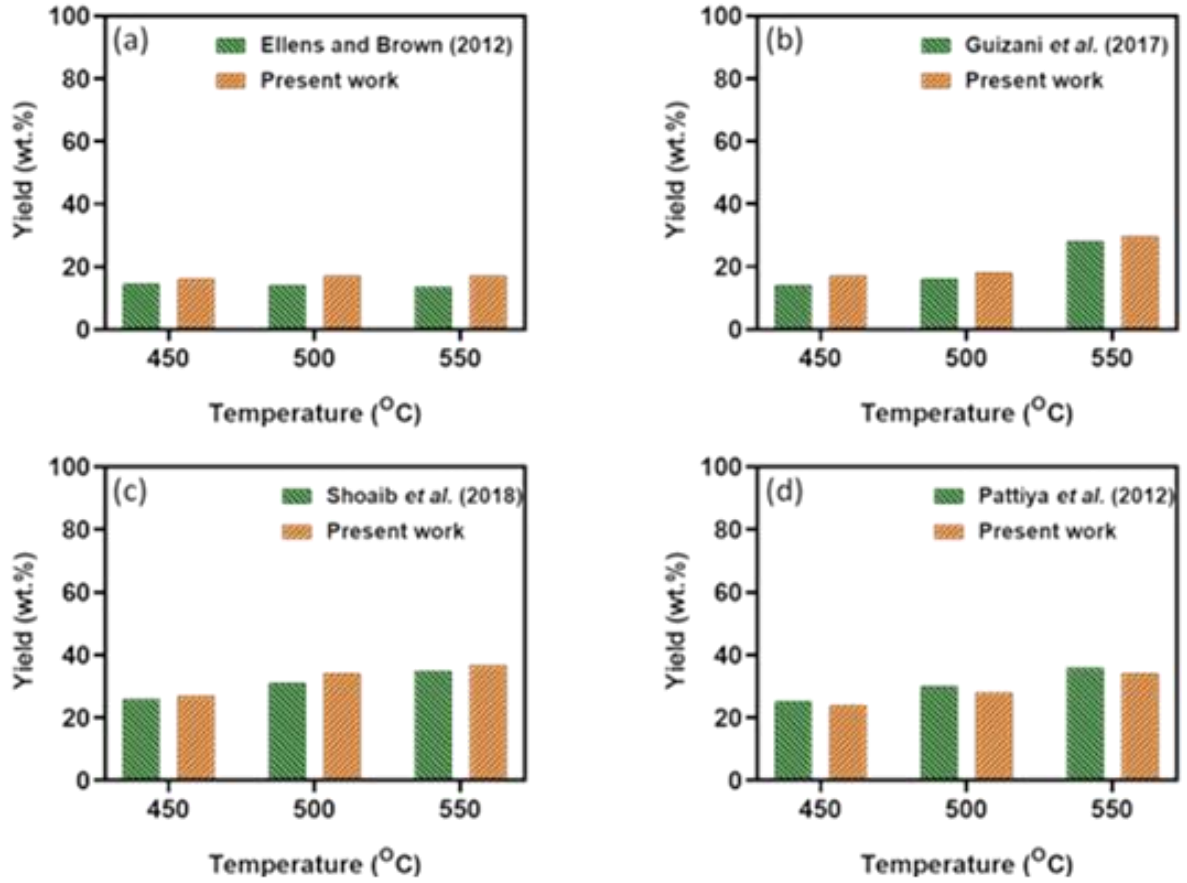

Figure 12. Gas yield distribution from different feedstocks; Oak (a), Beechwood (b), Rice straw (c) and Cassava stalk (d).

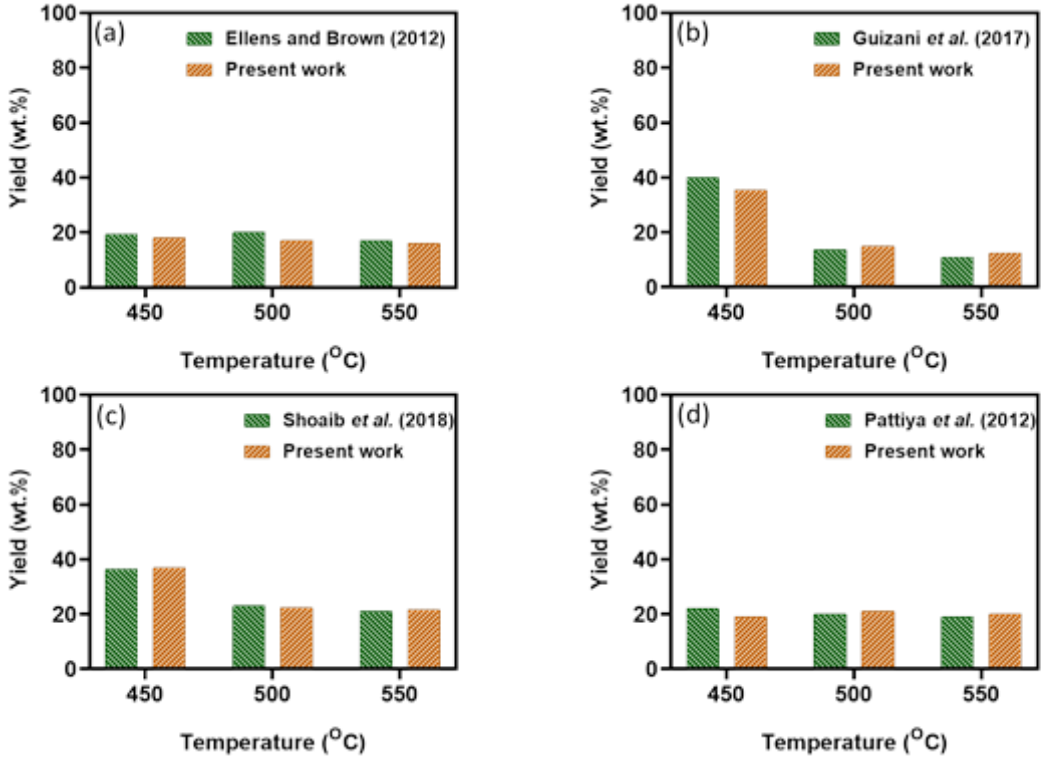

Figure 13. Char yield from different feedstocks; Oak (a), Beechwood (b), Rice straw (c) and Cassava stalk (d).

The yield of bio-oil from Oak, Beechwood, Rice straw and Cassava stalk obtained in the present study is shown in Figure 11(a – d). As can be seen from Figure 11(a) for oak feedstock, the yield of bio-oil shows almost a constant trend under the investigated pyrolysis temperature range. In the same way, from Figure 11(b), the yield of bio-oil obtained from beechwood pyrolysis increased from 49 wt.% to 64 wt.% as temperature increased from 450 to 500 ^{O}C. Further increasing the temperature to 550 ^{O}C decreases the yield of bio-oil. Besides, as shown in Figure 11(c & d) for rice straw and cassava stalk, respectively, the yield of the bio-oil increases with an increase in temperature from 450 – 500 ^{O}C and showed a decreasing trend with further increasing temperature. In all cases, the decrease in bio-oil yield with an increase in temperature is due to the initiation of the secondary reactions, favoring the yield of gas mixtures over liquid products. The difference in bio-oil yield based on feedstocks is attributed to variations in the initial composition of cellulose, hemicellulose and lignin. Overall, for the investigated biomasses, further increasing of temperature to 550 °C didn't favour the yield of liquid components and thus, the optimum pyrolysis temperature is found to be 500 °C.

On the other hand, the yield of gas is shown in Figure 12 (a – d). For all investigated feedstocks, the yield of gases increased with an increase in pyrolysis temperature which is due to the effect of secondary reactions at higher temperatures favoring the formation of gas components. In the same way, the difference in gas yield for all feedstocks is due to the difference in the fraction of cellulose, hemicellulose and lignin in the initial biomass feed. Comparably, rice straw and cassava stalk are found to have a high yield of gas than oak and beechwood, which could be due to the higher ash content in the feedstock. The same conclusion has been drawn by Trendewicz et al. [347].

Furthermore, the yields of char from the pyrolysis of oak, beechwood, rice straw and cassava stalk pyrolysis are depicted in Figure 13 (a – d). As can be seen from the figure, the yield of char decreased with increasing pyrolysis temperature which is associated with the increase in the reactivity of the reacting components favoring the production of liquid and gas products. The relatively high yield of char observed from rice straw could be related to the high ash content in the feed. Overall, the present study is in fair agreement with the pyrolysis yields of experimental results reported in the literature [348-351].

Detailed discussion on distribution of gases and char products from the different feedstocks and the accuracy of the kinetic model on capturing these yields can be found in the paper published by the author as part of this work as shown below.

FM Wako., G Pio., Ashraf L., Azhar U., E Salzano., Nader M., Performance Assessment of Drop Tube Reactor for Biomass Fast Pyrolysis Using Process Simulator, Can. J. Chem. Eng., 2023.

4.1.2 Validation of Detailed Kinetic Mechanisms

The reactivity of gaseous mixtures potentially produced by pyrolysis processes as well as oxidation and decomposition of large species have been investigated by using different approaches for the realization of a detailed kinetic mechanism. Considering the hierarchical nature of the mechanism, merging kinetic mechanisms focusing on specific species representative of commonly produced intermediates has been considered as per the possible procedure. Conversely, a theoretical-based kinetic mechanism developed from scratch has been realized and compared with existing ones. The detailed kinetic mechanisms (i.e., KiBo_MU and KiBo_AG) developed in the present study have been validated against experimental data considering low temperature, intermediate temperature and high-temperature combustions through the evaluation of fundamental combustion parameters, such as laminar burning velocity, species fraction and ignition delay times of methanol, ethanol, formic acid, acetic acid and acetaldehyde based on the availability of experimental data. The parameters and conditions accounted for validation might not be the same for each species. A detailed description of the parameter studied and results for each fuel component are described below.

4.1.2.1 Low-temperature combustion chemistry

The accuracy of the produced kinetic mechanisms at low temperatures has been studied through the evaluation of the laminar burning velocity of the target oxy-biofuels at wide ranges of reaction conditions. Indeed, laminar burning velocity is typically adopted as a standalone parameter for studying the low-temperature combustion phenomena. A detailed discussion of the results is provided below for each component.

4.1.2.1.1 Methanol

The Laminar burning velocity of methanol-air mixtures has been studied using KiBo_MU kinetic model under a wide range of reaction conditions as shown in Figures 14 – 17. For better evaluation of the models and comparison of results, results obtained using KiBo_MU have been compared with results obtained using other widely validated and commonly used

methanol kinetic models from the literature. Figure 14 (a – d) depicts the laminar burning velocity of methanol-air mixtures at an equivalence ratio range of 0.7 – 1.5, temperature range of 298 – 328 K and under atmospheric pressure. As can be seen from the figures, under the studied conditions, the laminar burning velocity obtained in the present study using KiBo_MU is in excellent agreement with the experimental result obtained using the heat flux method by Vancoillie et al. [189]. Regardless of the initial temperatures and kinetic models used, the maximum laminar burning velocity is obtained at an equivalence ratio of 1.1, which is consistent with the experimental results. Comparably, KiBo_MU showed better accuracy than the other investigated models. In the same way, Figure 15 (a – d) shows the laminar burning velocity of methanol-air mixtures at an equivalence ratio range of 0.7 – 1.5, atmospheric pressure and temperature range of 338 – 358 K. The result from the present study was compared with the experimental result obtained using heat flux [189] and counterflow [45] methods. Under the studied conditions, KiBo_MU mimicked the laminar burning velocity fairly and agreed well with the experimental results [45, 189]. However, Li et al and San Diego kinetic models over-predicted the burning velocity for an equivalence ratio of 0.9 and 1.0, whereas showed fair agreement at other conditions. For all the investigated initial temperatures, the maximum burning velocity is obtained at stoichiometric conditions, which agrees with the experimental studies. Overall, KiBo_MU fairly captured laminar burning velocity under a wide range of temperatures and equivalence ratios and showed better accuracy than the other kinetic models.

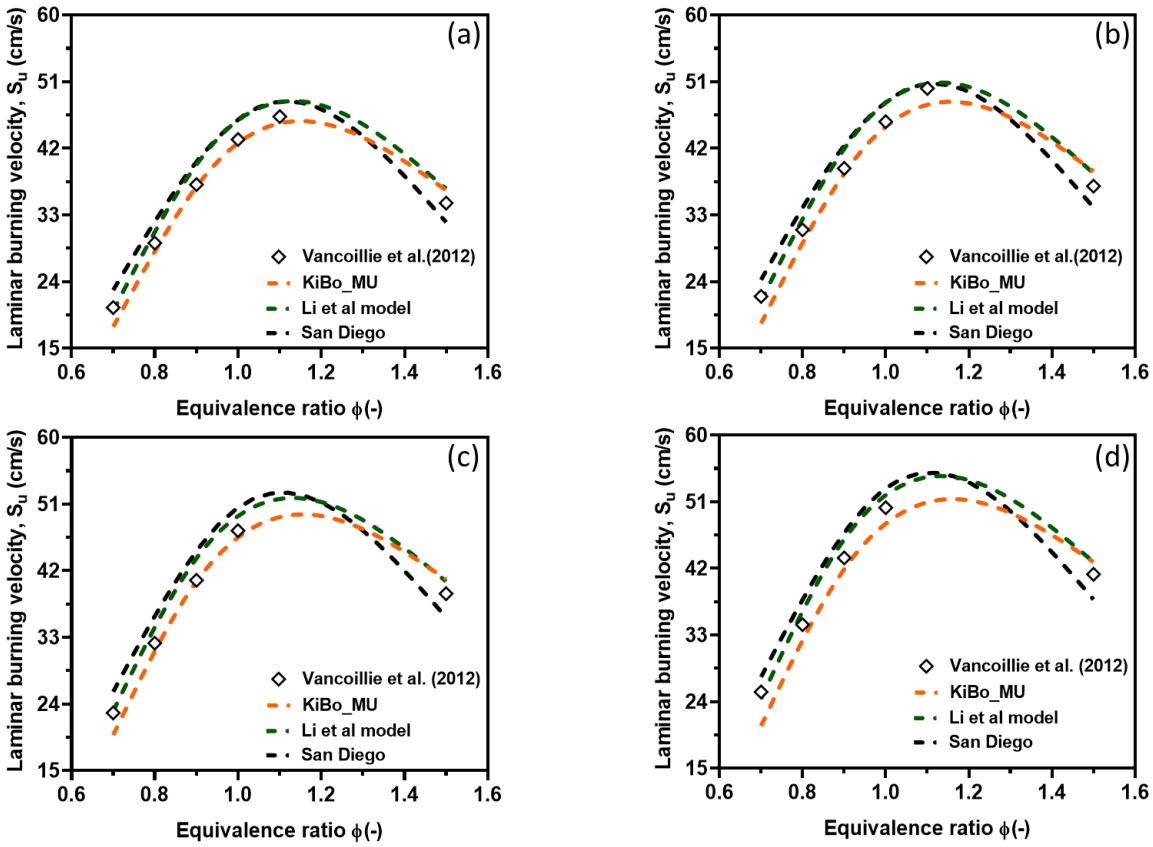

Figure 14. Laminar burning velocity of methanol-air mixtures at atmospheric pressure and initial temperatures of; 298 K (a), 308 K (b), 318 K (c) and 328 K (d).

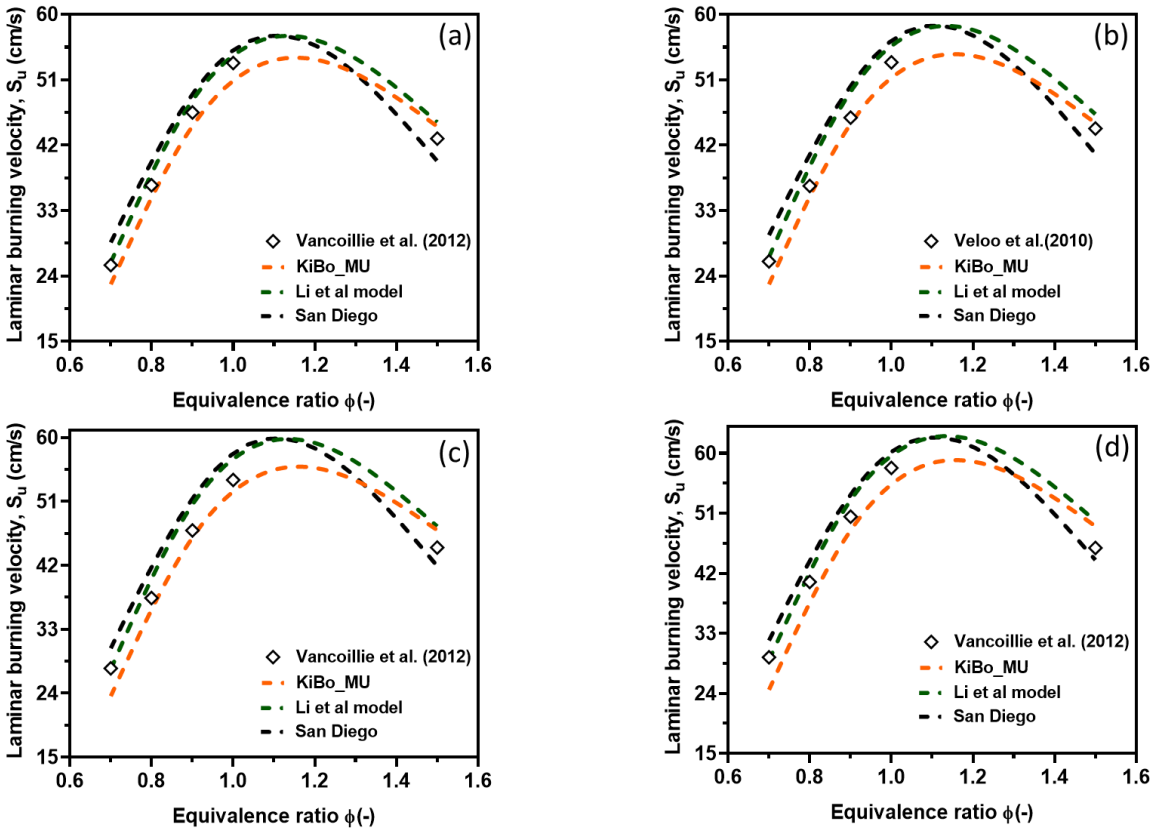

Figure 15. Laminar burning velocity of methanol-air mixtures at atmospheric pressure and initial temperatures of; 338 K (a), 343 K (b), 348 K (c) and 358 K (d).

Moreover, the validation has been extended to another laminar burning velocity data from the heat flux method reported by Sileghem et al. [193] for different initial temperatures (i.e., 298, 318, 328, 338 and 358 K) as shown in Figure 16 (a – d) and Figure 17, respectively. As can be seen from the figures, KiBo_MU fairly captured burning velocities under the investigated conditions. Nevertheless, Li et al and San Diego kinetic models showed some discrepancies for an equivalence ratio of 0.9 and 1.0, while showing good agreement at other conditions. Comparably, as can be seen from the figures, KiBo_MU showed better agreement than the other models.

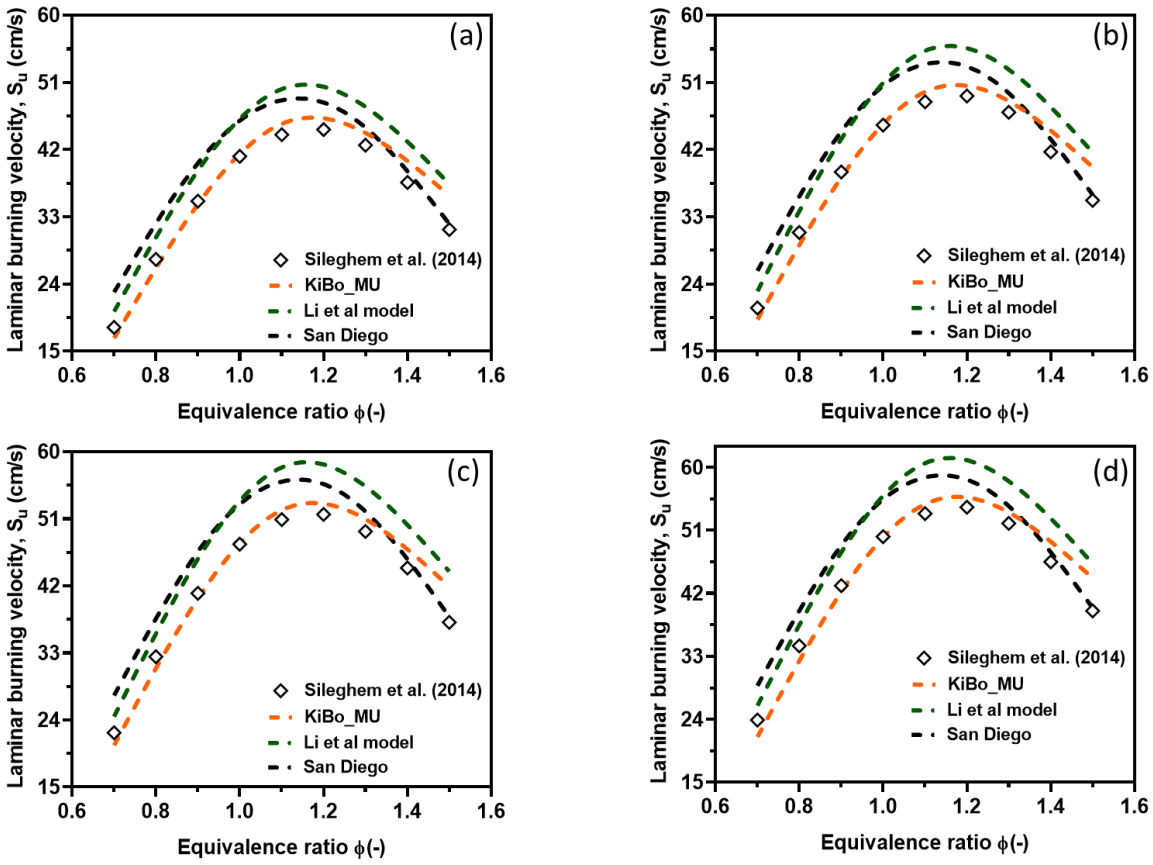

Figure 16. Laminar burning velocity of methanol-air mixtures at atmospheric pressure and initial temperatures of; 298 K (a), 318 K (b), 328 K (c) and 338 K (d).

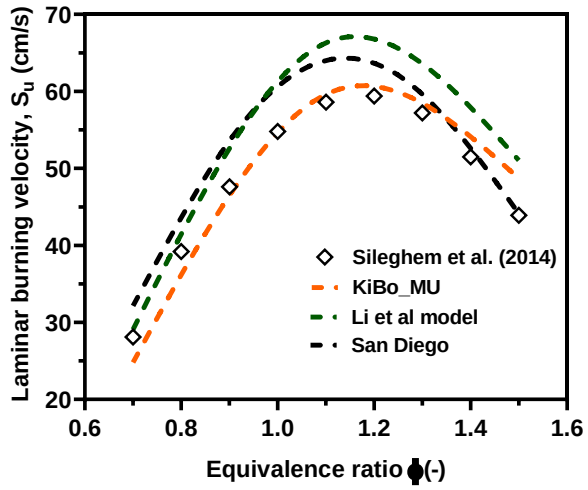

Figure 17. Laminar burning velocity of methanol-air mixtures at atmospheric pressure and initial temperatures of; 358 K.

To better understand the main reactions playing a key role during low-temperature combustion of methanol, sensitivity analysis considering lean, stoichiometric and rich flames has been

performed at 298 K and 358 K. The lists of influential reactions have been shown in Figures 18 & 19.

Under lean and stoichiometric conditions, CO + OH ↔ CO_2 + H, H + O_2 ↔ O + OH, HCO + M ↔ CO + H + M and H + HO_2 ↔ 2 OH, respectively are the first four key reactions having a promoting effect on the laminar burning velocity of methanol at an initial temperature of 298 K. Whereas, HCO + O_2 ↔ CO + HO_2, H + O_2 (+M) ↔ HO_2 (+M), HO_2 + OH ↔ H_2O + O_2 and H_2 + O_2 ↔ H + HO_2, respectively are the first four reactions having a limiting effect on the laminar burning velocity of methanol. From the main fuel reactions, CH_3OH + OH ↔ CH_2OH + H_2O and CH_3OH + OH ↔ CH_3O + H_2O were found to have a positive sensitivity coefficient towards the burning velocity. However, in rich flames, H + O_2 ↔ O + OH, HCO + M ↔ CO + H + M, H + HO_2 ↔ 2 OH and CH_2OH + M ↔ CH_2O + H + M, respectively are key reactions favoring the burning velocity while, H_2 + O_2 ↔ H + HO_2, H + HCO ↔ CO + H_2, HO_2 + OH ↔ H_2O + O_2 and H + OH + M ↔ H_2O + M, respectively key reactions inhibiting the burning velocity of methanol oxidation. From the main fuel reactions, CH_2OH + M ↔ CH_2O + H + M, CH_3OH + OH ↔ CH_2OH + H_2O and CH_3OH + HO_2 ↔ CH_2OH + H_2O_2 are the key reactions promoting the laminar burning velocity of methanol oxidation in rich flames at an initial temperature of 298 K. On the other hand, at 358 K in lean condition, H + O_2 ↔ O + OH, HCO + M ↔ CO + H + M, H + HO_2 ↔ 2 OH and CH_2OH + M ↔ CH_2O + H + M, respectively are key reactions promoting burning velocity of methanol. Whereas, H_2 + O_2 ↔ H + HO_2, H + HCO ↔ CO + H_2, HO_2 + OH ↔ H_2O + O_2 and H + OH + M ↔ H_2O + M, respectively key reactions inhibiting the burning velocity of methanol oxidation. From the main fuel reactions, CH_2OH + M ↔ CH_2O + H + M, CH_3OH + OH ↔ CH_2OH + H_2O and CH_3OH + HO_2 ↔ CH_2OH + H_2O_2 are the key reactions promoting the laminar burning velocity of methanol oxidation in rich flames at an initial temperature of 358 K. In the same way, reactions having a promoting effect on the burning velocity at stoichiometric condition are listed as; H + O_2 ↔ O + OH, HCO + M ↔ CO + H + M, CO + OH ↔ CO_2 + H and H + HO_2 ↔ 2 OH, respectively and those inhibiting the burning rate includes, H_2 + O_2 ↔ H + HO_2, HCO + O_2 ↔ CO + HO_2, H + HCO ↔ CO + H_2 and HO_2 + OH ↔ H_2O + O_2, respectively. Likewise, in rich flames; H + O_2 ↔ O + OH, HCO + M ↔ CO + H + M, CO + OH ↔ CO_2 + H and H + HO_2 ↔ 2 OH, respectively found to have a favoring effect on laminar burning velocity while, H_2 + O_2 ↔ H + HO_2, HCO + O_2 ↔ CO + HO_2, H + HCO ↔ CO + H_2 and HO_2 + OH ↔ H_2O + O_2, respectively are hindering the burning velocity. From the main fuel reactions, CH_3OH + OH

↔ $CH_2OH + H_2O$ and $CH_3OH + OH$ ↔ $CH_3O + H_2O$ were found to have a positive sensitivity coefficient towards the burning velocity in both stoichiometric and rich conditions.

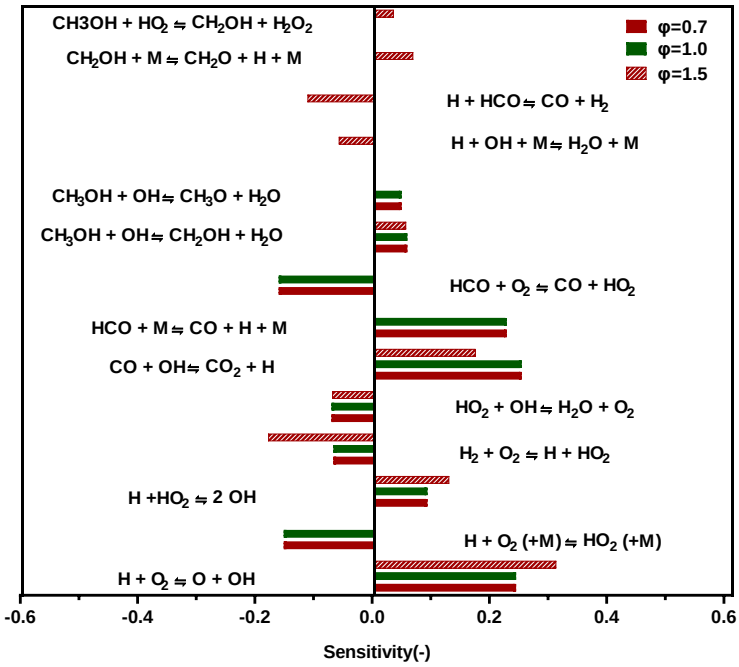

Figure 18. Sensitivity coefficients for laminar burning velocity of CH_3OH-air mixtures, T = 298 K, φ =0.7, 1.0, 1.5 using KiBo_MU.

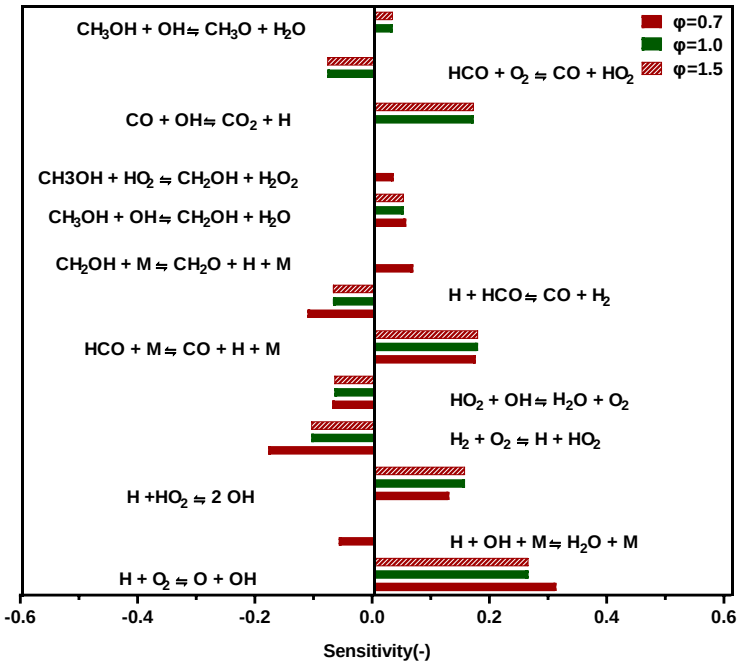

Figure 19. Sensitivity coefficients for laminar burning velocity of CH_3OH-air mixtures, T = 358 K, φ =0.7, 1.0, 1.5 using KiBo_MU.

4.1.2.1.2 Ethanol

The laminar burning velocity of ethanol flames has been investigated under ranges of reaction conditions using KiBo_MU kinetic model as shown in Figures 20 & 21. Results from the present study have been compared with experimental results from Konnov et al. [55] and numerical results obtained using the widely used and validated ethanol kinetic mechanisms such as the ethanol kinetic model from Lund university developed by Christensen and Konnov [264] (Konnov kinetic model), Politecnico di Milano (CRECK) [131] kinetic models.

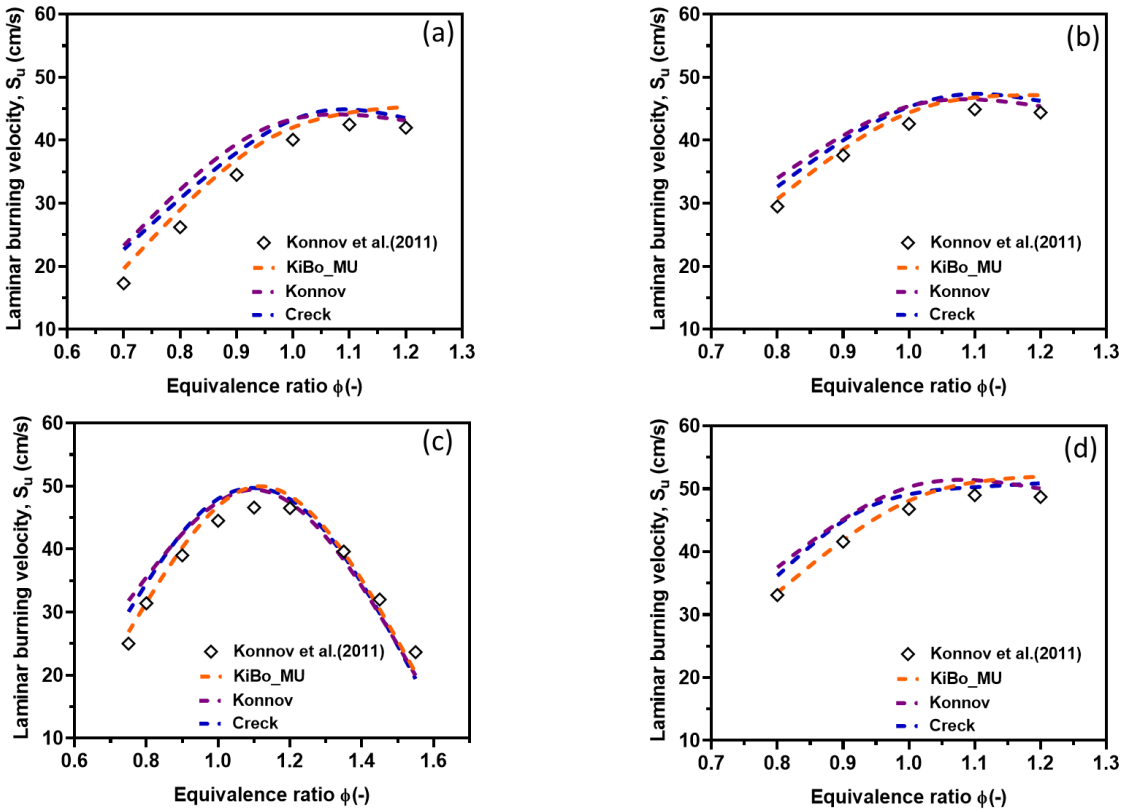

Figure 20. Laminar burning velocity of ethanol-air mixtures at atmospheric pressure and initial temperatures of; 298 K (a), 308 K (b), 318 K (c) and 328 K (d).

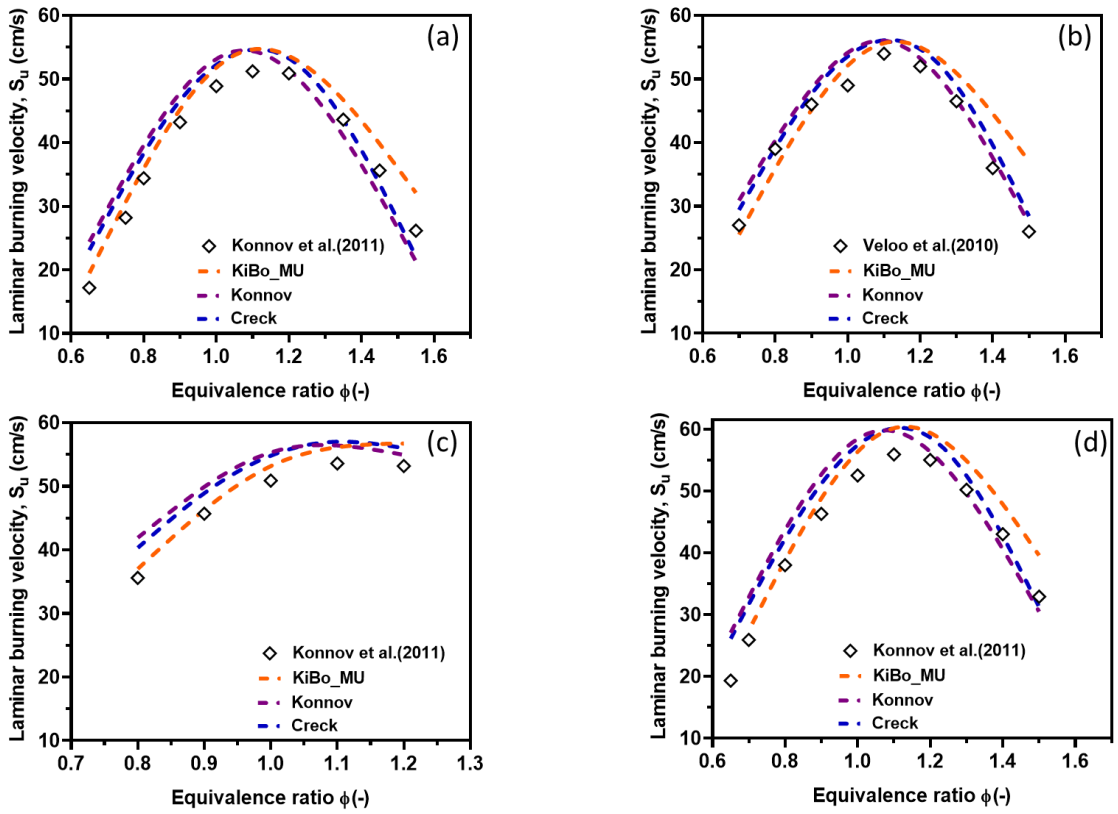

Figure 21. Laminar burning velocity of ethanol-air mixtures at atmospheric pressure and initial temperatures of; 338 K (a), 343 K (b), 348 K (c) and 358 K (d).

The laminar burning velocity of ethanol-air flames under a temperature range of 298 – 358 K, equivalence ratio of 0.6 – 1.6 and a pressure of 1 atm are shown in Figures 20 & 21. From the result shown in Figure 20 (a – d), for reaction temperature of 298 – 328 K and equivalence ratio range of 0.7 – 1.6, KiBo_MU kinetic model showed good agreement with the experimental result obtained using a perforated plate burner as reported in the literature [55]. As can be seen from the laminar burning velocity curves, under the investigated conditions, maximum burning velocity has been found at the onset of rich flames (i.e., around φ = 1.1) which is consistent with the experimental result. In the same way, as can be seen from the laminar burning velocity curves shown in Figure 21 (a – d) for a temperature range of 338 – 358 K and equivalence ratio range of 0.65 – 1.55, results from KiBo_MU agreed well with experimental data from the literature obtained using a perforated burner and counterflow methods. Overall, the current model captured the burning velocity very well and comparably, showed low uncertainty when compared with other kinetic models (i.e., Konnov, CRECK).

The key reactions playing an important role during low-temperature ethanol combustion and mostly governing the flame propagation have been revealed through the evaluation of laminar

burning velocity sensitivity analysis. Considering the relatively lower and higher temperatures of the investigated conditions, sensitivity analysis of ethanol-air flames at 298 and 358 K has been performed in all flame conditions and the results are shown in Figures 22 & 23.

In lean and rich conditions (φ =0.7, 1.5) and T=298 K, CO + OH ↔ CO_2 + H, H + O_2 ↔ O + OH, HCO + M ↔ CO + H + M and H + HO_2 ↔ 2 OH, respectively are the first four key reactions having a strong positive sensitivity coefficient towards burning velocity of ethanol. While H + O_2 (+ M) ↔ HO_2 (+ M), HCO + O_2 ↔ CO + HO_2, SC_2H_4OH + O_2 ↔ CH_3CHO + HO_2 and C_2H_5OH + H ↔ SC_2H_4OH + H_2, respectively are the first four reactions limiting ethanol burning rate. Under the stoichiometric condition, H + O_2 ↔ O + OH was found to have a strong promoting effect than CO + OH ↔ CO_2 + H, and the order of the first four reactions favoring laminar burning velocity are listed as; H + O_2 ↔ O + OH, CO + OH ↔ CO_2 + H, HCO + M ↔ CO + H + M and CH_3 + O ↔ CH_2O + H. Whereas, H + OH (+ M) ↔ H_2O (+ M) and CH_3 + H (+ M) ↔ CH_4 (+ M) are the two key reactions hindering ethanol burning rate. Similarly, from the sensitivity result shown in Figure 23 for 358 K and equivalence ratios of φ =0.7, 1.0 and 1.5, it can be seen that H + O_2 ↔ O + OH, CO + OH ↔ CO_2 + H and HCO + M ↔ CO + H + M are the first 3 key reactions favoring ethanol burning rate under lean and stoichiometric conditions. Likewise, from the fuel reactions, the unimolecular decomposition of SC_2H_4OH intermediate forming acetaldehyde and hydrogen is found to have a relatively large positive sensitivity coefficient. In contrast, HCO + O_2 ↔ CO + H_2O and SC_2H_4OH + O_2 ↔ CH_3CHO + HO_2 have strong negative coefficients at φ =0.7 while, H + O_2 (+ M) ↔ HO_2 (+ M) and H + OH (+ M) ↔ H_2O (+ M) are reactions having an inhibiting effect on the laminar burning velocity at φ =1.0. On the other hand, in rich conditions, H + O_2 ↔ O + OH, HCO + M ↔ CO + H + M, C_2H_3 + O_2 ↔ CH_2CHO + O, and CH_3 + HO_2 ↔ CH_3O + OH, respectively are reactions with strong promoting effect while, C_2H_3 + H ↔ C_2H_2 + H_2, 2 CH_3 (+M) ↔ C_2H_6 (+M), H + HCO ↔ CO + H_2 and H_2 + O_2 ↔ H + HO_2, respectively are the list of reactions that inhibit the burning velocity.

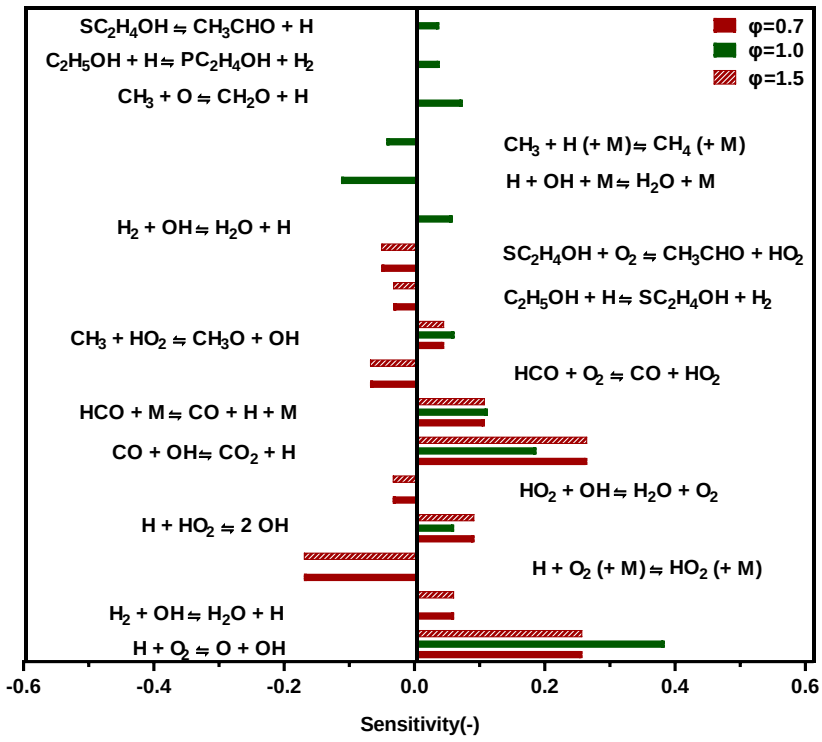

Figure 22. Sensitivity coefficients for laminar burning velocity of C_2H_5OH-air mixtures, T = 298 K, φ =0.7, 1.0, 1.5 using KiBo_MU.

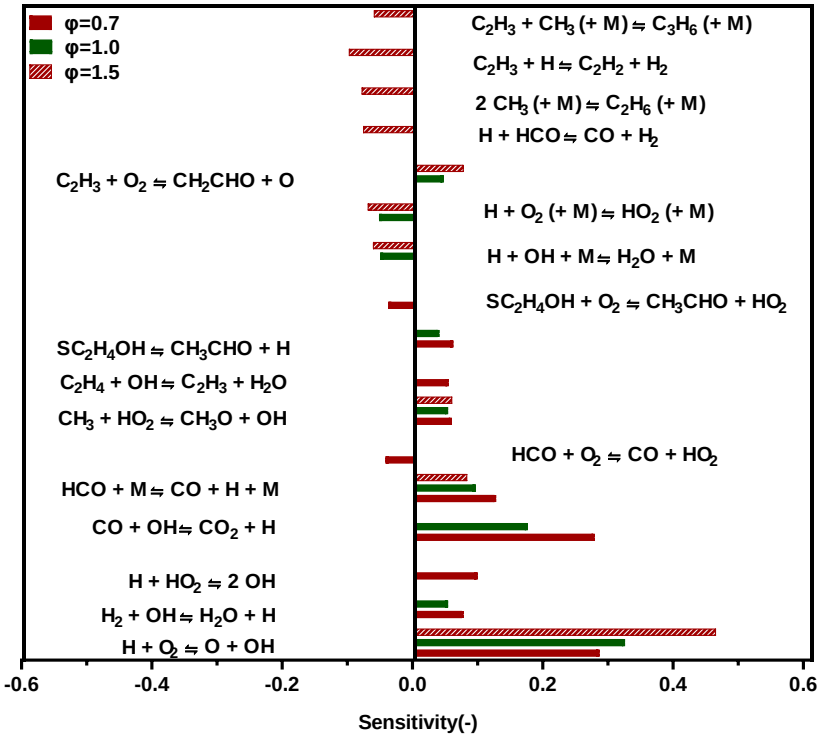

Figure 23. Sensitivity coefficients for laminar burning velocity of C_2H_5OH-air mixtures, T = 358 K, φ =0.7, 1.0, 1.5 using KiBo_MU.

4.1.2.1.3 Formic acid

The two kinetic mechanisms developed in this work have been used for the investigation of laminar burning velocity of formic acid oxidation in different diluents (i.e., N_2, Ar) concentration, ranges of initial temperatures and equivalence ratios, and atmospheric pressure and the results are shown in Figures 24 – 27.

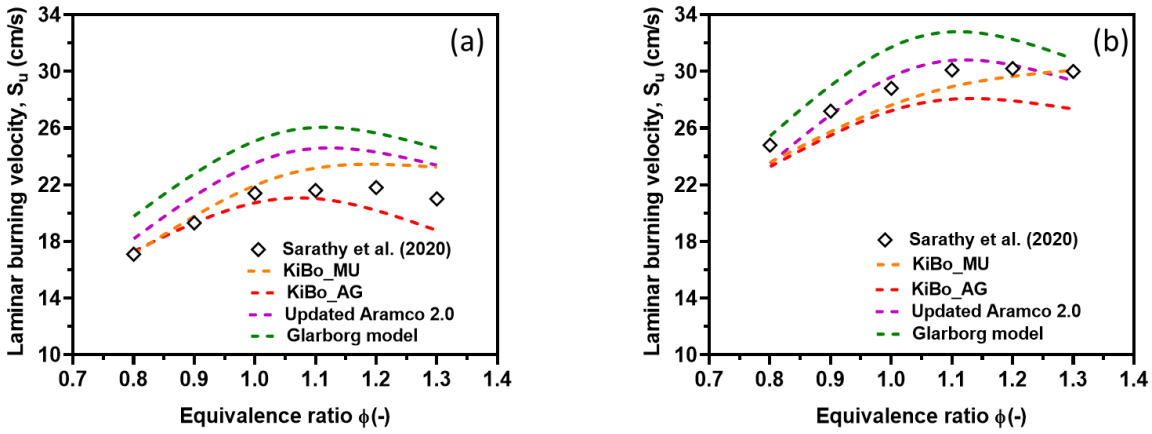

Figure 24. Laminar burning velocity for HOCHO/air mixtures at 373 K (a) and 423 K (b).

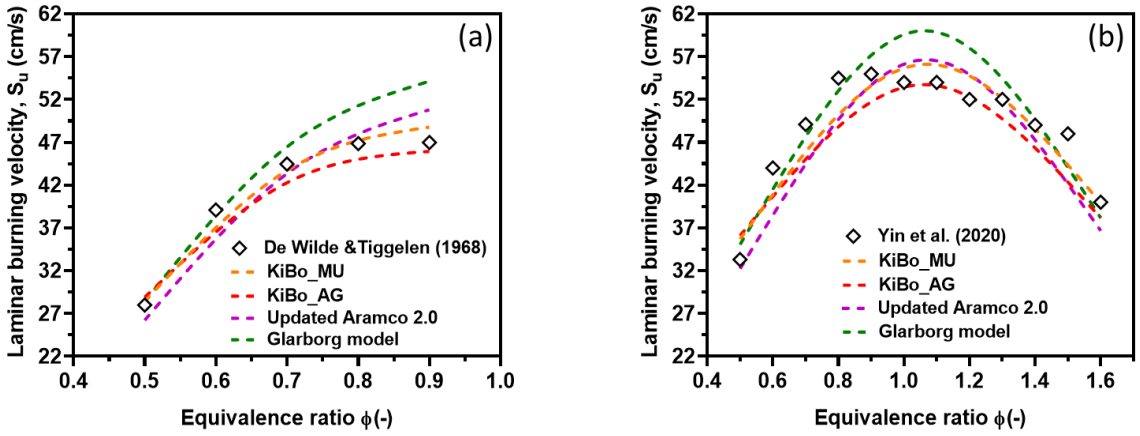

Figure 25. Laminar burning velocity for HOCHO/O_2/N_2 mixtures at 433K (a) and 453K (b); 35 % O_2, 65 % N_2.

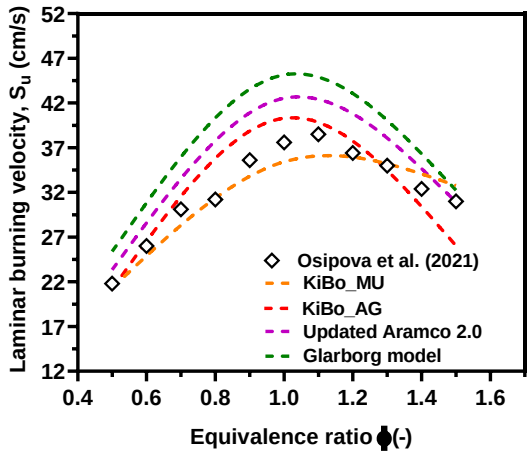

Figure 26. Laminar burning velocity for HOCHO/O_2/Ar blends at 368 K, the mole fraction of Ar is 0.55.

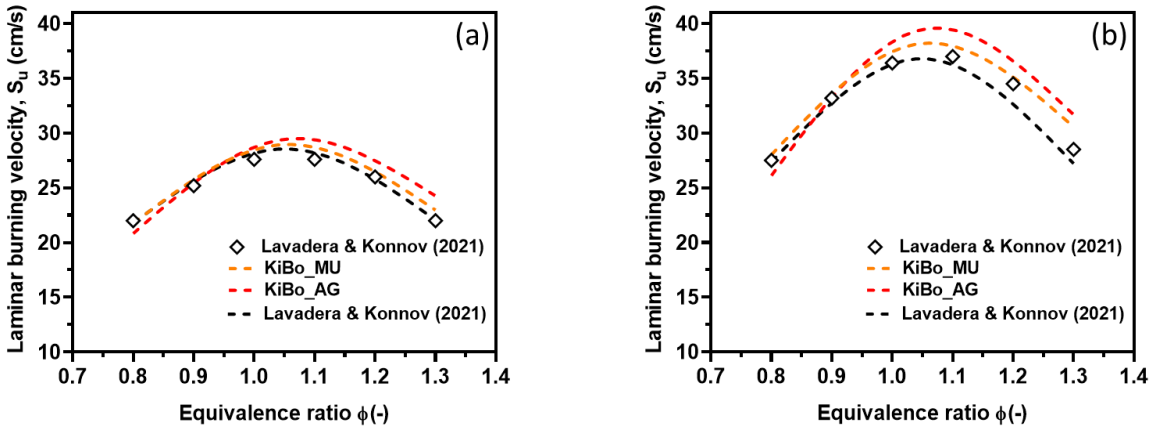

Figure 27. Laminar burning velocities of 0.75 HOCHO + 0.25 CH_4 + air (a) and 0.5 HOCHO + 0.5 CH_4 + air (b) at 353 K.

As can be seen from Figure 24 (a & b), under the investigated conditions, KiBo_MU and KiBo_AG kinetic models are in good agreement with the experimental results. The laminar burning velocity increases with increasing equivalence ratio and reached its peak value at fuel to air ratio of 1.1 using all the investigated kinetic mechanisms which are consistent with the experimental study reported by Sarathy et al. [99]. The equivalence ratio where the fundamental laminar burning velocity is observed is in line with most hydrocarbons, as it is related to the compositions showing the maximum adiabatic temperature and maximum concentration of H radicals [352]. Besides, results from the current models have been compared with the existing formic acid kinetic models and found to show a better agreement, however, there happen to be discrepancies in rich flames for Glarborg whereas, the updated Aramco 2.0 kinetic model fairly agreed with the measured burning velocity.

On the other hand, as can be seen from Figure 25 (a & b) for 433 and 453 K respectively, KiBo_MU and KiBo_AG apparently predicted the laminar burning velocities well and the results satisfactorily agreed with the experimental results from De Wilde and Van Tiggelen [353] and Yin et al. [232]. Given the limited equivalence ratio considered in the case of 433 K temperature, at both 433 and 453 K, the numerical and experimental value of maximum laminar burning velocity was found to be obtained at an equivalence ratio of 0.9 which might be due to the increased oxygen composition in the fuel mixture. The increase in 20 K (i.e., 433 – 453 K), increases the laminar burning velocity by 8 cm/s which is equivalent to a 50 K increase (i.e., 373 – 423 K) as shown in Figure 24 (a & b) where argon was used as a diluent. From this, it can be said that the increase in oxygen composition in the fuel mixture increases the burning rate more than the increase in temperature leading to peak laminar burning velocity happening in a lean condition.

The laminar burning velocity of HOCHO/Ar mixtures at reaction temperatures of 368 K, atmospheric pressure and equivalence ratio ranging from 0.5 – 1.5 is shown in Figure 26. In the same way, the current kinetic models well mimicked the experimental laminar burning velocity and comparably showed better agreement than the existing kinetic models. Furthermore, as shown in Figure 27 (a & b), the laminar burning velocity of fuel mixtures (i.e., HOCHO/CH_4/air mixture) has been studied in the equivalence ratio range of 0.8 – 1.3 and the initial temperature of 353 K. From the result, it has been observed that methane addition was found to increase the reaction rate and apparently favouring laminar burning velocity. Maximum reactivity of the fuel mixture is achieved at equivalence ratios of 1.0 and 1.1, as is the maximum laminar burning velocity. From both figures, the laminar burning velocity result from the present study using KiBo_MU and KiBo_AG is in good agreement with the experimental data reported by Lavadera and Konnov [345], and the model result obtained by the same author. Overall, under the studied conditions, KiBo_MU and KiBo_AG reasonably predicted the burning velocity and showed better accuracy than the existing kinetic models.

The most influential reactions at lean, stoichiometric and rich conditions during formic acid oxidation were analysed through sensitivity analysis using KiBo_MU and KiBo_AG kinetic models. The analysis was performed at a temperature of 453 K, atmospheric pressure and equivalence ratio of 0.8, 1.0, and 1.5, and the results are shown below in Figure 28. The effects of reactions involving small radicals such as $H + O_2 \leftrightarrow O + OH$, $H + O_2 \leftrightarrow 2\ OH$, $H_2 + O_2 \leftrightarrow H + HO_2$, $H + OH + M \leftrightarrow H_2O + M$, $H + O_2\ (+ M) \leftrightarrow HO_2\ (+ M)$, $H + HO_2 \leftrightarrow H_2 + O_2$ on the

laminar burning velocity of formic acid are not shown here as they are widely studied in the literature [99, 232, 345] as well as in common with species previously investigated in this work. This observation suggests that a common decomposition pathway can be assumed for light species typically produced by the decomposition of biofuels as well as confirms the validity of the hierarchical structure of detailed kinetic mechanisms.

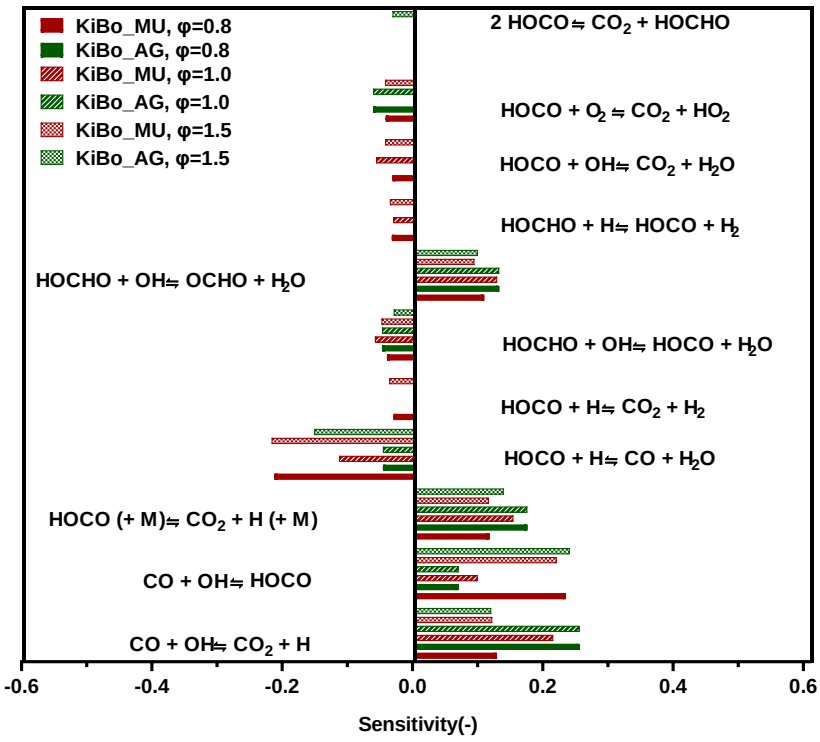

Figure 28. Sensitivity coefficients for laminar burning velocity in the oxidation of HOCHO/O_2/N_2, 35% O_2, 65% N_2, T = 453 K, φ =0.8, 1.0, 1.5 using KiBo_MU and KiBo_AG.

As can be seen from Figure 28, using the two kinetic models, radical reactions such as CO + OH ↔ CO_2 + H, CO + OH ↔ HOCO, HOCO + M ↔ CO_2 + H + M and HOCHO + OH ↔ OCHO + H_2O have a dominant promoting effect on the overall reactivity under the investigated conditions resulting from the generation of active H radical. Comparably, at φ = 0.8 and stoichiometric conditions, CO + OH ↔ CO_2 + H and HOCO + M ↔ CO_2 + H + M showed a strong positive sensitivity coefficient in KiBo_AG than KiBo_MU while, the opposite is true in the case of CO + OH ↔ HOCO reaction. However, in rich flames, CO + OH ↔ HOCO and HOCO + M ↔ CO_2 + H + M the reactions show a relatively lower sensitivity coefficient in the case of KiBo_MU than KiBo_AG whereas, CO + OH ↔ CO_2 + H is equally sensitive to laminar burning velocity in both mechanisms.

On the other hand, in lean and rich flames using KiBo_MU, HOCO + H ↔ CO + H_2O, HOCHO + OH ↔ HOCO + H_2O, HOCO + O_2 ↔ CO_2 + H_2, HOCHO + H ↔ HOCO + H_2, HOCO + OH ↔ CO_2 + H_2O and HOCO + H ↔ CO_2 + H_2 were orderly found to have negative sensitivity effects on the laminar burning velocity of formic acid, in which HOCO + H ↔ CO + H_2O had a strong hindering effect on the burning rate. Except for the last reaction (i.e., HOCO + H ↔ CO_2 + H_2), which is insensitive under stoichiometric conditions, all other reactions also show negative sensitivity to combustion rate under stoichiometric conditions. In the same way, using KiBo_AG, in lean and stoichiometric, and rich conditions, reactions having an obstructing effect on the laminar burning velocity are listed in order of their impact as; HOCO + O_2 ↔ CO_2 + HO_2, HOCHO + OH ↔ HOCO + H_2O, HOCO + H ↔ CO + H_2O, and HOCO + O_2 ↔ CO_2 + HO_2, 2 HOCO ↔ HOCHO + CO_2, HOCHO + OH ↔ HOCO + H_2O, respectively.

Under the investigated conditions, HOCO + H ↔ CO_2 + H_2, HOCHO + H ↔ HOCO + H_2 and HOCO + OH ↔ CO_2 + H_2O are insensitive to laminar burning rates in the case of KiBo_AG, but they had a hindering effect on burning rate in case of KiBo_MU. Likewise, 2 HOCO ↔ HOCHO + CO_2 is only sensitive in rich flame in the case of KiBo_AG. It is worth mentioning that this reaction was not included in KiBo_MU. Indeed, the procedure implemented for the realization of this mechanism considered only the H abstraction by small radicals as primary reactions, to limit the number of reactions.

4.1.2.1.4 Acetic Acid

Similar to formic acid, the kinetic study of acetic acid has been performed by the two currently developed kinetic models (i.e., KiBo_MU and KiBo_AG). The laminar burning velocity of acetic acid-air mixtures at different initial temperatures (i.e., 338, 348, and 358 K) and ranges of equivalence ratios computed in the current study are depicted in Figure 29. Results from the two kinetic models developed in the present study have been compared with the kinetic model developed by Christensen and Konnov [78].

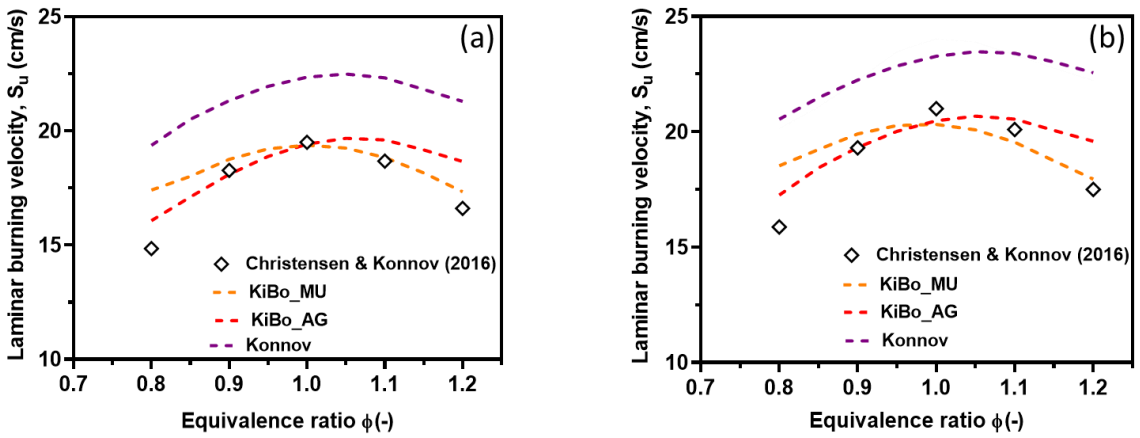

Figure 29: Laminar burning velocity of acetic acid at 338 K (a), 348 K (b) and pressure of 1 atm.

As can be seen from the figure; at 338 K, KiBo_AG kinetic model quite perfectly reproduced the experimental data in all flame conditions, especially in lean and stoichiometric flames. However, the model relatively overestimated the burning velocity in rich flames, whereas KiBo_MU reproduced the burning velocity very well and the results in all flame conditions showed a good agreement against experimental data, nevertheless, slight discrepancies were observed in lean flames at an equivalence ratio of 0.8.

On the other hand, at 348 K, KiBo_AG kinetic model captured the burning velocity well and are in good agreement with the experimental data at lean and stoichiometric compositions, whereas, the overall reactivity of richer flames is slightly overestimated. Likewise, despite the few underestimations observed at an equivalence ratio of 0.8, KiBo_MU kinetic model perfectly mimicked the investigated parameter at all flame conditions. Under the investigated conditions, KiBo_MU kinetic model attempted the laminar burning velocity with almost negligible deviations at stoichiometric and rich flames. Furthermore, results from KiBo_MU and KiBo_AG have been also compared with other kinetic mechanism from the literature (e.g. Konnov kinetic model). Under the investigated conditions, Konnov kinetic model overpredicted the laminar burning velocity, showing a poorer estimation quality when compared to KiBo_MU and KiBo_AG kinetic models. The observations reported so far may be strongly influenced by the lack of experimental data. However, it is worth noting that the fundamental burning velocity was obtained under stoichiometric conditions using the KiBo_MU and KiBo_AG kinetic models, which agrees with the experimentally reported data, indicating the maximum reactivity under stoichiometric conditions. Overall, despite the few

discrepancies, under the studied conditions KiBo_MU and KiBo_AG kinetic models fairly mimicked the laminar burning velocity and the results are in good agreement with the experimental results.

Important reactions governing the reactivity of acetic acid in the oxidative environment have been analysed and lists of main reactions affecting the laminar burning velocity of acetic acid at 338 K are provided in Figure 30.

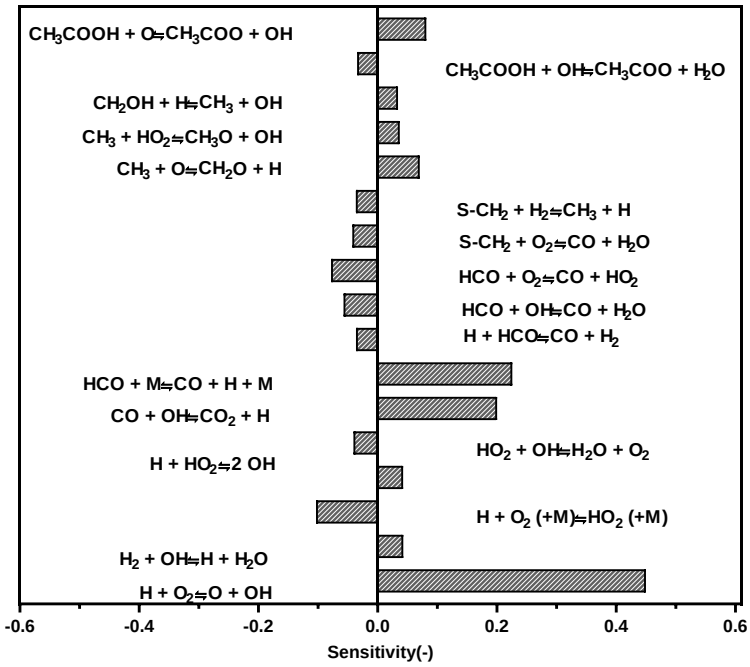

Figure 30: Sensitivity coefficients for laminar burning velocity of acetic acid at; T = 338 K, P = 1 atm, φ = 1.0 using KiBo_MU kinetic mechanism.

Reactions with the highest values (in modulus) in the sensitivity coefficients and playing key roles in acetic acid oxidation at low initial temperatures are listed as; $H + O_2 \leftrightarrow O + OH$, $CO + OH \leftrightarrow CO_2 + H$, $HCO (+ M) \leftrightarrow CO + H (+ M)$, $H + O_2 (+ M) \leftrightarrow HO_2 (+ M)$ and $CH_3COOH + O \leftrightarrow CH_3COO + OH$. Additional insights and elements useful for the discussion on the main reactions and their rate parameters source can be found in the paper reported below, published by the author as part of this work.

FM *Wako., G Pio., E Salzano., Modelling of acetaldehyde and acetic acid combustion., Combustion Theory and Modelling, 2023.*

4.1.2.1.5 Acetaldehyde

The laminar burning velocity of acetaldehyde-air flames was computed at two different initial temperatures (298 K, 338 K), atmospheric pressure and equivalence ratio range of 0.6 – 1.6 using KiBo_MU and KiBo_AG kinetic models as shown in Figure 31.

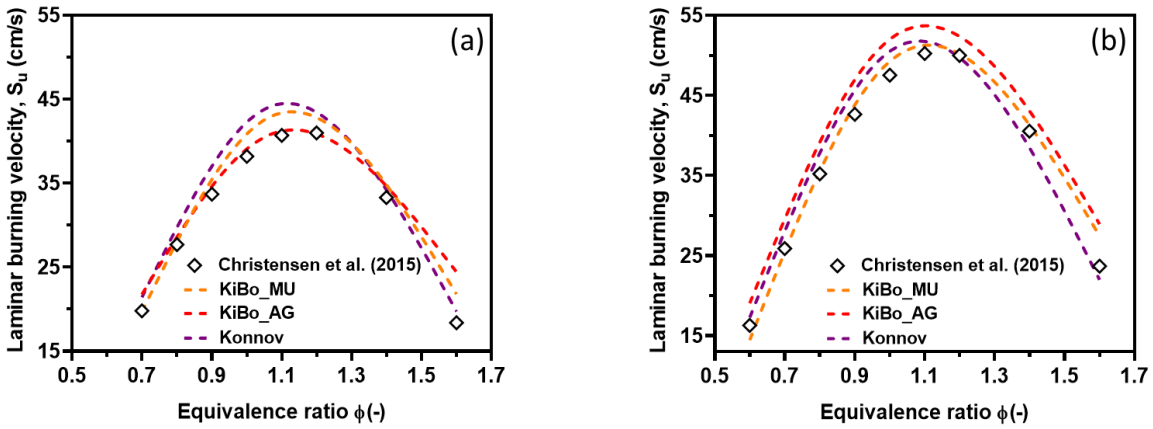

Figure 31: Laminar burning velocity of acetaldehyde/air flames at the temperature of 298 K (a), 338 K (b) and atmospheric pressure.

In lean and stoichiometric flames for an initial temperature of 298 K, kinetic models from the present study reproduced the experimental data very well. However, the investigated mechanisms showed a minor deviation in burning velocity in rich flames particularly, at φ = 1.6. The maximum flame reactivity and burning velocity was obtained at φ = 1.2, which is consistent with the experimental report. Likewise, at 338 K the maximum laminar burning velocity was obtained at φ = 1.2 by using KiBo_MU and Konnov mechanism, and at φ = 1.1 by using KiBo_AG, whereas experiments show the maximum reactivity at φ=1.1. Comparably, KiBo_AG kinetic mechanism for both initial reaction temperatures, the relatively larger deviation was observed in rich flames at an equivalence ratio of 1.6 while KiBo_MU kinetic mechanism showed an opposite trend at 298 K. Despite the few discrepancies, both KiBo_MU and KiBo_AG kinetic models fairly reproduced the experimental data under the studied conditions.

The main reactions influencing the low-temperature combustion chemistry of acetaldehyde have been reported in Figure 32 and analysed in the following. As can be seen from the figure, reactions; $H + O_2 \leftrightarrow O + OH$, $HCO + M \leftrightarrow CO + H + M$, $HCO + H \leftrightarrow CO + H_2$, $H + OH (+ M) \leftrightarrow H_2O (+ M)$ and $CH_3 + HO_2 \leftrightarrow CH_3O + OH$, respectively were found to be the first five

reactions in lean and rich flames having high sensitivity values (in modulus). Similarly, at stoichiometric conditions, $H + O_2 \leftrightarrow O + OH$, $CO + OH \leftrightarrow CO_2 + H$, $HCO + M \leftrightarrow CO + H + M$, $CH_3 + HO_2 \leftrightarrow CH_3O + OH$ and $H_2 + O \leftrightarrow H + OH$, respectively were key reactions affecting the burning velocity of acetaldehyde. The complete list of sensible reactions in lean, stochiometric and rich conditions are shown in Figure 32.

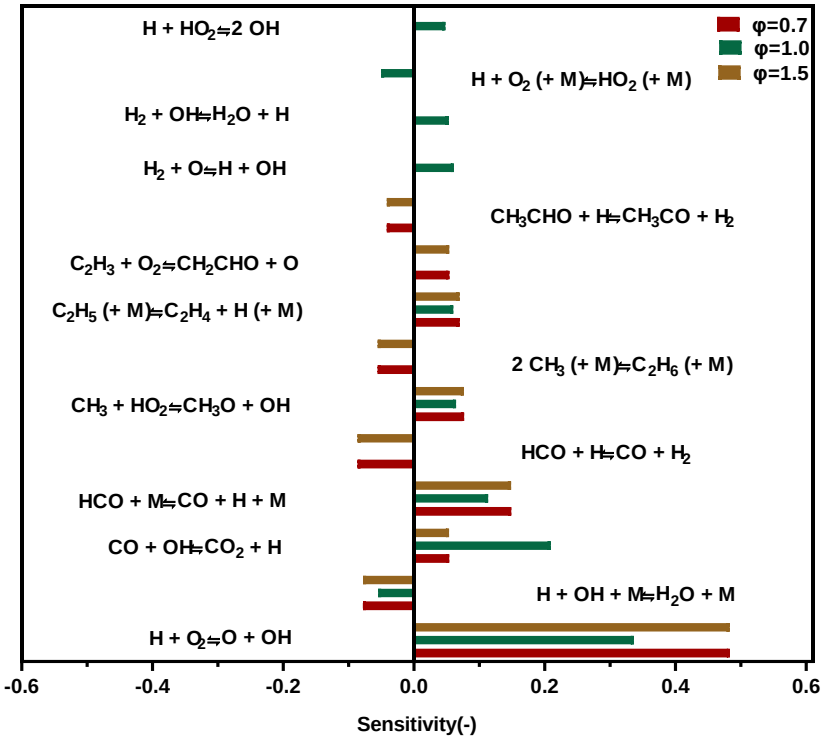

Figure 32. Sensitivity coefficients for laminar burning velocity of CH_3CHO-air mixtures, T = 298 K, φ =0.7, 1.0, 1.5 using KiBo_MU.

Additional information on the current understanding and existing numerical and experimental data sources for laminar burning velocity can be found in the paper published by the author as part of this work as shown below.

FM Wako., G Pio., E Salzano., Modelling of acetaldehyde and acetic acid combustion., Combustion Theory and Modelling, 2023.

4.1.2.2 Intermediate temperature combustion

The kinetic model has been used for studying intermediate temperature combustion phenomena. To this aim, the concentration profile of the most relevant species from the jet-stirred reactor and the overall reactivity intended as the ignition delay times from rapid

compression machine are the two parameters studied for guaranteeing the validity of the kinetic models in intermediate temperature combustion.

4.1.2.2.1 Methanol

The intermediate combustion chemistry of methanol/O_2/Ar mixtures has been studied through the evaluation of ignition delay times from rapid compression machines. Due to the limitation of experimental studies in the literature, validation has been limited to stoichiometric condition and the results are shown in Figure 33. From the IDT results shown in Fig. 33, at the temperature range of 842 – 1012 K, the average pressure of 15 bar and φ =1.0, KiBo_MU kinetic model showed fair agreement with the experimental data from the rapid compression machine reported by Wang et al. [177]. More specifically, very good agreement has been realized for temperatures greater than 900 K while a few variations have been observed for temperatures less than 900 K. Even though, KiBo_MU, Zhang and Li et al kinetic models showed better attempts at lesser temperatures, San Diego and Aramco1.3 kinetic models showed large variations. Overall, KiBo_MU showed a very fair attempt even in combustion conditions where other models failed in a narrow range of attempts and can be considered as a detailed and comprehensive kinetic model.

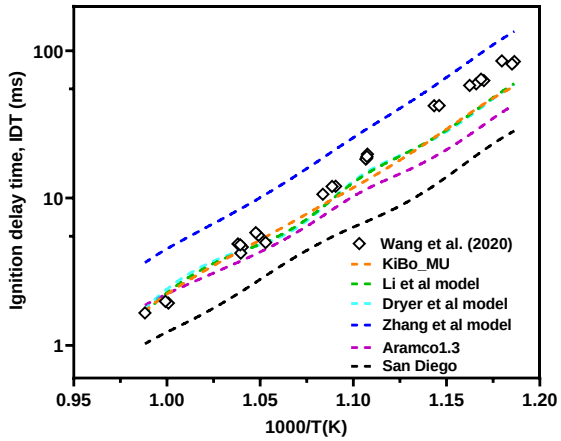

Figure 33. Ignition delay time of methanol/O_2/Ar mixtures at φ = 1.0, 8.08% CH_3OH, 12.13% O_2, 79.19% average pressure of 15 bar.

4.1.2.2.2 Ethanol

Intermediate temperature ignition delay times of ethanol/O_2/Ar mixtures at φ= 0.5, 1.0, T = 835 – 1005 K and average pressure of 15 bar is shown in Figure 34. Results obtained using KiBo_MU is in good agreement with the RCM experimental result in both lean and stoichiometric flames particularly, the model excellently mimicked the IDT at stoichiometric

condition. Similarly, from the simulation study in rich conditions as shown in Figure 35 for the temperature range of 825 – 940 K and average pressure of 15 bar, KiBo_MU fairly captured the IDT and showed better accuracy than the other models within the studied reaction conditions.

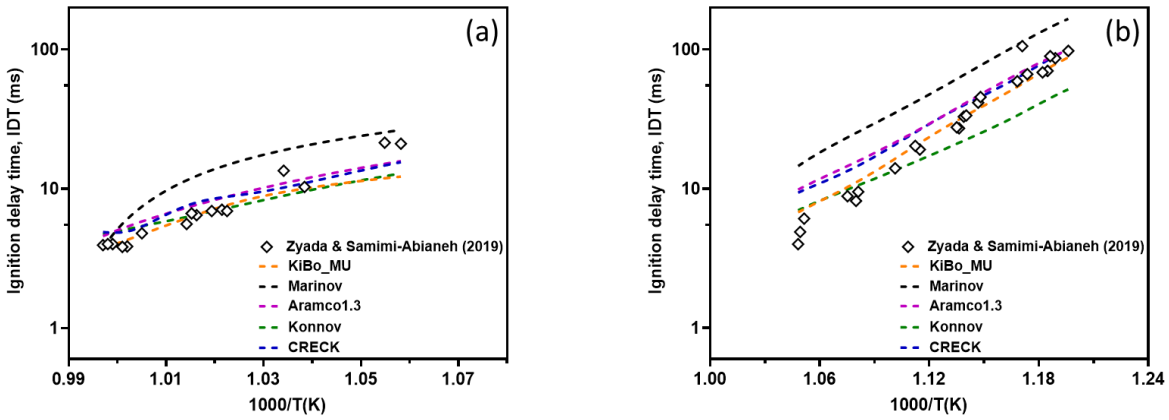

Figure 34. Ignition delay time of ethanol/O_2/Ar mixtures at φ = 0.5, 1.25% C_2H_5OH, 7.55% O_2 and 91.25% Ar (a), φ = 1.0, 2.5035% C_2H_5OH, 7.508% O_2, 7.985% N_2 and 82.0035% Ar (b), and average pressure of 15 bar.

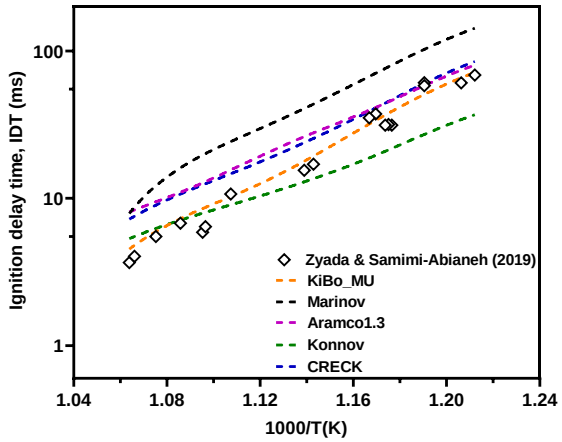

Figure 35. Ignition delay time of ethanol/O_2/Ar mixtures at φ = 2.0, 15 bar. 4.9309% C_2H_5OH, 7.3892% O_2 and 87.6799% Ar.

4.1.2.2.3 Formic acid

The species profiles from the jet-stirred reactor (JSR) reported by Yin et al. [346] at a temperature range of 500 – 1100 K, atmospheric pressure, and an equivalence ratio ranging from 0.5 – 2.0 were considered for intermediate temperature validation. The numerical results obtained in this work along with the experimental measurements from a recent study reported by Yin et al. [346] are shown in Figures 36 – 38.

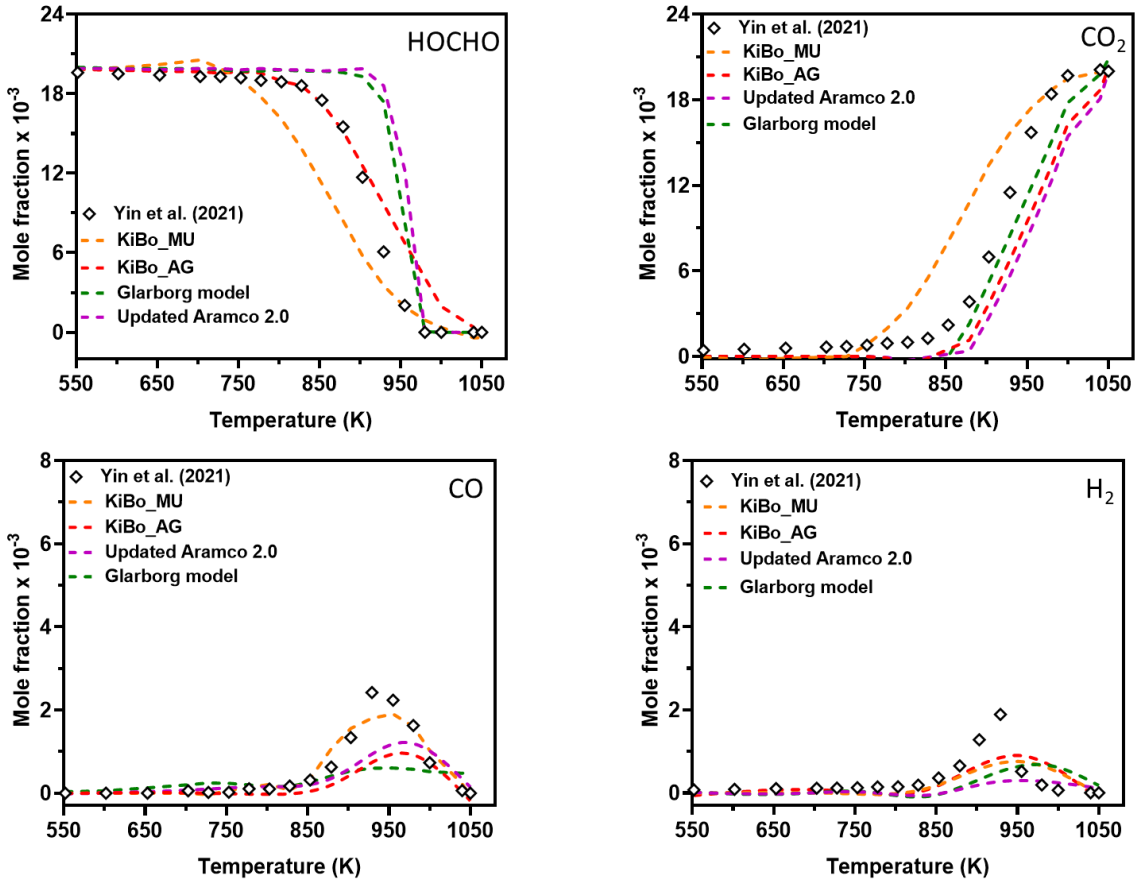

Figure 36. Mole fraction profiles of HOCHO, CO_2, CO and H_2 at temperatures of 500 – 1100 K, equivalence ratio of 0.5, atmospheric pressure, and residence time of 2 s.

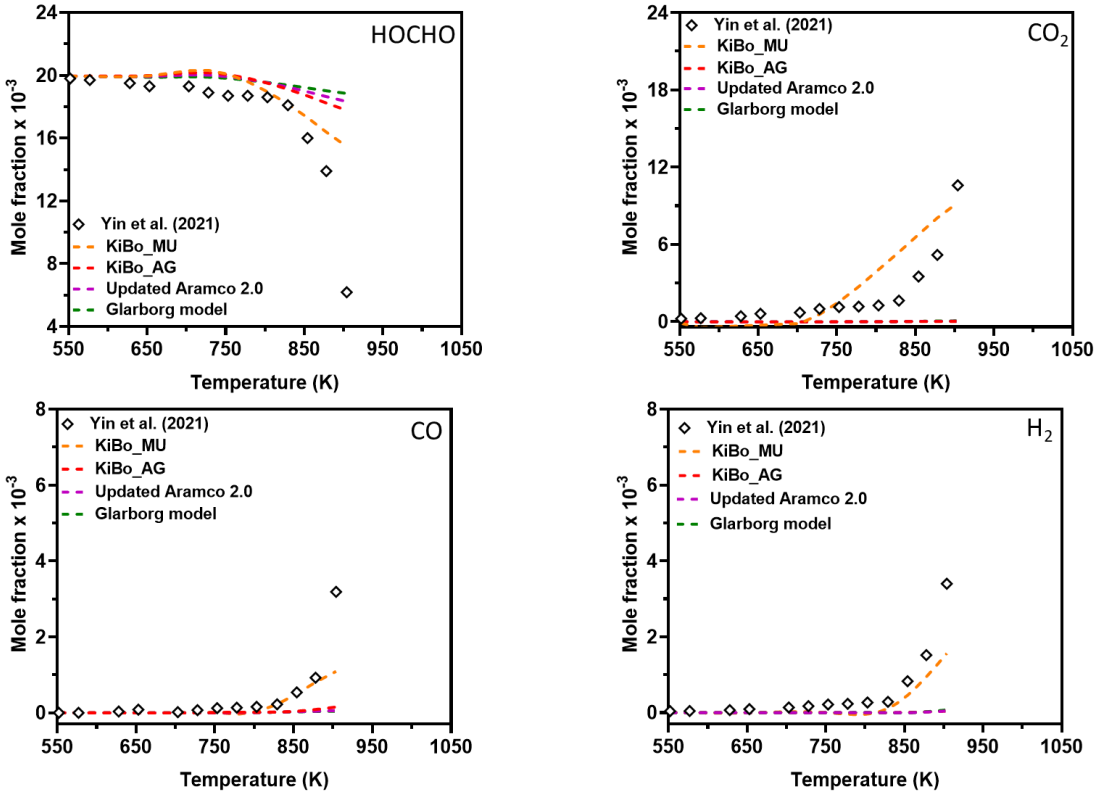

Figure 37. Mole fraction profiles of HOCHO, CO_2, CO and H_2 at temperatures of 500 – 1100 K, equivalence ratio of 1.0, atmospheric pressure, and residence time of 2 s.

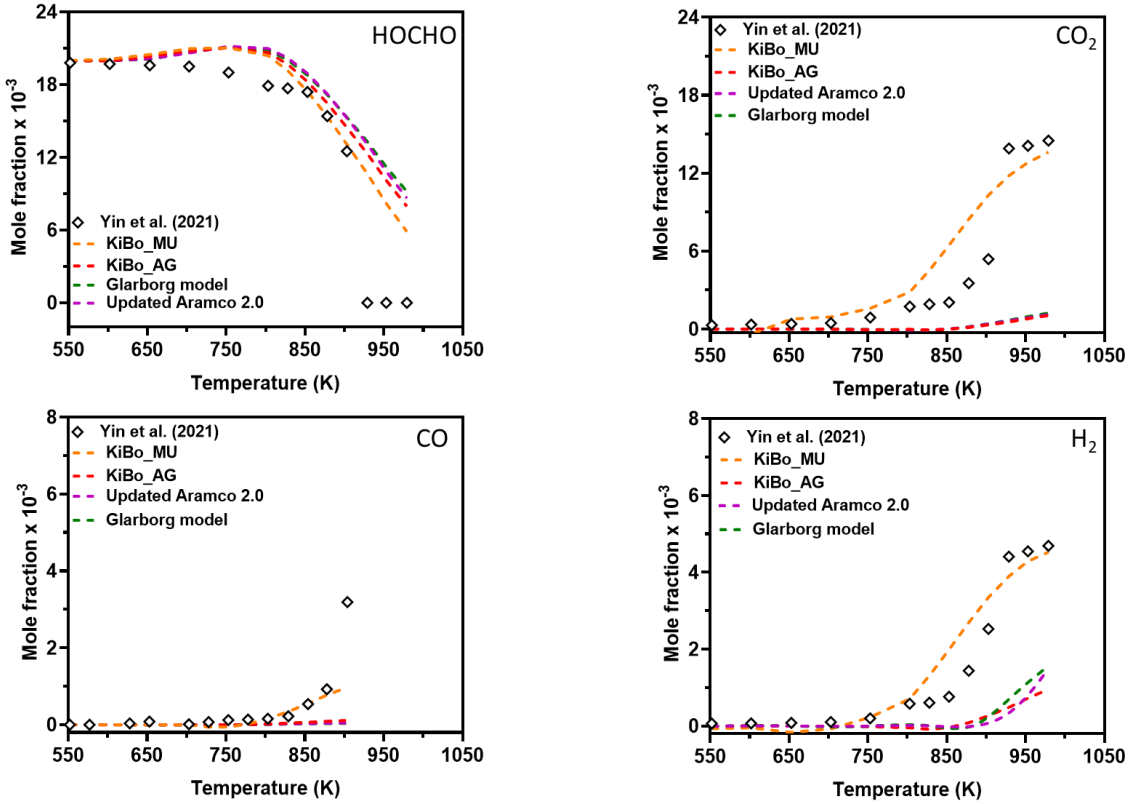

Figure 38. Mole fraction profiles of HOCHO, CO_2, CO and H_2 at temperatures of 500 – 1100 K, equivalence ratio of 2.0, atmospheric pressure, and residence time of 2 s.

Regardless of the investigated composition, numerical models show that formic acid does not auto-ignite at intermediate temperatures, as also observed at higher pressure [354]. From the thermal decomposition of HOCHO at intermediate temperatures, the active onset decomposition temperature and complete consumption of HOCHO are found to be at 803 K, and 1050 K, respectively. From the simulation result using KiBo_MU at lean conditions, around 42 % of HOCHO was consumed at 903 K and 36 % consumed within a temperature range of 929 – 955 K whereas, 14 % and 50 % of HOCHO were consumed, respectively at 903 K and 929 – 955 K in case of KiBo_AG. From the experimental result reported by Yin et al. [346], 30 % of HOCHO was consumed at 903 K while 31 % was consumed within a temperature range of 929 – 955K. Similarly, under stoichiometric condition, more than 95 % of HOCHO get consumed within a temperature range of 878 – 903 K using KiBo_MU and KiBo_AG, where around 70 % of HOCHO decomposed according to the experimental result from Yin et al. [346] under the same temperature range. According to KiBo_MU, in rich flames 1/3 of HOCHO gets consumed within the temperature range of 803 – 903 K. Conversely, KiBo_AG indicates that only 1/10 of HOCHO gets consumed within a temperature range of 803 – 903 K. Both mechanisms agree on the whole consumption before the reaching 1000 K. The reason for the difference in KiBo_MU and KiBo_AG in predicting the decomposition of formic acid might be due to the difference in rate coefficients associated with reactions at intermediate temperatures; HOCHO + O ↔ HOCO + OH, HOCHO + O ↔ OCHO + OH and 2 HOCO ↔ CO_2 + HOCHO which are only incorporated in KiBo_AG and the rate coefficients derive from estimations. However, from the jet-stirred result, around 85% of formic acid gets consumed between 803 – 903 K.

The decarboxylation reaction (i.e., HOCHO ↔ CO_2 + H_2) and hydrogen abstraction reaction by HO_2 (i.e., HOCHO + HO_2 ↔ HOCO + H_2O_2, HOCHO + HO_2 ↔ OCHO + H_2O_2), OCHO ↔ CO_2 + H and abstraction reaction of hyroxycarboxyl radical by O_2 (i.e., HOCO + O_2 ↔ CO_2 + H_2O_2) are found to be the key reactions affecting decomposition of HOCHO under the probed condition. Even though, the rate coefficients of these reactions were taken from *ab initio* it seems they have to be revised for better agreement of the HOCHO consumption and production of combustion products. The current models' results are also compared with the recently reported formic acid mechanism from the Saudi Aramco research group (Updated Aramco 2.0) and the first formic acid kinetic model (i.e., Glarborg kinetic model). Overall, KiBo_MU showed better agreement for all species however, KiBo_AG showed some variation, especially

for CO_2 and H_2. Comparably, our models capture fairly the experimental observations than the Updated Aramco 2.0 and Glarborg kinetic models.

4.1.2.3 High-temperature combustion

The kinetic models have been validated and used for the evaluation of the high-temperature combustion phenomena through the investigation of ignition delay times from shock tubes at ranges of reaction conditions. Details of the results are shown below for each species.

4.1.2.3.1 Methanol

In this section, shock tube ignition delay time has been investigated using KiBo_MU kinetic model under ranges of reaction conditions (i.e., temperature, pressure) and equivalence ratios have been studied. The numerical results obtained in the present study with the corresponding experimental result from literature and results using widely validated models from literature are shown below in Figures 39 – 41. The IDT of methanol/O_2/Ar mixtures under lean conditions and ranges of reaction temperatures has been shown in Figure 39 (a & b).

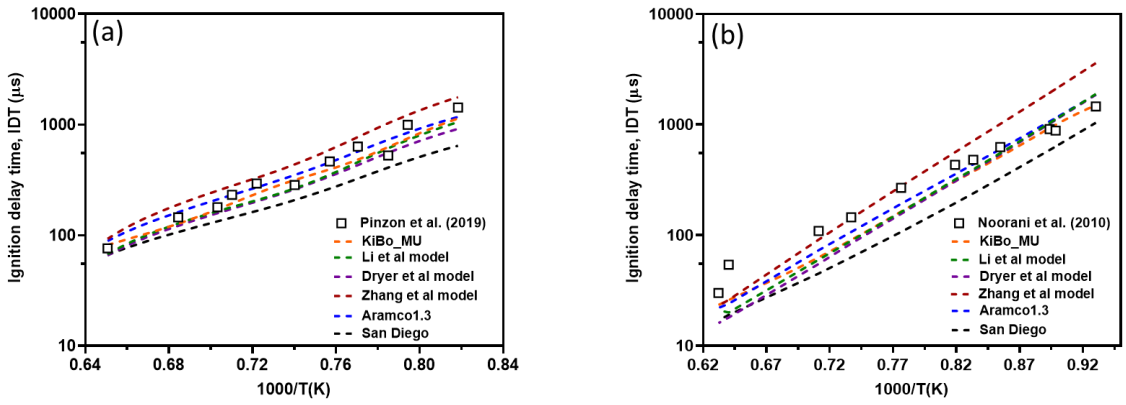

Figure 39. Ignition delay time of methanol/O_2/Ar mixtures at φ = 0.5, 1.3 bar (a) and 11.6 bar (b).

For average pressure of 1.3 bar and temperature range of 1220 –1540 K, KiBo_MU captured the IDT very well. In the same way for an average pressure of 11.6 bar and temperature range of 1075 – 1582 K, KiBo_MU kinetic model mimicked well the experimental ignition delay times. Under the tested conditions, KiBo_MU predicted results are in the range of less than 10 % variations from the experimental results and showed better accuracy than Li et al, Dryer et al, Zhang et al, Aramco1.3 and San Diego kinetic models. Comparably, San Diego kinetic model showed a large variation than the others. The reason for such variation could be

associated with rate coefficients of reactions; $CH_3OH + HO_2 \leftrightarrow CH_2OH + H_2O_2$ and H_2O_2 (+ M) ↔ 2 OH (+ M) which are the most sensitive reactions having strong positive sensitivity effect on IDT at an equivalence ratio of 0.5 and average pressure of 1.3 bar. The rate coefficients of these reactions incorporated in KiBo_MU respectively were taken from ab initio calculations [355] and [356] while the source of the reaction parameters was not mentioned in the case of the San Diego kinetic model.

Even though all the investigated models showed fair agreement against experimental IDT at a temperature greater than 1200 K, only KiBo_MU captured the IDT fairly at all investigated temperatures. More specifically, the model from Zhang et al overpredicted the IDT for temperatures less than 1200 K while San Diego kinetic model under-predicted. Overall, it can be seen from both plots (Figures 39 (a & b) that a 10-fold increase in pressure leads to a sharp drop in IDT. For example, at a temperature of 1222 K and an average pressure of 1.3 bar, an IDT value of 1425 µs was obtained, while at the same temperature, increasing the pressure by a factor of 10 reduced the IDT to 275 µs.

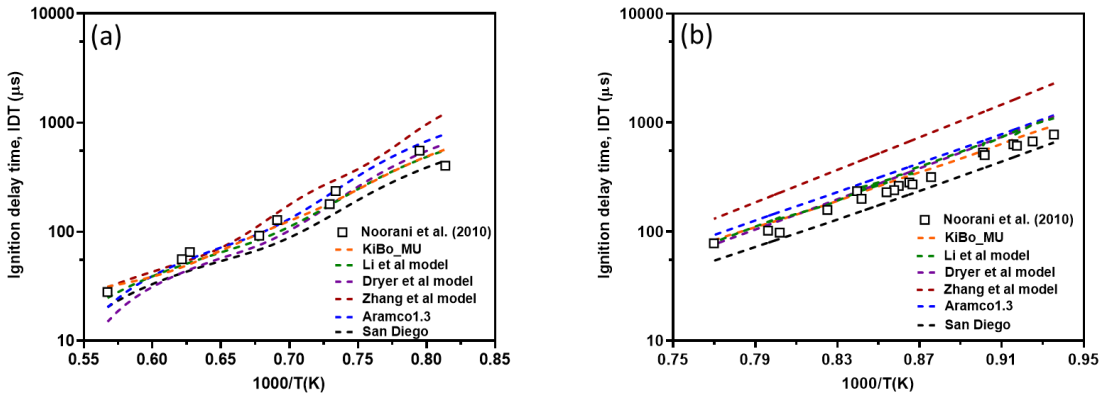

Figure 40. Ignition delay time of methanol/O_2/Ar mixtures at φ = 1.0, 2.0 bar (a) and 10 bar (b).

On the other hand, ignition delay times data of methanol/O_2/Ar mixtures at stoichiometric conditions and ranges of temperatures is depicted in Figure 40 (a & b). From Figure 40(a), for an average pressure of 2 bar and temperature range of 1229 – 1763 K, the numerical results obtained by KiBo_MU showed a fair agreement with the experimental result [54] and indeed all the investigated mechanisms showed good agreement with experimental data. Likewise, for a pressure of 10 bar and temperature range of 1069 – 1299 K, the present study is in excellent agreement with the experimental result, and apart from Zhang et al kinetic model which over-predicted the IDT, all the investigated mechanisms captured the experimental result well.

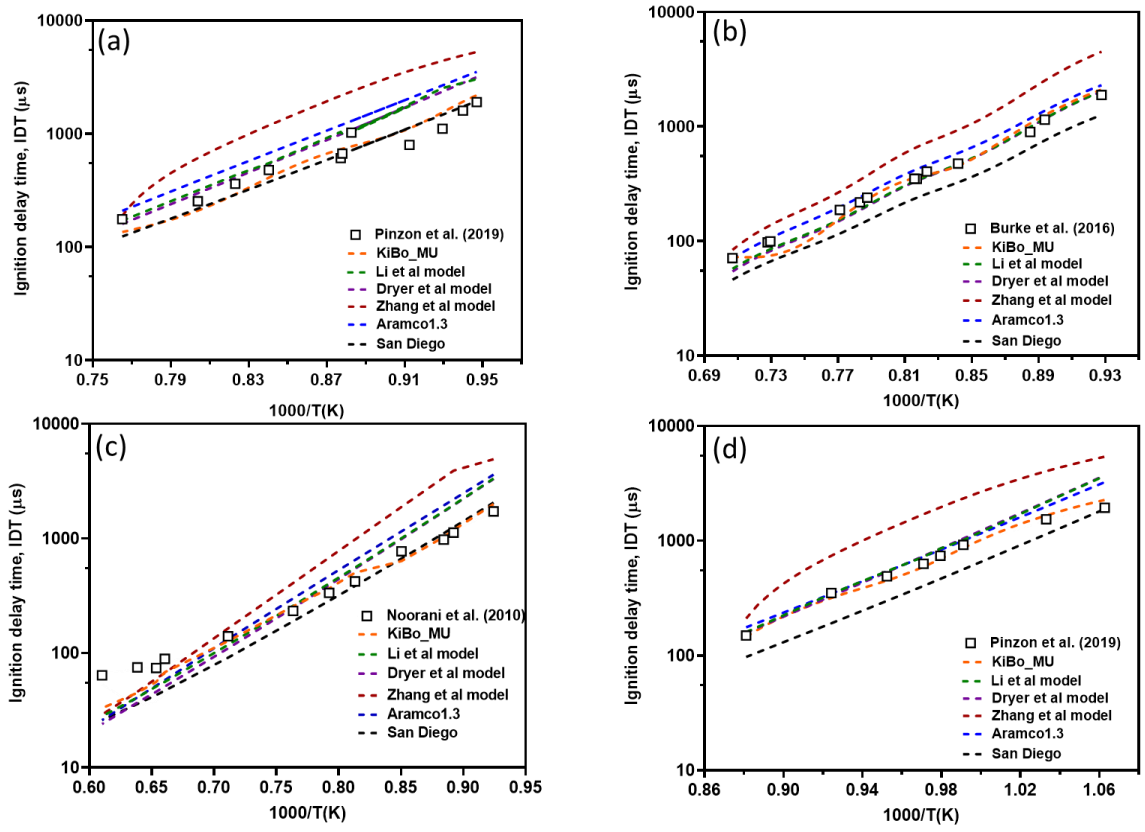

Figure 41. Ignition delay time of methanol/O_2/Ar mixtures at φ = 2.0, 1.6 bar (a), 1.8 bar (b), 2.2 bar (c) and 12.4 bar (d).

Furthermore, in the case of rich flames, an investigation of IDT has been performed at temperature 1055 – 1640 K, pressure 1.5 – 12.5 bar, and the results are shown in Figure 41 (a – d). As can be seen from figure 41 (a – c) for pressures 1.6 bar, 1.8 bar, 2.2 bar and temperature ranges, 1056 – 1307 K, 1078 – 1415 K, and 1082 – 1639 K, respectively, KiBo_MU kinetic model mimicked the experimental data very well. Apart from Zhang et al kinetic model, which over-predicted the IDT, all the investigated mechanisms captured the IDT fairly. Comparably, KiBo_MU again showed lower uncertainty towards IDT under the investigated conditions when compared to the other kinetic models. Likewise, for a pressure of 12.4 bar and temperature range of 941 – 1135 K, as shown in Figure 41(d), KiBo_MU fairly captured the IDT and shows better consistency. However, Zhang et al kinetic model again showed a large variation by overpredicting IDT followed by San Diego kinetic model which underestimated the IDT.

In general, from the ignition delay time study of methanol combustion performed at different reaction conditions, it has been observed that $CH_3OH + HO_2 \leftrightarrow CH_2OH + H_2O_2$, H_2O_2 (+ M) $\leftrightarrow$ 2 OH (+ M), 2 $HO_2 \leftrightarrow H_2O_2 + O_2$ and H + OH (+ M) $\leftrightarrow H_2O$ (+ M) were key reactions impacting methanol oxidation in intermediate and high temperatures. Overall, except for a few conditions (i.e., φ = 2.0, T= 122 K), $CH_3OH + HO_2 \leftrightarrow CH_2OH + H_2O_2$ was found to be very sensitive to IDT and largely dominates uncertainty in the predicted ignition delay time of methanol. For instance, the variation in ignition delay time data observed for the investigated models is mostly derived from the difference in rate coefficients of this reaction. In particular, the noticeable effect of the kinetics of this reaction on the ignition delay times is more profound at high pressures and low temperatures, relevant to real combustion engines (>10 atm and 1000 − 1200 K). There have been theoretical studies on the effect of this reaction on the ignition delay time with the recent study reported by Klippenstein et al.[197] but, the literature provides no direct experimental measurement for this reaction. Overall, the current model fairly captured the experimental ignition delay time data under the investigated conditions and even in some cases showed better accuracy than the other investigated methanol kinetic models.

4.1.2.3.2 Ethanol

The high-temperature combustion of ethanol oxidation has been studied through the investigation of ignition delay time under different reaction conditions and fuel compositions. Results from the present kinetic model and other kinetic models from the literature, as well as experimental results from literature, are provided in Figures 42 – 44.

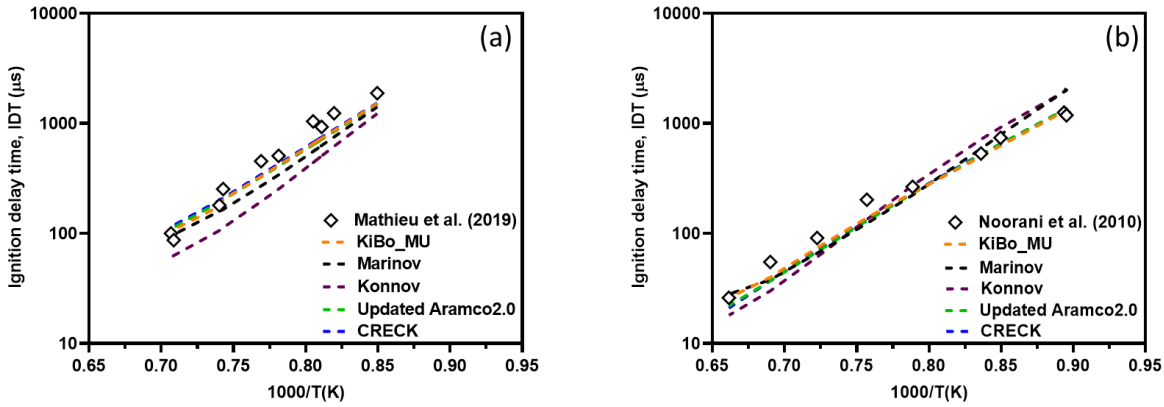

Figure 42. Ignition delay time of ethanol/O_2/Ar mixtures at φ = 0.5, 1.3 bar (a) and 11.6 bar (b).

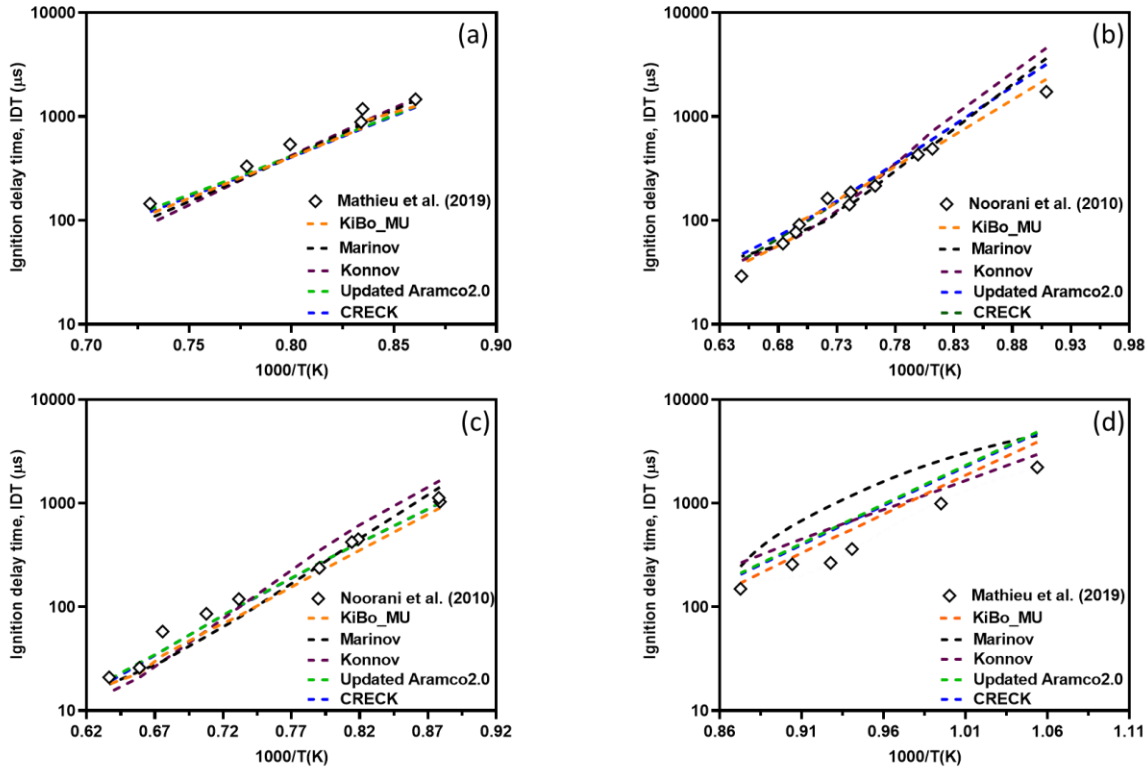

Figure 43. Ignition delay time of ethanol/O_2/Ar mixtures at φ = 1.0, 1.3 bar (a), 2.3 bar (b), 9.8 bar (c) and 12.6 bar (d).

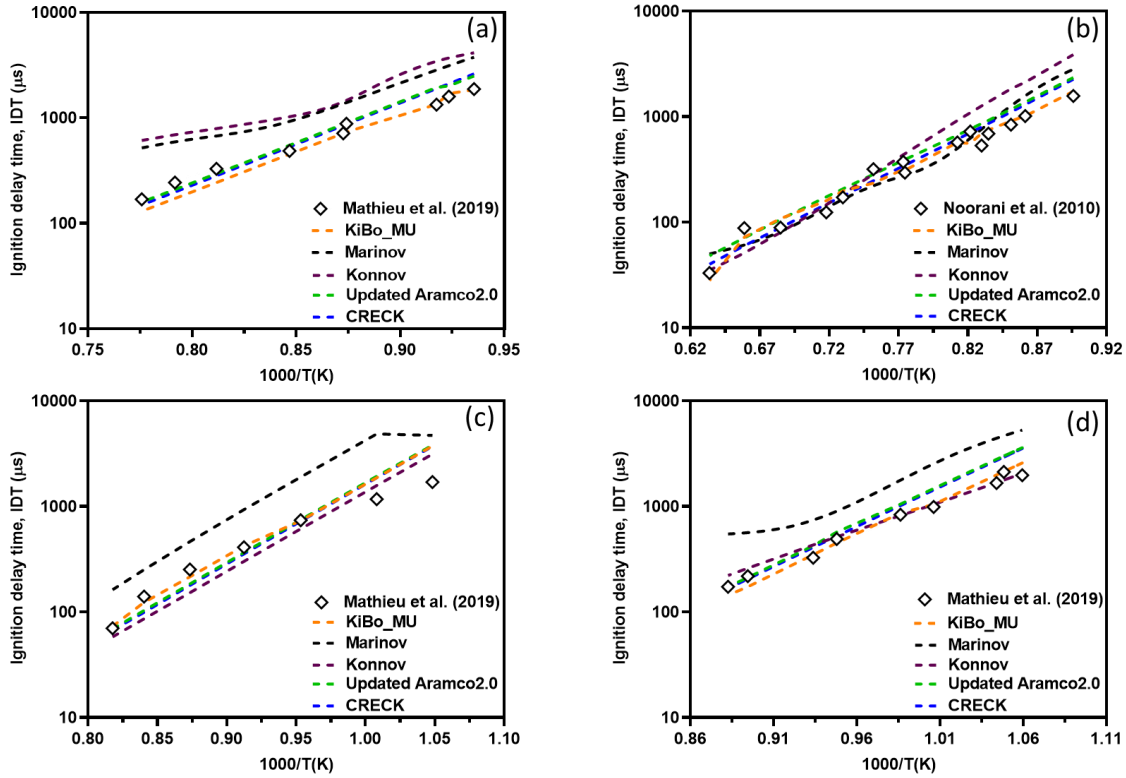

Figure 44. Ignition delay time of ethanol/O_2/Ar mixtures at φ = 2.0, 1.7 bar (a), 2.2 bar (b), 10 bar (c) and 12.9 bar (d).

Figures 42 (a & b) depicts the ignition delay times of ethanol/O_2/Ar mixtures at φ = 0.5, an average pressure of 1.3 and 11.6 bar, and a reaction temperature range of 1177 – 1411 K, and T = 1117 – 1512 K, respectively. As can be seen from the figures, under the investigated conditions, KiBo_MU attempted the IDT fairly and the results are in good agreement with the shock tube experimental data reported here [54, 214]. Increasing the mean pressure from 1.3 bar to 11.6 bar significantly reduced the IDT. For example, at 1177 K, the IDT was found to be 1513 μs for 1.3 bar, which decreased to 625 μs when the average pressure was increased by a factor of 10. This shift in IDT with pressure is consistent with the experimental results considered for validation. Overall, the present study showed a consistent trend with experimental results and results obtained using other available ethanol kinetic models such as Marinov [95], Konnov [357], Aramco1.3 [206] and CRECK [222] kinetic models. Moreover, IDT results for pressure ranges of 1.3 – 12.6 bar, temperature range of 950 – 1570 K and stoichiometric conditions are shown in Figure 43 (a – d). Experimental results considered for validation were taken from a shock tube study reported by Mathieu et al. [214] and Noorani et al. [54]. Under the studied conditions, KiBo_MU predicted the IDT well and is in good agreement with the experimental results. Overall, apart from a few variations observed at 949 K and 12.6 bar, the present study is in excellent agreement. Even though discrepancies at this particular condition are the case for all the investigated mechanisms, compared to others, KiBo_MU showed fewer deviations while Marinov kinetic model presented large variations. The overprediction at this particular condition could be due to rate coefficients associated with H_2O_2 (+ M) ↔ 2 OH (+ M), $C_2H_5OH + HO_2 \leftrightarrow C_2H_5O + H_2O_2$ and $H + HO_2 \leftrightarrow SC_2H_4OH + H_2O_2$ reactions which are important reactions promoting the IDT at the aforementioned conditions. Thus, the difference in prediction accuracy of the kinetic models can be related to the differences in kinetic parameters of these reactions incorporated in the mechanisms.

Furthermore, the numerical study of the IDT of ethanol/O_2/Ar mixtures at φ = 2.0, T = 1069 – 1578 K and average pressure range of 1.7 – 12.9 bar are shown in Figures 44 (a – d). Under the investigated conditions, the present study agreed well with the experimental results, and even compared with the other models, KiBo_MU showed better agreement, especially at 1069 and 1083 K where the other mechanisms showed larger discrepancies, KiBo_MU attempted well.

4.1.2.3.3 Acetaldehyde

The shock-tube ignition delay time of acetaldehyde/O_2/Ar mixtures within the temperature range of 1250 – 1700 K, pressure range of 1.6 – 4.0 atm and equivalence ratios of 0.5, 1, 1.5 and 2 were studied using KiBo_MU and KiBo_AG kinetic models. The computed ignition delay times at lean, stoichiometric and rich conditions are shown in Figures 45 – 47, respectively.

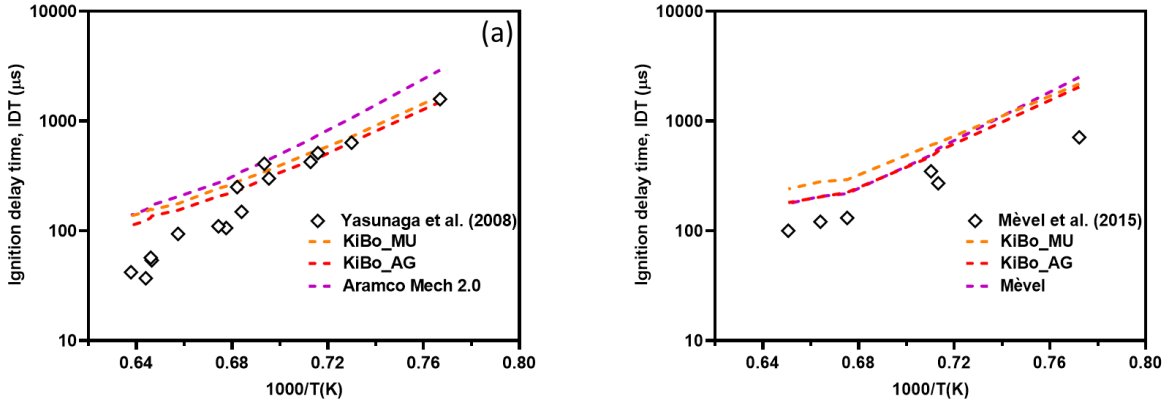

Figure 45: Ignition delay times of acetaldehyde/oxygen/argon mixtures: a) φ = 0.5, P = 1.6 – 2.3 atm, 94 %v/v Ar, b) φ = 0.5, P = 3.2 – 3.9 atm, 97 %v/v Ar.

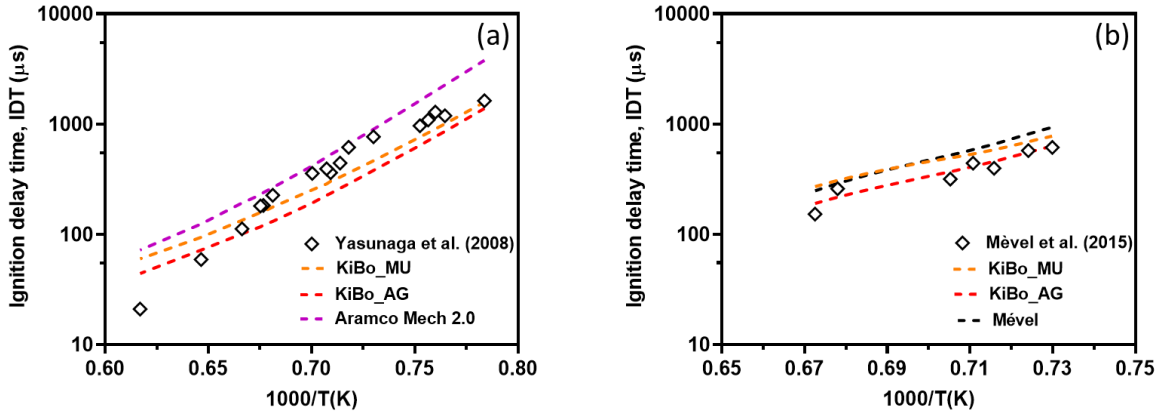

Figure 46: Ignition delay times of acetaldehyde/oxygen/argon mixtures: a) φ = 1.0, P = 1.7 – 2.6 atm, 93 %v/v Ar; b) φ = 1.0, P = 3.6 – 4.0 atm, 97 % v/v Ar.

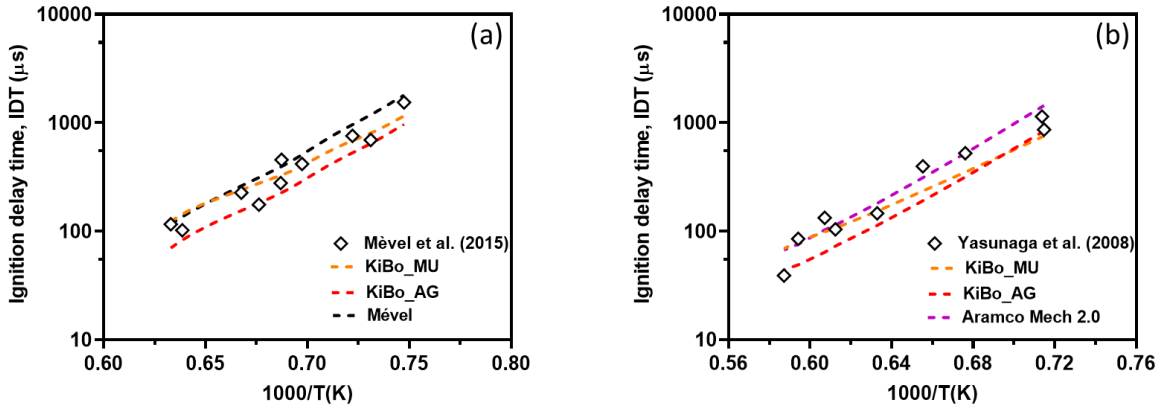

Figure 47: Ignition delay times of acetaldehyde/oxygen/argon mixtures: a) φ = 1.5, P = 3.0 – 3.5 atm, 94 %v/v Ar; b) φ = 2.0, P = 1.9 – 2.7 atm, 96 %v/v Ar.

As shown in Figure 45(a), KiBo_MU and KiBo_AG kinetic models better reproduced the experimental data at all initial temperatures, whereas Aramco Mech2.0 over-predicted the IDT data at temperatures < 1300 K. Similarly, from Figure 45(b), it can be seen that KiBo_MU and KiBo_AG kinetic models fairly mimicked the experimental data for temperatures > 1300 K. However, both kinetic models over-predicted the ignition delay time at an initial temperature of 1295 K. The same behaviour has been observed for the kinetic model developed by Mevel [259]. To better understand the reactions causing the over-prediction, sensitivity analysis was performed at T = 1295 K, P = 3.4 atm, φ = 0.5 and the result is shown in the following section. Despite a few discrepancies shown in Figure 46(a), KiBo_MU and KiBo_AG kinetic models reproduced the ignition delay time quite fairly. Whereas, Aramco Mech2.0, showed larger deviations, especially for temperatures < 1400 K. Comparably, KiBo_MU and KiBo_AG showed better agreement than Aramco Mech2.0, which tends to overpredict this parameter. Conversely, as shown in Figure 46(b), only KiBo_AG can accurately catch the trend at moderate pressure while KiBo_MU kinetic model slightly over-predicted. The same trend of over-prediction is observed in the case of the Mevel kinetic model. Lastly, under rich conditions, as shown in Figure 47(a), KiBo_MU and KiBo_AG kinetic models fairly mimicked the IDT even though KiBo_MU kinetic model looks to show better agreement. In the same way, the Mevel kinetic model was attempted quite reasonably. Similarly, as shown in Figure 47(b) for rich conditions, KiBo_MU kinetic model better predicted the IDT at higher temperatures however, slightly under-predicted at moderate temperatures. Whereas, KiBo_AG kinetic model is slightly under-predicted at moderate temperatures but shows better agreement at higher temperatures. In general, the oxidation chemistry of acetaldehyde is mainly affected

by unimolecular decomposition reaction via C–C fission (i.e., CH_3CHO (+ M) ↔ CH_3 + HCO (+ M)) forming methyl and formyl radicals. Besides, acetaldehyde can undergo H atom abstraction reactions either at methyl group forming methylene radical (CH_2CHO) via $CH_3CHO + H \leftrightarrow CH_3CO + H_2$ reaction or at acetyl group resulting in acetyl radical (CH_3CO) through $CH_3CHO + H \leftrightarrow CH_2CHO + H_2$. The rate parameters of these important reactions have been taken from the study reported by Harding et al. [358] and Hashemi et al. [223], respectively. The rate coefficients considered in the present study are in good agreement with experimental and theoretical rate constants under the studied conditions. Overall, despite the few deviations, KiBo_MU and KiBo_AG kinetic models fairly reproduced the experimental IDT.

Besides, the evaluation of the overall reactivity and concentration profile, the availability of numerical tools like the detailed kinetic mechanisms developed in this work allows for the evaluation of the chemistry and reactions ruling the whole process. In this view, a sensitivity analysis was performed to elucidate the effect of specific rate constants that contributed to the differences between the model and experiments as shown in Figure 48. Considering the size of the mechanism, sensitivity analysis has been performed using KiBo_MU at conditions where a large deviation has been observed (i.e., at 1295 K, 3.4 bar and φ = 0.5).

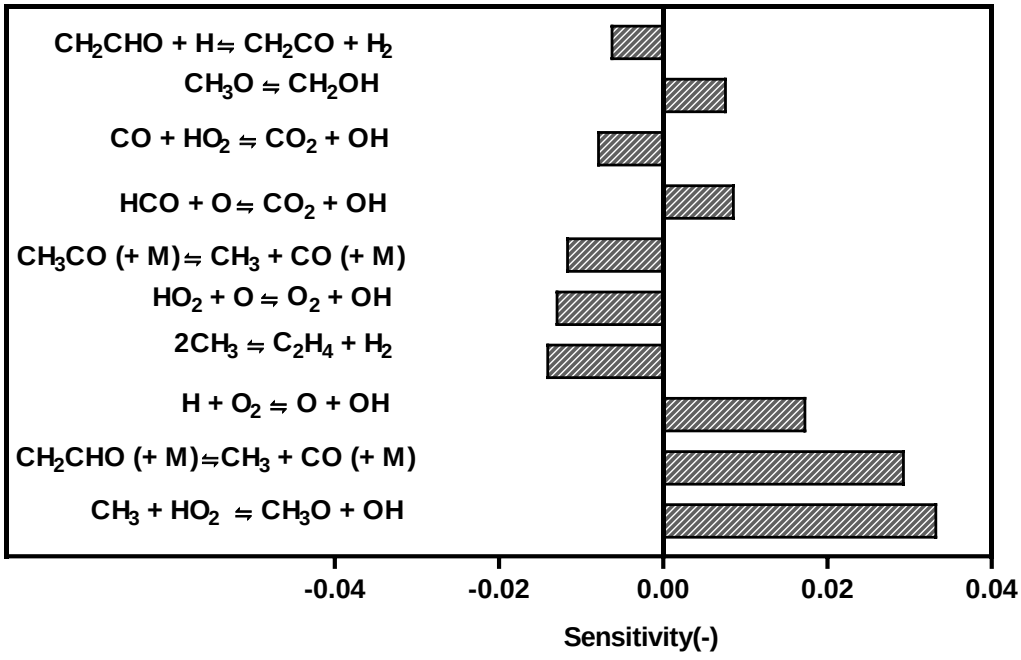

Figure 48: Sensitivity coefficients for ignition delay times of acetaldehyde/O_2/Ar mixtures at; T = 1295 K, P = 3.4 atm, φ = 0.5 using KiBo_MU kinetic model.

As can be seen from the figure, $CH_3 + HO_2 \leftrightarrow CH_3O + OH$, $CH_2CHO (+ M) \leftrightarrow CH_3 + CO (+ M)$ and $H + O_2 \leftrightarrow O + OH$, respectively are the most influential reactions promoting the IDT of acetaldehyde at the aforementioned reaction condition. On the other hand, $2\ CH_3 \leftrightarrow C_2H_4 + H_2$, $HO_2 + O \leftrightarrow O_2 + OH$ and $CH_3CO (+ M) \leftrightarrow CH_3 + CO (+ M)$ are the main reactions inhibiting the reactivity of acetaldehyde oxidation. Detailed discussion on the main reactions and their rate parameters sources can be found in the paper published by the author as part of this work as shown below.

FM Wako., G Pio., E Salzano., Modelling of acetaldehyde and acetic acid combustion., Combustion Theory and Modelling, 2023

Theoretical kinetics provides a valuable means for improving the fidelity of chemical kinetic mechanisms for conditions that are difficult to explore experimentally. In this regard, kinetic mechanisms accounting for the chemistry of biomass components and different light-oxygenated compounds have been developed. Pyrolyzed product distributions and relevant combustion parameters (i.e., laminar burning velocity, species profile and ignition delay times) addressing the low-temperature, intermediate-temperature and high-temperature combustion were investigated. A wide range of reaction conditions and fuel compositions have been addressed during the validation. Under the studied conditions, kinetic mechanisms from the present study showed a very good agreement with the experimental studies reported in the current literature. Overall, KiBo_MU and KiBo_AG showed good estimation quality with a narrow range of uncertainty which can be observed from the results shown above. The accuracy of the mechanisms also allowed for further analysis of the detailed chemistry of the systems and investigation of key important radicals and reactions governing the oxidation of oxygenated components.

Chapter 5: Conclusion and Future directions

5.1 Conclusive remarks

The development of sustainable solutions to tackle climate change is one of the major challenges facing humanity. The need to reduce these environmental impacts requires complex and multidisciplinary approaches to be truly effectively overcome. The investigation of biomass energy as one possible alternative source for energy supply requires accurate models simulating biomass pyrolysis and biofuel oxidation.

The present work aimed at the characterization of chemical and physical phenomena ruling the decomposition and oxidation of bio-based fuels. Theoretical-based approaches as well as empirical methods were tested and compared. The quality of the produced models was tested against experimental data from the literature in a wide range of operative conditions and compositions. Safety and kinetic aspects were addressed and combined to identify the most relevant features for energy production. The observations and analyses of the gathered data have allowed for the acquisition of further knowledge on the topic. The main findings related to this work are listed below:

- Heat transfer and reaction rates during biomass conversion are strongly influenced by biomass composition and reactor configuration, thereby affecting yield profiles and compositions. Ultimately, the variations in biofuel composition will eventually dictate the combustion characteristics. Indeed, the presence of oxygen atoms limits the production of aromatic compounds, improves combustion efficiency (thus heat production) and alleviates the formation of carbon soot. On the other hand, the variability of their composition has represented one of the major challenges for the complete characterization of combustion behaviour. With different technologies in development to increase efficiency in ICEs, enabling the almost immediate implementation of alternative fuels requires effective characterization of the individual biofuel components.
- From a kinetics perspective, accurately capturing the molecular conversion kinetics requires in-depth knowledge of how the sub-components of the feedstocks decompose, intermediate species formed/consumed and desired products produced. Pyrolysis being the first step in the energy recovery process and combustion being the subsequent process, the knowledge of both solid-phase and gas-phase chemistry is vital for the

complete characterization of oxy-biofuels. Solid-phase kinetics describe the degradation kinetic chemistry of how individual biomass reference components degrade to form intermediate species and light oxygenates, while gas-phase kinetics address how the light-oxygenated components oxidize in an oxidative environment.

- For the gaseous phase, two different strategies were followed; a simplified kinetic mechanism; KiBo_MU and an automated mechanism; KiBo_AG. The former contains 141 species and 453 reactions, whereas, the latter comprises 631 species and 28329 reactions. The solid-phase kinetics (i.e., pyrolysis kinetic mechanism) was tested using Aspen plus to simulate the biomass pyrolysis process and evaluate pyrolysis product distribution profiles while, KiBo_MU and KiBo_AG were used to study combustion phenomena and validated against experimental combustion data available in the literature.
- Different combustion parameters have been investigated for the sake of model validation to be representative of a wide range of conditions. More specifically, laminar burning velocity was considered as representative for the overall reactivity at low temperatures combustion, species profile from jet-stirred reactor and ignition delay times from RCM for intermediate temperatures, and ignition delay times from shock tubes for high-temperature combustion.
- Under the studied conditions, the kinetic mechanism, KiBo_MU and KiBo_AG showed good agreement with the experimental data reported in the works of literature. The accuracy of the generated mechanisms allowed for further analysis of the chemistry of the system, enlightening some determining aspects of the chemistry of the oxygenated species. Overall, KiBo_MU and KiBo_AG showed better accuracy than the other investigated kinetic models from the literature and proved to be robust mechanisms for light-oxygenated species, and can also be used as seed mechanisms for developing kinetic models for larger biofuel components.

Overall, the work combines newly developed detailed kinetic mechanisms for solid-phase and gas-phase reactions governing biomass pyrolysis process and biofuel combustion chemistry, respectively. The influence of feedstock variability and structural differences of biomass sub-components on the chemistry of the process and product distribution was emphasized. In addition, overall reactivity, energy production, intermediates and product distributions from combustion of biofuel components from different chemical families has been investigated. The

realization of a model integrating these chemical processes plays a fundamental role in designing of efficient reactors and combustors based on biofuels. Moreover, the acquired knowledge can be adopted to accurately predict the production and consumption pathway of common species, as well as the entire energy production processes, which could contribute to overcoming main biofuel application challenges.

5.2 Future directions

All the analyses performed in this project have been used as a way to illustrate physical-chemical phenomena of biomass components and predict the overall reactivity of common oxy-biofuels from different chemical families. The accuracy of the kinetic mechanisms in mimicking the fundamental phenomena indicates the ability and relevance of the mechanisms to explore experimental conditions. Even though, the kinetic models can potentially be used for characterizing the physical-chemical aspects of the target components, the basic idea to meet ever tighter efficiency and emission limits requires investigation of different practical fuel components and intermediate radicals at engine relevant conditions from both chemical and safety practical aspects. In this view, the results presented in this thesis can be also considered as an essential building block for future technological developments and research activities. As a way of example, a shortlist of activities debottlenecked by the obtained data is reported below:

- Although pyrolysis oil is environmentally friendly, its fuel performance is still lower than that of fossil fuels, especially in terms of combustion efficiency. The high content of oxygen molecules in the pyrolysis oil is the cause of the problem. Furthermore, representing biomass pyrolysis by unimolecular decomposition reactions of biomass sub-components and some intermediate species alone is insufficient to represent the entire pyrolysis process as important chemical components are likely to be missed. In this regard, enlarging the kinetic mechanism by including further breakdown of major intermediate pyrolysis products (i.e., levoglucosans, phenols, high molecular weight alcohols and aldehydes, and lignin intermediates) into lighter components can help improve the yield of desired fractions and at same time reduce oxygen functionality of the components apparently improving the heating value.
- The lack of experimental data limited the range of operative conditions to be considered for validation goals. As a way of example, validation was limited to low temperature and intermediate temperatures for acetic acid and formic acid. Thus, the

future activities could be devoted to the collection of additional data at intermediate and high temperatures of these carboxylic acids.

- Unbalanced reaction conditions can lead to safety problems in chemical plants. The role of chemical kinetic model in revealing the optimal safe conditions is crucial in this aspect due to costs associated with experimental approaches. So, the future work may include extending the validation of these documented chemistry databases to study the safety aspects of the chemical systems
- Further upgrading the mechanisms to include the chemistry of larger biofuel components which are being commercialized and potentially replace fossil fuels.
- The detailed kinetic mechanism developed in this project (KiBo_AG) is huge in size as it comprises large number of species and reactions, which is computationally costly to run. Thus, systematic reduction of the skeletal mechanism without compromising its accuracy is undoubtedly important for the wide application of the model in industrial sectors. To this aim, the future work will focus on further reducing the size of KiBo_AG kinetic mechanism for the convenience of its use.

Reference

[1] S. Solomon, M. Manning, M. Marquis, and D. Qin, *Climate change 2007-the physical science basis: Working group I contribution to the fourth assessment report of the IPCC*, Vol. 4, Cambridge university press, 2007.

[2] K. Yasunaga, T. Mikajiri, S.M. Sarathy, T. Koike, F. Gillespie, T. Nagy, J.M. Simmie, and H.J. Curran, *A shock tube and chemical kinetic modeling study of the pyrolysis and oxidation of butanols*, Combustion and Flame 159 (2012), pp. 2009-2027.

[3] S. Ma, G. Chen, M. Guo, L. Zhao, T. Han, and S. Zhu, *Path analysis on CO2 resource utilization based on carbon capture using ammonia method in coal-fired power plants*, Renewable and Sustainable Energy Reviews 37 (2014), pp. 687-697.

[4] Y. Yang, P.E. Campana, and J. Yan, *Potential of unsubsidized distributed solar PV to replace coal-fired power plants, and profits classification in Chinese cities*, Renewable and Sustainable Energy Reviews 131 (2020), p. 109967.

[5] N. Maamoun, R. Kennedy, X. Jin, and J. Urpelainen, *Identifying coal-fired power plants for early retirement*, Renewable and Sustainable Energy Reviews 126 (2020), p. 109833.

[6] R. Clark, N. Zucker, and J. Urpelainen, *The future of coal-fired power generation in Southeast Asia*, Renewable and Sustainable Energy Reviews 121 (2020), p. 109650.

[7] C.-k. Gao, H.-m. Na, K.-h. Song, N. Dyer, F. Tian, Q.-j. Xu, and Y.-h. Xing, *Environmental impact analysis of power generation from biomass and wind farms in different locations*, Renewable and Sustainable Energy Reviews 102 (2019), pp. 307-317.

[8] P. Das, V. Chandramohan, T. Mathimani, and A. Pugazhendhi, *Recent advances in thermochemical methods for the conversion of algal biomass to energy*, Science of The Total Environment 766 (2021), p. 144608.

[9] ---, *A comprehensive review on the factors affecting thermochemical conversion efficiency of algal biomass to energy*, Science of The Total Environment 766 (2021), p. 144213.

[10] X. Hu, and M. Gholizadeh, *Biomass pyrolysis: A review of the process development and challenges from initial researches up to the commercialisation stage*, Journal of Energy Chemistry 39 (2019), pp. 109-143.

[11] A.V. Bridgwater, *Review of fast pyrolysis of biomass and product upgrading*, Biomass and bioenergy 38 (2012), pp. 68-94.

[12] K. Openshaw, *Biomass energy: employment generation and its contribution to poverty alleviation*, Biomass and bioenergy 34 (2010), pp. 365-378.

[13] T. Mathimani, A. Baldinelli, K. Rajendran, D. Prabakar, M. Matheswaran, R.P. van Leeuwen, and A. Pugazhendhi, *Review on cultivation and thermochemical conversion of microalgae to fuels and chemicals: process evaluation and knowledge gaps*, Journal of cleaner production 208 (2019), pp. 1053-1064.

[14] A.P. Saravanan, A. Pugazhendhi, and T. Mathimani, *A comprehensive assessment of biofuel policies in the BRICS nations: Implementation, blending target and gaps*, Fuel 272 (2020), p. 117635.

[15] R.N. Colvile, E.J. Hutchinson, J.S. Mindell, and R.F. Warren, *The transport sector as a source of air pollution*, Atmospheric Environment 35 (2001), pp. 1537-1565.

[16] J. Cho, and H.H. Song, *Understanding the effect of inhomogeneous fuel–air mixing on knocking characteristics of various ethanol reference fuels with RON 100 using rapid*

compression machine, Proceedings of the Combustion Institute 37 (2019), pp. 4911-4919.

[17] S. Shaheen, E. Martin, and H. Totte, *Zero-emission vehicle exposure within US carsharing fleets and impacts on sentiment toward electric-drive vehicles*, Transport Policy 85 (2020), pp. A23-A32.

[18] O.A. Towoju, and F.A. Ishola, *A case for the internal combustion engine powered vehicle*, Energy Reports 6 (2020), pp. 315-321.

[19] G. Kalghatgi, *Development of fuel/engine systems—the way forward to sustainable transport*, Engineering 5 (2019), pp. 510-518.

[20] *Buji ile Ateşlemeli Motor Kullanılan Seri Hibrit Elektrikli Bir Aracın Modellenmesi*.

[21] I. Taymaz, and M. Benli, *Emissions and fuel economy for a hybrid vehicle*, Fuel 115 (2014), pp. 812-817.

[22] E.E. Kahveci, and I. Taymaz, *Experimental study on performance evaluation of PEM fuel cell by coating bipolar plate with materials having different contact angle*, Fuel 253 (2019), pp. 1274-1281.

[23] S.S. Kumar, V. Kumar, S.K. Malyan, J. Sharma, T. Mathimani, M.S. Maskarenj, P.C. Ghosh, and A. Pugazhendhi, *Microbial fuel cells (MFCs) for bioelectrochemical treatment of different wastewater streams*, Fuel 254 (2019), p. 115526.

[24] Y.E. Ekici, and T. Nusret, *Charge and discharge characteristics of different types of batteries on a hybrid electric vehicle model and selection of suitable battery type for electric vehicles*, International Journal of Automotive Science and Technology 3 (2019), pp. 62-70.

[25] A. Uyumaz, *An experimental investigation into combustion and performance characteristics of an HCCI gasoline engine fueled with n-heptane, isopropanol and n-butanol fuel blends at different inlet air temperatures*, Energy Conversion and Management 98 (2015), pp. 199-207.

[26] A. Uyumaz, B. Aydoğan, A. Calam, F. Aksoy, and E. Yılmaz, *The effects of diisopropyl ether on combustion, performance, emissions and operating range in a HCCI engine*, Fuel 265 (2020), p. 116919.

[27] S. Polat, A. Uyumaz, D. İpci, H.S. Yücesu, H. Solmaz, and E. Yılmaz, *Doğalgaz yakıtlı HCCI bir motorda hidrojen ilavesinin yanma karakteristikleri üzerindeki etkilerinin nümerik olarak incelenmesi*, Makine Teknolojileri Elektronik Dergisi 12 (2015), pp. 15-26.

[28] C.F. dos Santos Vieira, F. Maugeri Filho, R. Maciel Filho, and A.P. Mariano, *Isopropanol-butanol-ethanol (IBE) production in repeated-batch cultivation of Clostridium beijerinckii DSM 6423 immobilized on sugarcane bagasse*, Fuel 263 (2020), p. 116708.

[29] Ö. Can, E. Öztürk, H. Solmaz, F. Aksoy, C. Çinar, and H.S. Yücesu, *Combined effects of soybean biodiesel fuel addition and EGR application on the combustion and exhaust emissions in a diesel engine*, Applied thermal engineering 95 (2016), pp. 115-124.

[30] İ. Çelikten, E. Mutlu, and H. Solmaz, *Variation of performance and emission characteristics of a diesel engine fueled with diesel, rapeseed oil and hazelnut oil methyl ester blends*, Renewable Energy 48 (2012), pp. 122-126.

[31] A. Uyumaz, B. Aydoğan, H. Solmaz, E. Yılmaz, D.Y. Hopa, T.A. Bahtli, Ö. Solmaz, and F. Aksoy, *Production of waste tyre oil and experimental investigation on combustion, engine performance and exhaust emissions*, Journal of the Energy Institute 92 (2019), pp. 1406-1418.

[32] A. Uyumaz, *Experimental evaluation of linseed oil biodiesel/diesel fuel blends on combustion, performance and emission characteristics in a DI diesel engine*, Fuel 267 (2020), p. 117150.
[33] A. UYUMAZ, F. AKSOY, A. Fatih, Ş.A. BAYDIR, H. SOLMAZ, E. YILMAZ, B. Aydoğan, and A. Calam, *An Experimental Investigation on The Effects of Waste Olive Oil Biodiesel on Combustion, Engine Performance and Exhaust Emissions*, International Journal of Automotive Engineering and Technologies 8 (2019), pp. 103-116.
[34] Q.M. Rahman, B. Zhang, L. Wang, and A. Shahbazi, *A combined pretreatment, fermentation and ethanol-assisted liquefaction process for production of biofuel from Chlorella sp*, Fuel 257 (2019), p. 116026.
[35] U. EIA, *Use of energy explained*, Energy Use in Homes. June (2021).
[36] R.D. Schnepf, and B.D. Yacobucci, *Renewable fuel standard (RFS): overview and issues*, Vol. 40155, Congressional Research Service Washington, DC, 2010.
[37] J.R. Serrano, R. Novella, and P. Piqueras, *Why the development of internal combustion engines is still necessary to fight against global climate change from the perspective of transportation*, MDPI, 2019, pp. 4597.
[38] F.Z. Sánchez, C.V. Braga, L.C. Braga, S.L. Braga, F.G. Dias, F.Y. Turkovics, and R.N. De Souza, *Ethanol-powered combustion experimental study in a rapid compression machine*, 0148-7191, SAE Technical Paper, 2013.
[39] V.B. Pedrozo, I. May, W. Guan, and H. Zhao, *High efficiency ethanol-diesel dual-fuel combustion: A comparison against conventional diesel combustion from low to full engine load*, Fuel 230 (2018), pp. 440-451.
[40] R.B.R. da Costa, R.M. Valle, J.J. Hernández, A.C.T. Malaquias, C.J. Coronado, and F.J.P. Pujatti, *Experimental investigation on the potential of biogas/ethanol dual-fuel spark-ignition engine for power generation: Combustion, performance and pollutant emission analysis*, Applied Energy 261 (2020), p. 114438.
[41] M. Joyce, *Developments in US alternative fuel markets*, Energy Information Administration, 2000.
[42] M. Pelucchi, M. Bissoli, C. Rizzo, Y. Zhang, K. Somers, A. Frassoldati, H. Curran, and T. Faravelli, *A kinetic modelling study of alcohols operating regimes in a HCCI engine*, SAE International Journal of Engines 10 (2017), pp. 2354-2370.
[43] S. Namysl, M. Pelucchi, O. Herbinet, A. Frassoldati, T. Faravelli, and F. Battin-Leclerc, *A first evaluation of butanoic and pentanoic acid oxidation kinetics*, Chemical Engineering Journal 373 (2019), pp. 973-984.
[44] M. Pelucchi, S. Namysl, E. Ranzi, A. Rodriguez, C. Rizzo, K. Somers, Y. Zhang, O. Herbinet, H. Curran, and F. Battin-Leclerc, *Combustion of n-C3–C6 Linear Alcohols: An Experimental and Kinetic Modeling Study. Part I: Reaction Classes, Rate Rules, Model Lumping, and Validation*, Energy & Fuels 34 (2020), pp. 14688-14707.
[45] P.S. Veloo, Y.L. Wang, F.N. Egolfopoulos, and C.K. Westbrook, *A comparative experimental and computational study of methanol, ethanol, and n-butanol flames*, Combustion and Flame 157 (2010), pp. 1989-2004.
[46] D. Liu, C. Togbé, L.-S. Tran, D. Felsmann, P. Oßwald, P. Nau, J. Koppmann, A. Lackner, P.-A. Glaude, and B. Sirjean, *Combustion chemistry and flame structure of furan group biofuels using molecular-beam mass spectrometry and gas chromatography–Part I: Furan*, Combustion and flame 161 (2014), pp. 748-765.

[47] A. García, J. Monsalve-Serrano, S. Martínez-Boggio, V.R. Roso, and N.D.S.A. Santos, *Potential of bio-ethanol in different advanced combustion modes for hybrid passenger vehicles*, Renewable Energy 150 (2020), pp. 58-77.

[48] A.K. Agarwal, *Biofuels (alcohols and biodiesel) applications as fuels for internal combustion engines*, Progress in energy and combustion science 33 (2007), pp. 233-271.

[49] S. Kim, and B.E. Dale, *Environmental aspects of ethanol derived from no-tilled corn grain: nonrenewable energy consumption and greenhouse gas emissions*, Biomass and bioenergy 28 (2005), pp. 475-489.

[50] A.B. Taylor, D.P. Moran, A.J. Bell, N.G. Hodgson, I.S. Myburgh, and J.J. Botha, *Gasoline/alcohol blends: exhaust emissions, performance and burn-rate in a multi-valve production engine*, 0148-7191, SAE Technical Paper, 1996.

[51] N.D.S.A. Santos, V.R. Roso, A.C.T. Malaquias, and J.G.C. Baeta, *Internal combustion engines and biofuels: Examining why this robust combination should not be ignored for future sustainable transportation*, Renewable and Sustainable Energy Reviews 148 (2021), p. 111292.

[52] F. Thomaz, A.C. Teixeira Malaquias, G.A. Resende de Paula, and J.G.C. Baêta, *Thermal management of an internal combustion engine focused on vehicle performance maximization: A numerical assessment*, Proceedings of the Institution of Mechanical Engineers, Part D: Journal of Automobile Engineering 235 (2021), pp. 2296-2310.

[53] S.M. Sarathy, *Chemical kinetic modeling of biofuel combustion*. 2010.

[54] K.E. Noorani, B. Akih-Kumgeh, and J.M. Bergthorson, *Comparative high temperature shock tube ignition of C1− C4 primary alcohols*, Energy & fuels 24 (2010), pp. 5834-5843.

[55] A. Konnov, R. Meuwissen, and L. De Goey, *The temperature dependence of the laminar burning velocity of ethanol flames*, Proceedings of the Combustion Institute 33 (2011), pp. 1011-1019.

[56] A. Uyumaz, H. Solmaz, E. Yılmaz, H. Yamık, and S. Polat, *Experimental examination of the effects of military aviation fuel JP-8 and biodiesel fuel blends on the engine performance, exhaust emissions and combustion in a direct injection engine*, Fuel Processing Technology 128 (2014), pp. 158-165.

[57] C. Cinar, A. Uyumaz, H. Solmaz, F. Sahin, S. Polat, and E. Yilmaz, *Effects of intake air temperature on combustion, performance and emission characteristics of a HCCI engine fueled with the blends of 20% n-heptane and 80% isooctane fuels*, Fuel Processing Technology 130 (2015), pp. 275-281.

[58] Z. Chen, L. Wang, and K. Zeng, *Comparative study of combustion process and cycle-by-cycle variations of spark-ignition engine fueled with pure methanol, ethanol, and n-butanol at various air–fuel ratios*, Fuel 254 (2019), p. 115683.

[59] J. Yanowitz, E. Christensen, and R.L. McCormick, *Utilization of renewable oxygenates as gasoline blending components*, (2011).

[60] Ö. İlker, B. SAYIN, and M. Ciniviz, *A comparative study of ethanol and methanol addition effects on engine performance, combustion and emissions in the SI engine*, International Journal of Automotive Science and Technology 4 (2020), pp. 59-69.

[61] M.K. Yeşilyurt, B. Doğan, and E. Derviş, *Experimental assessment of a CI engine operating with 1-pentanol/diesel fuel blends*, International Journal of Automotive Science and Technology 4 (2020), pp. 70-89.

[62] U. EPA, *Renewable fuel standard program (RFS2) regulatory impact analysis*, United States Environmental Protection Agency, Washington, DC (2010).
[63] F.D. Stump, K.T. Knapp, and W.D. Ray, *Influence of ethanol-blended fuels on the emissions from three pre-1985 light-duty passenger vehicles*, Journal of the Air & Waste Management Association 46 (1996), pp. 1149-1161.
[64] J.H. Perry, and C.P. Perry, *Methanol: Bridge to a renewable energy future*, University Press of America, 1990.
[65] E.I. Administration, N. Office of Coal, Electric,, and A. Fuels, *Alternatives to Traditional Transportation Fuels: An Overview*, 1994.
[66] D.A. Guerrieri, P.J. Caffrey, and V. Rao, *Investigation into the vehicle exhaust emissions of high percentage ethanol blends*, 0148-7191, SAE Technical Paper, 1995.
[67] D.C. PJ, and V. Rao, *Investigation into the vehicular exhaust emission of high percentage Ethanol blends*, SAE paper (1995).
[68] A. Panahi, M. Dehhaghi, J. Kinder, and T. Ezeji, *review on green liquid fuels for the transportation sector: a prospect of microbial solutions to climate change, Biofuel Res*, J 6 (2019), pp. 995-1024.
[69] O.I. Awad, R. Mamat, O.M. Ali, N.C. Sidik, T. Yusaf, K. Kadirgama, and M. Kettner, *Alcohol and ether as alternative fuels in spark ignition engine: A review*, Renewable and Sustainable Energy Reviews 82 (2018), pp. 2586-2605.
[70] K. Kohse-Höinghaus, P. Oßwald, T.A. Cool, T. Kasper, N. Hansen, F. Qi, C.K. Westbrook, and P.R. Westmoreland, *Biofuel combustion chemistry: from ethanol to biodiesel*, Angewandte Chemie International Edition 49 (2010), pp. 3572-3597.
[71] J.H. Seinfeld, and S.N. Pandis, *From air pollution to climate change*, Atmospheric chemistry and physics 1326 (1998).
[72] E. Grosjean, D. Grosjean, M.P. Fraser, and G.R. Cass, *Air quality model evaluation data for organics. 2. C1− C14 carbonyls in Los Angeles air*, Environmental science & technology 30 (1996), pp. 2687-2703.
[73] D. Grosjean, E. Grosjean, and A.W. Gertler, *On-road emissions of carbonyls from light-duty and heavy-duty vehicles*, Environmental Science & Technology 35 (2001), pp. 45-53.
[74] X. Pang, Y. Mu, J. Yuan, and H. He, *Carbonyls emission from ethanol-blended gasoline and biodiesel-ethanol-diesel used in engines*, Atmospheric Environment 42 (2008), pp. 1349-1358.
[75] B.-Q. He, M.-B. Liu, J. Yuan, and H. Zhao, *Combustion and emission characteristics of a HCCI engine fuelled with n-butanol–gasoline blends*, Fuel 108 (2013), pp. 668-674.
[76] M. Pelucchi, C. Cavallotti, E. Ranzi, A. Frassoldati, and T. Faravelli, *Relative reactivity of oxygenated fuels: alcohols, aldehydes, ketones, and methyl esters*, Energy & Fuels 30 (2016), pp. 8665-8679.
[77] K. Doolan, J. Mackie, and C. Reid, *High temperature kinetics of the thermal decomposition of the lower alkanoic acids*, International journal of chemical kinetics 18 (1986), pp. 575-596.
[78] M. Christensen, and A.A. Konnov, *Laminar burning velocity of acetic acid+ air flames*, Combustion and Flame 170 (2016), pp. 12-29.
[79] A. Elwardany, E.F. Nasir, E. Es-Sebbar, and A. Farooq, *Unimolecular decomposition of formic and acetic acids: A shock tube/laser absorption study*, Proceedings of the Combustion Institute 35 (2015), pp. 429-436.

[80] S.M. Sarathy, S. Vranckx, K. Yasunaga, M. Mehl, P. Oßwald, W.K. Metcalfe, C.K. Westbrook, W.J. Pitz, K. Kohse-Höinghaus, and R.X. Fernandes, Henry J.Curran, *A comprehensive chemical kinetic combustion model for the four butanol isomers*, combustion and flame 159 (2012), pp. 2028-2055.

[81] H. Curran, W. Pitz, C. Westbrook, P. Dagaut, J.C. Boettner, and M. Cathonnet, *A wide range modeling study of dimethyl ether oxidation*, International Journal of Chemical Kinetics 30 (1998), pp. 229-241.

[82] M.S. Graboski, and R.L. McCormick, *Combustion of fat and vegetable oil derived fuels in diesel engines*, Progress in energy and combustion science 24 (1998), pp. 125-164.

[83] J.E. Lawrence, and P. Koutrakis, *Measurement of atmospheric formic and acetic acids: Methods evaluation and results from field studies*, Environmental science & technology 28 (1994), pp. 957-964.

[84] A. Chebbi, and P. Carlier, *Carboxylic acids in the troposphere, occurrence, sources, and sinks: A review*, Atmospheric Environment 30 (1996), pp. 4233-4249.

[85] E. Zervas, X. Montagne, and J. Lahaye, *The influence of gasoline formulation on specific pollutant emissions*, Journal of the Air & Waste Management Association 49 (1999), pp. 1304-1314.

[86] E. Zervas, X. Montagne, and J. Lahaye, *Emission of specific pollutants from a compression ignition engine. Influence of fuel hydrotreatment and fuel/air equivalence ratio*, Atmospheric Environment 35 (2001), pp. 1301-1306.

[87] J.J. Schauer, M.J. Kleeman, G.R. Cass, and B.R. Simoneit, *Measurement of emissions from air pollution sources. 3. C1− C29 organic compounds from fireplace combustion of wood*, Environmental science & technology 35 (2001), pp. 1716-1728.

[88] E. Zervas, X. Montagne, and J. Lahaye, *C1− C5 organic acid emissions from an SI engine: Influence of fuel and air/fuel equivalence ratio*, Environmental science & technology 35 (2001), pp. 2746-2751.

[89] E. Biagini, F. Barontini, and L. Tognotti, *Devolatilization of biomass fuels and biomass components studied by TG/FTIR technique*, Industrial & Engineering Chemistry Research 45 (2006), pp. 4486-4493.

[90] A.M. Zaras, M. Szőri, S.b. Thion, P. Van Cauwenberghe, F. Deguillaume, Z. Serinyel, G. Dayma, and P. Dagaut, *A Chemical Kinetic Investigation on Butyl Formate Oxidation: Ab Initio Calculations and Experiments in a Jet-Stirred Reactor*, Energy & Fuels 31 (2017), pp. 6194-6205.

[91] T.J. Held, and F.L. Dryer, *A comprehensive mechanism for methanol oxidation*, International Journal of Chemical Kinetics 30 (1998), pp. 805-830.

[92] A.T. Blades, *The kinetics of the pyrolysis of ethyl and isopropyl formates and acetates*, Canadian Journal of Chemistry 32 (1954), pp. 366-372.

[93] S. Fischer, F. Dryer, and H. Curran, *The reaction kinetics of dimethyl ether. I: High-temperature pyrolysis and oxidation in flow reactors*, International Journal of Chemical Kinetics 32 (2000), pp. 713-740.

[94] K.B. Ansari, J.S. Arora, J.W. Chew, P.J. Dauenhauer, and S.H. Mushrif, *Fast pyrolysis of cellulose, hemicellulose, and lignin: Effect of operating temperature on bio-oil yield and composition and insights into the intrinsic pyrolysis chemistry*, Industrial & Engineering Chemistry Research 58 (2019), pp. 15838-15852.

[95] N.M. Marinov, *A detailed chemical kinetic model for high temperature ethanol oxidation*, International Journal of Chemical Kinetics 31 (1999), pp. 183-220.

[96] F. Battin-Leclerc, A. Konnov, J.-L. Jaffrezo, and M. Legrand, *To better understand the formation of short-chain acids in combustion systems*, Combustion science and technology 180 (2007), pp. 343-370.
[97] J.r. Eppinger, and K.-W. Huang, *Formic acid as a hydrogen energy carrier*, ACS Energy Letters 2 (2017), pp. 188-195.
[98] S. Hafeez, E. Harkou, A. Spanou, S. Al-Salem, A. Villa, N. Dimitratos, G. Manos, and A. Constantinou, *Review on recent progress and reactor set-ups for hydrogen production from formic acid decomposition*, Materials Today Chemistry 26 (2022), p. 101120.
[99] S.M. Sarathy, P. Brequigny, A. Katoch, A.M. Elbaz, W.L. Roberts, R.W. Dibble, and F. Foucher, *Laminar burning velocities and kinetic modeling of a renewable e-fuel: formic acid and its mixtures with H2 and CO2*, Energy & Fuels 34 (2020), pp. 7564-7572.
[100] C.K. Dyer, P.T. Moseley, Z. Ogumi, D.A. Rand, and B. Scrosati, *Encyclopedia of electrochemical power sources*, Elsevier Science & Technology., 2009.
[101] W. Park, S. Park, R.D. Reitz, and E. Kurtz, *The effect of oxygenated fuel properties on diesel spray combustion and soot formation*, Combustion and Flame 180 (2017), pp. 276-283.
[102] A. Oasmaa, Y. Solantausta, V. Arpiainen, E. Kuoppala, and K. Sipila, *Fast pyrolysis bio-oils from wood and agricultural residues*, Energy & fuels 24 (2010), pp. 1380-1388.
[103] H. Heeres, E. Leijenhorst, and L. van de Beld, *Project title: Renewable residential heating with fast pyrolysis bio-oil*.
[104] W. Sun, T. Tao, R. Zhang, H. Liao, C. Huang, F. Zhang, X. Zhang, Y. Zhang, and B. Yang, *Experimental and modeling efforts towards a better understanding of the high-temperature combustion kinetics of C3-C5 ethyl esters*, Combustion and Flame 185 (2017), pp. 173-187.
[105] O. Herbinet, B. Husson, Z. Serinyel, M. Cord, V. Warth, R. Fournet, P.-A. Glaude, B. Sirjean, F. Battin-Leclerc, Z. Wang, M. Xie, Z. Cheng, and F. Qi, *Experimental and modeling investigation of the low-temperature oxidation of an-heptane*, Combustion and flame 159 (2012), pp. 3455-3471.
[106] A. Fukutome, H. Kawamoto, and S. Saka, *Gas-and coke/soot-forming reactivities of cellulose-derived tar components under nitrogen and oxygen/nitrogen*, Journal of Analytical and Applied Pyrolysis 108 (2014), pp. 98-108.
[107] R.W. Jenkins, C.M. Moore, T.A. Semelsberger, C.J. Chuck, J.C. Gordon, and A.D. Sutton, *The Effect of Functional Groups in Bio-Derived Fuel Candidates*, ChemSusChem 9 (2016), pp. 922-931.
[108] T. Ohra-Aho, L. Rohrbach, J.G. Winkelman, H.J. Heeres, A. Mikkelson, A. Oasmaa, B. Van De Beld, E.J. Leijenhorst, and H. Heeres, *Evaluation of Analysis Methods for Formaldehyde, Acetaldehyde, and Furfural from Fast Pyrolysis Bio-oil*, Energy & Fuels 35 (2021), pp. 18583-18591.
[109] A. Abdel-Rahman, *On the emissions from internal-combustion engines: a review*, International Journal of Energy Research 22 (1998), pp. 483-513.
[110] J.P. Senosiain, S.J. Klippenstein, and J.A. Miller, *Pathways and rate coefficients for the decomposition of vinoxy and acetyl radicals*, The Journal of Physical Chemistry A 110 (2006), pp. 5772-5781.
[111] J.A. Miller, R.J. Kee, and C.K. Westbrook, *Chemical kinetics and combustion modeling*, Annual Review of Physical Chemistry 41 (1990), pp. 345-387.

[112] E. Ranzi, A. Frassoldati, R. Grana, A. Cuoci, T. Faravelli, A. Kelley, and C.K. Law, *Hierarchical and comparative kinetic modeling of laminar flame speeds of hydrocarbon and oxygenated fuels*, Progress in Energy and Combustion Science 38 (2012), pp. 468-501.
[113] S. Dooley, S.H. Won, J. Heyne, T.I. Farouk, Y. Ju, F.L. Dryer, K. Kumar, X. Hui, C.-J. Sung, H. Wang, M.A. Oehlschlaeger, V. Lyer, S. Lyer, T.A. Litzinger, R.J. Santoro, T. Malewicki, and K. Brezinsky, *The experimental evaluation of a methodology for surrogate fuel formulation to emulate gas phase combustion kinetic phenomena*, Combustion and Flame 159 (2012), pp. 1444-1466.
[114] C. Treviño, and T. Turányi, *Low temperature first ignition of n-butane*, Combustion Theory and Modelling 23 (2019), pp. 1150-1168.
[115] J. Warnatz, *Rate coefficients in the C/H/O system*, in *Combustion chemistry*, Springer, 1984, pp. 197-360.
[116] G. Issayev, S.M. Sarathy, and A. Farooq, *Autoignition of diethyl ether and a diethyl ether/ethanol blend*, Fuel 279 (2020), p. 118553.
[117] A. Saylam, B. Atakan, and S. Kaiser, *Modeling study of reactive species formation from C1–C3 alkanes in an HCCI engine*, Combustion Theory and Modelling 23 (2019), pp. 1119-1133.
[118] F. Ferfecki, and S. Sorenson, *Performance of ethanol blends in gasoline engines*, Transactions of the ASAE 26 (1983), pp. 38-0043.
[119] S. Poulopoulos, and C. Philippopoulos, *Influence of MTBE addition into gasoline on automotive exhaust emissions*, Atmospheric Environment 34 (2000), pp. 4781-4786.
[120] A.K. Agarwal, A.P. Singh, and R.K. Maurya, *Evolution, challenges and path forward for low temperature combustion engines*, Progress in energy and combustion science 61 (2017), pp. 1-56.
[121] J.E. Dec, *A conceptual model of DL diesel combustion based on laser-sheet imaging*, SAE transactions (1997), pp. 1319-1348.
[122] C.K. Westbrook, Y. Mizobuchi, T.J. Poinsot, P.J. Smith, and J. Warnatz, *Computational combustion*, Proceedings of the Combustion Institute 30 (2005), pp. 125-157.
[123] C.K. Westbrook, W.J. Pitz, and H.J. Curran, *Chemical kinetic modeling study of the effects of oxygenated hydrocarbons on soot emissions from diesel engines*, The journal of physical chemistry A 110 (2006), pp. 6912-6922.
[124] C.K. Westbrook, *Biofuels combustion*, Annual review of physical chemistry 64 (2013).
[125] H. Wang, and D.A. Sheen, *Combustion kinetic model uncertainty quantification, propagation and minimization*, Progress in Energy and Combustion Science 47 (2015), pp. 1-31.
[126] A.S. Tomlin, *The role of sensitivity and uncertainty analysis in combustion modelling*, Proceedings of the Combustion Institute 34 (2013), pp. 159-176.
[127] S.M. Sarathy, P. Oßwald, N. Hansen, and K. Kohse-Höinghaus, *Alcohol combustion chemistry*, Progress in energy and Combustion Science 44 (2014), pp. 40-102.
[128] M. Mehl, J.-Y. Chen, W.J. Pitz, S.M. Sarathy, and C.K. Westbrook, *An approach for formulating surrogates for gasoline with application toward a reduced surrogate mechanism for CFD engine modeling*, Energy & Fuels 25 (2011), pp. 5215-5223.
[129] S.M. Sarathy, T. Javed, F. Karsenty, A. Heufer, W. Wang, S. Park, A. Elwardany, A. Farooq, C.K. Westbrook, and W.J. Pitz, *A comprehensive combustion chemistry study of 2, 5-dimethylhexane*, Combustion and Flame 161 (2014), pp. 1444-1459.

[130] G. Kalghatgi, *Fuel/engine interactions*, SAE, 2014.
[131] E. Ranzi, A. Frassoldati, R. Grana, A. Cuoci, T. Faravelli, A.P. Kelley, and C.K. Law, *Hierarchical and comparative kinetic modeling of laminar flame speeds of hydrocarbon and oxygenated fuels*, Progress in Energy and Combustion Science 38 (2012), pp. 468-501.
[132] P. Nau, A. Seipel, A. Lucassen, A. Brockhinke, and K. Kohse-Höinghaus, *Intermediate species detection in a morpholine flame: contributions to fuel-bound nitrogen conversion from a model biofuel*, Experiments in fluids 49 (2010), pp. 761-773.
[133] M. Pelucchi, S. Namysl, E. Ranzi, A. Frassoldati, O. Herbinet, F. Battin-Leclerc, and T. Faravelli, *An experimental and kinetic modelling study of n-C4C6 aldehydes oxidation in a jet-stirred reactor*, Proceedings of the Combustion Institute 37 (2019), pp. 389-397.
[134] M. Pelucchi, E. Ranzi, A. Frassoldati, and T. Faravelli, *Alkyl radicals rule the low temperature oxidation of long chain aldehydes*, Proceedings of the Combustion Institute 36 (2017), pp. 393-401.
[135] M. Pelucchi, C. Cavallotti, A. Cuoci, T. Faravelli, A. Frassoldati, and E. Ranzi, *Detailed kinetics of substituted phenolic species in pyrolysis bio-oils*, Reaction Chemistry & Engineering 4 (2019), pp. 490-506.
[136] S. Namysl, M. Pelucchi, L.P. Maffei, O. Herbinet, A. Stagni, T. Faravelli, and F. Battin-Leclerc, *Experimental and modeling study of benzaldehyde oxidation*, Combustion and Flame 211 (2020), pp. 124-132.
[137] J.M. Simmie, *Detailed chemical kinetic models for the combustion of hydrocarbon fuels*, Progress in energy and combustion science 29 (2003), pp. 599-634.
[138] F. Mosisa Wako, G. Pio, and E. Salzano, *Laminar Burning Velocity and Ignition Delay Time of Oxygenated Biofuel*, Energies 14 (2021), p. 3562.
[139] E.M. Fisher, W.J. Pitz, H.J. Curran, and C.K. Westbrook, *Detailed chemical kinetic mechanisms for combustion of oxygenated fuels*, CORNELL UNIV ITHACA NY DEPT OF MECHANICAL AND AEROSPACE ENGINEERING, 2000.
[140] I. Dafnomilis, R. Hoefnagels, Y.W. Pratama, D.L. Schott, G. Lodewijks, and M. Junginger, *Review of solid and liquid biofuel demand and supply in Northwest Europe towards 2030–A comparison of national and regional projections*, Renewable and Sustainable Energy Reviews 78 (2017), pp. 31-45.
[141] W. Griffin, B. Saville, and H. MacLean, *Ethanol use in the United States: status, threats and the potential future*, Global Bioethanol (2016), pp. 34-62.
[142] S. Hameed, A. Sharma, V. Pareek, H. Wu, and Y. Yu, *A review on biomass pyrolysis models: Kinetic, network and mechanistic models*, Biomass and bioenergy 123 (2019), pp. 104-122.
[143] C. Koufopanos, A. Lucchesi, and G. Maschio, *Kinetic modelling of the pyrolysis of biomass and biomass components*, The Canadian Journal of Chemical Engineering 67 (1989), pp. 75-84.
[144] G. Varhegyi, M.J. Antal Jr, E. Jakab, and P. Szabó, *Kinetic modeling of biomass pyrolysis*, Journal of analytical and Applied Pyrolysis 42 (1997), pp. 73-87.
[145] E. Ranzi, A. Cuoci, T. Faravelli, A. Frassoldati, G. Migliavacca, S. Pierucci, and S. Sommariva, *Chemical kinetics of biomass pyrolysis*, Energy & Fuels 22 (2008), pp. 4292-4300.

[146] T. Faravelli, A. Frassoldati, E. Barker Hemings, and E. Ranzi, *Multistep Kinetic Model of Biomass Pyrolysis*, in *Cleaner Combustion*, Springer, 2013, pp. 111-139.
[147] R. Vinu, and L.J. Broadbelt, *Unraveling reaction pathways and specifying reaction kinetics for complex systems*, Annual review of chemical and biomolecular engineering 3 (2012), pp. 29-54.
[148] A. Anca-Couce, *Reaction mechanisms and multi-scale modelling of lignocellulosic biomass pyrolysis*, Progress in Energy and Combustion Science 53 (2016), pp. 41-79.
[149] M.B. Pecha, J.I.M. Arbelaez, M. Garcia-Perez, F. Chejne, and P.N. Ciesielski, *Progress in understanding the four dominant intra-particle phenomena of lignocellulose pyrolysis: chemical reactions, heat transfer, mass transfer, and phase change*, Green chemistry 21 (2019), pp. 2868-2898.
[150] C. Di Blasi, *Modeling and simulation of combustion processes of charring and non-charring solid fuels*, Progress in energy and combustion science 19 (1993), pp. 71-104.
[151] A.G. Bradbury, Y. Sakai, and F. Shafizadeh, *A kinetic model for pyrolysis of cellulose*, Journal of applied polymer science 23 (1979), pp. 3271-3280.
[152] F. Shafizadeh, R.H. Furneaux, T.G. Cochran, J.P. Scholl, and Y. Sakai, *Production of levoglucosan and glucose from pyrolysis of cellulosic materials*, Journal of Applied Polymer Science 23 (1979), pp. 3525-3539.
[153] F. Shafizadeh, *Thermal conversion of cellulosic materials to fuel and chemicals*, (1983).
[154] J. Piskorz, D. Radlein, and D.S. Scott, *On the mechanism of the rapid pyrolysis of cellulose*, Journal of Analytical and Applied pyrolysis 9 (1986), pp. 121-137.
[155] J. Piskorz, D.S.A. Radlein, D.S. Scott, and S. Czernik, *Liquid products from the fast pyrolysis of wood and cellulose*, in *Research in thermochemical biomass conversion*, Springer, 1988, pp. 557-571.
[156] G.N. Richards, *Glycolaldehyde from pyrolysis of cellulose*, Journal of Analytical and Applied Pyrolysis 10 (1987), pp. 251-255.
[157] A.D. Pouwels, G.B. Eijkel, and J.J. Boon, *Curie-point pyrolysis-capillary gas chromatography-high-resolution mass spectrometry of microcrystalline cellulose*, Journal of Analytical and Applied Pyrolysis 14 (1989), pp. 237-280.
[158] J. Lomax, J. Commandeur, P. Arisz, and J. Boon, *Characterisation of oligomers and sugar ring-cleavage products in the pyrolysate of cellulose*, Journal of Analytical and Applied Pyrolysis 19 (1991), pp. 65-79.
[159] J. Piskorz, D.S.A. Radlein, D.S. Scott, and S. Czernik, *Pretreatment of wood and cellulose for production of sugars by fast pyrolysis*, Journal of Analytical and Applied Pyrolysis 16 (1989), pp. 127-142.
[160] J.L. Banyasz, S. Li, J.L. Lyons-Hart, and K.H. Shafer, *Cellulose pyrolysis: the kinetics of hydroxyacetaldehyde evolution*, Journal of Analytical and Applied Pyrolysis 57 (2001), pp. 223-248.
[161] J. Banyasz, S. Li, J. Lyons-Hart, and K. Shafer, *Gas evolution and the mechanism of cellulose pyrolysis*, Fuel 80 (2001), pp. 1757-1763.
[162] Z. Luo, S. Wang, Y. Liao, and K. Cen, *Mechanism study of cellulose rapid pyrolysis*, Industrial & engineering chemistry research 43 (2004), pp. 5605-5610.
[163] X. Zhou, W. Li, R. Mabon, and L.J. Broadbelt, *A critical review on hemicellulose pyrolysis*, Energy Technology 5 (2017), pp. 52-79.
[164] P. Giudicianni, V. Gargiulo, M. Alfè, R. Ragucci, A.I. Ferreiro, M. Rabacal, and M. Costa, *Slow pyrolysis of xylan as pentose model compound for hardwood hemicellulose: A*

study of the catalytic effect of Na ions, Journal of Analytical and Applied Pyrolysis 137 (2019), pp. 266-275.
[165] V. Gargiulo, P. Giudicianni, M. Alfe, and R. Ragucci, *About the influence of doping approach on the alkali metal catalyzed slow pyrolysis of xylan*, Journal of Chemistry 2019 (2019).
[166] V. Gargiulo, A.I. Ferreiro, P. Giudicianni, S. Tomaselli, M. Costa, R. Ragucci, and M. Alfe, *Insights about the effect of composition, branching and molecular weight on the slow pyrolysis of xylose-based polysaccharides*, Journal of Analytical and Applied Pyrolysis 161 (2022), p. 105369.
[167] D. Shen, S. Gu, and A.V. Bridgwater, *Study on the pyrolytic behaviour of xylan-based hemicellulose using TG–FTIR and Py–GC–FTIR*, Journal of analytical and applied pyrolysis 87 (2010), pp. 199-206.
[168] X. Zhou, W. Li, R. Mabon, and L.J. Broadbelt, *A mechanistic model of fast pyrolysis of hemicellulose*, Energy & environmental science 11 (2018), pp. 1240-1260.
[169] P.R. Patwardhan, R.C. Brown, and B.H. Shanks, *Product distribution from the fast pyrolysis of hemicellulose*, ChemSusChem 4 (2011), pp. 636-643.
[170] T. Faravelli, A. Frassoldati, G. Migliavacca, and E. Ranzi, *Detailed kinetic modeling of the thermal degradation of lignins*, Biomass and bioenergy 34 (2010), pp. 290-301.
[171] B.R. Hough, D.T. Schwartz, and J. Pfaendtner, *Detailed kinetic modeling of lignin pyrolysis for process optimization*, Industrial & Engineering Chemistry Research 55 (2016), pp. 9147-9153.
[172] C.T. Bowman, *A shock-tube investigation of the high-temperature oxidation of methanol*, Combustion and Flame 25 (1975), pp. 343-354.
[173] K. Fieweger, R. Blumenthal, and G. Adomeit, *Self-ignition of SI engine model fuels: a shock tube investigation at high pressure*, Combustion and Flame 109 (1997), pp. 599-619.
[174] K. Kumar, and C.J. Sung, *Autoignition of methanol: experiments and computations*, International Journal of Chemical Kinetics 43 (2011), pp. 175-184.
[175] M. Cathonnet, and B. JC, *Étude expérimentale et simulation de la pyrolyse du méthanol*, (1979).
[176] K. Aniolek, and R. Wilk, *Preflame oxidation characteristics of methanol*, Energy & fuels 9 (1995), pp. 395-405.
[177] Y. Wang, Y. Qi, W. Liu, and Z. Wang, *Investigation of methanol ignition phenomena using a rapid compression machine*, Combustion and Flame 211 (2020), pp. 147-157.
[178] C.K. Westbrook, and F.L. Dryer, *Comprehensive mechanism for methanol oxidation*, Combustion Science and Technology 20 (1979), pp. 125-140.
[179] U. Burke, W.K. Metcalfe, S.M. Burke, K.A. Heufer, P. Dagaut, and H.J. Curran, *A detailed chemical kinetic modeling, ignition delay time and jet-stirred reactor study of methanol oxidation*, Combustion and Flame 165 (2016), pp. 125-136.
[180] L. Pinzón, O. Mathieu, C. Mulvihill, I. Schoegl, and E. Petersen, *Ignition delay time and H2O measurements during methanol oxidation behind reflected shock waves*, Combustion and Flame 203 (2019), pp. 143-156.
[181] J. Li, Z. Zhao, A. Kazakov, M. Chaos, F.L. Dryer, and J.J. Scire Jr, *A comprehensive kinetic mechanism for CO, CH2O, and CH3OH combustion*, International Journal of Chemical Kinetics 39 (2007), pp. 109-136.

[182] A. Fomin, T. Zavlev, V.A. Alekseev, I. Rahinov, S. Cheskis, and A.A. Konnov, *Experimental and modelling study of 1CH2 in premixed very rich methane flames*, Combustion and Flame 171 (2016), pp. 198-210.
[183] C.-W. Zhou, Y. Li, U. Burke, C. Banyon, K.P. Somers, S. Ding, S. Khan, J.W. Hargis, T. Sikes, and O. Mathieu, *An experimental and chemical kinetic modeling study of 1, 3-butadiene combustion: Ignition delay time and laminar flame speed measurements*, Combustion and Flame 197 (2018), pp. 423-438.
[184] V. Aranda, J. Christensen, M.U. Alzueta, P. Glarborg, S. Gersen, Y. Gao, and P. Marshall, *Experimental and kinetic modeling study of methanol ignition and oxidation at high pressure*, International Journal of Chemical Kinetics 45 (2013), pp. 283-294.
[185] M. Figueroa-Labastida, M.B. Luong, J. Badra, H.G. Im, and A. Farooq, *Experimental and computational studies of methanol and ethanol preignition behind reflected shock waves*, Combustion and Flame 234 (2021), p. 111621.
[186] R. Akrich, C. Vovelle, and R. Delbourgo, *Flame profiles and combustion mechanisms of methanol-air flames under reduced pressure*, Combustion and Flame 32 (1978), pp. 171-179.
[187] F.N. Egolfopoulos, D. Du, and C. Law, *A comprehensive study of methanol kinetics in freely-propagating and burner-stabilized flames, flow and static reactors, and shock tubes*, Combustion science and technology 83 (1992), pp. 33-75.
[188] S. Liao, D. Jiang, Z. Huang, W. Shen, C. Yuan, and Q. Cheng, *Laminar burning velocities for mixtures of methanol and air at elevated temperatures*, Energy conversion and management 48 (2007), pp. 857-863.
[189] J. Vancoillie, M. Christensen, E. Nilsson, S. Verhelst, and A. Konnov, *Temperature dependence of the laminar burning velocity of methanol flames*, Energy & Fuels 26 (2012), pp. 1557-1564.
[190] X. Zhang, G. Wang, J. Zou, Y. Li, W. Li, T. Li, H. Jin, Z. Zhou, and Y.-Y. Lee, *Investigation on the oxidation chemistry of methanol in laminar premixed flames*, Combustion and Flame 180 (2017), pp. 20-31.
[191] M. Raida, G. Hoetmer, A. Konnov, J. van Oijen, and L. de Goey, *Laminar burning velocity measurements of ethanol+ air and methanol+ air flames at atmospheric and elevated pressures using a new Heat Flux setup*, Combustion and Flame 230 (2021), p. 111435.
[192] F. Williams, *Chemical-kinetic mechanisms for combustion applications*, Center for Energy Research, UCSD, http://maeweb. ucsd. edu/~ combustion/cermech (2003).
[193] L. Sileghem, V. Alekseev, J. Vancoillie, E. Nilsson, S. Verhelst, and A. Konnov, *Laminar burning velocities of primary reference fuels and simple alcohols*, Fuel 115 (2014), pp. 32-40.
[194] J.D. Naucler, L. Sileghem, E.J. Nilsson, S. Verhelst, and A.A. Konnov, *Performance of methanol kinetic mechanisms at oxy-fuel conditions*, Combustion and Flame 162 (2015), pp. 1719-1728.
[195] S. Xu, and M.-C. Lin, *Theoretical study on the kinetics for OH reactions with CH3OH and C2H5OH*, Proceedings of the Combustion Institute 31 (2007), pp. 159-166.
[196] R. Meana-Pañeda, D.G. Truhlar, and A. Fernández-Ramos, *High-level direct-dynamics variational transition state theory calculations including multidimensional tunneling of the thermal rate constants, branching ratios, and kinetic isotope effects of the*

hydrogen abstraction reactions from methanol by atomic hydrogen, The Journal of chemical physics 134 (2011), p. 094302.

[197] S.J. Klippenstein, L.B. Harding, M.J. Davis, A.S. Tomlin, and R.T. Skodje, *Uncertainty driven theoretical kinetics studies for CH3OH ignition: HO2+ CH3OH and O2+ CH3OH*, Proceedings of the Combustion Institute 33 (2011), pp. 351-357.

[198] M. Christensen, E. Nilsson, and A. Konnov, *A systematically updated detailed kinetic model for CH2O and CH3OH combustion*, Energy & Fuels 30 (2016), pp. 6709-6726.

[199] J. Vancoillie, M. Christensen, E. Nilsson, S. Verhelst, and A. Konnov, *The effects of dilution with nitrogen and steam on the laminar burning velocity of methanol at room and elevated temperatures*, Fuel 105 (2013), pp. 732-738.

[200] C.R. Group, *Mechanical and Aerospace Engineering, San Diego Mechanism, Version 2016-12-14*, Chemical-Kinetic Mechanisms for Combustion Applications, University of California at San Diego, La Jolla, CA, accessed July 26 (2016), p. 2018.

[201] *Thermal Oxidation of Ethanol: Experimental and Numerical Analysis of Ignition Chemistry of Ethanol-Air Mixtures in Shock Heated Gases,* Vol. 27, 1.

[202] L. Cancino, M. Fikri, A. Oliveira, and C. Schulz, *Ignition delay times of ethanol-containing multi-component gasoline surrogates: Shock-tube experiments and detailed modeling*, Fuel 90 (2011), pp. 1238-1244.

[203] M. Aghsaee, D. Nativel, M. Bozkurt, M. Fikri, N. Chaumeix, and C. Schulz, *Experimental study of the kinetics of ethanol pyrolysis and oxidation behind reflected shock waves and in laminar flames*, Proceedings of the Combustion Institute 35 (2015), pp. 393-400.

[204] C.L. Barraza-Botet, S.W. Wagnon, and M.S. Wooldridge, *Combustion chemistry of ethanol: ignition and speciation studies in a rapid compression facility*, The Journal of Physical Chemistry A 120 (2016), pp. 7408-7418.

[205] C. Lee, S. Vranckx, K.A. Heufer, S.V. Khomik, Y. Uygun, H. Olivier, and R.X. Fernandez, *On the chemical kinetics of ethanol oxidation: shock tube, rapid compression machine and detailed modeling study*, Zeitschrift für Physikalische Chemie 226 (2012), pp. 1-28.

[206] G. Mittal, S.M. Burke, V.A. Davies, B. Parajuli, W.K. Metcalfe, and H.J. Curran, *Autoignition of ethanol in a rapid compression machine*, Combustion and Flame 161 (2014), pp. 1164-1171.

[207] J. Van Lipzig, E. Nilsson, L. De Goey, and A. Konnov, *Laminar burning velocities of n-heptane, iso-octane, ethanol and their binary and tertiary mixtures*, Fuel 90 (2011), pp. 2773-2781.

[208] P. Dirrenberger, P.-A. Glaude, R. Bounaceur, H. Le Gall, A.P. Da Cruz, A. Konnov, and F. Battin-Leclerc, *Laminar burning velocity of gasolines with addition of ethanol*, Fuel 115 (2014), pp. 162-169.

[209] *Further considerations on the determination of laminar flame speeds with the counterflow twin-flame technique,* Vol. 25, 1, Elsevier.

[210] T. Fiala, and T. Sattelmayer, *Nonpremixed counterflow flames: scaling rules for batch simulations*, Journal of Combustion 2014 (2014).

[211] X. Liu, H. Wang, Z. Zheng, J. Liu, R.D. Reitz, and M. Yao, *Development of a combined reduced primary reference fuel-alcohols (methanol/ethanol/propanols/butanols/n-pentanol) mechanism for engine applications*, Energy 114 (2016), pp. 542-558.

[212] N. Hinton, R. Stone, R. Cracknell, and C. Olm, *Aqueous ethanol laminar burning velocity measurements using constant volume bomb methods*, Fuel 214 (2018), pp. 127-134.
[213] *Chemical kinetics of ethanol oxidation,* Vol. 26, University of California at San Diego San Diego, CA.
[214] O. Mathieu, L.T. Pinzón, T.M. Atherley, C.R. Mulvihill, I. Schoel, and E.L. Petersen, *Experimental study of ethanol oxidation behind reflected shock waves: Ignition delay time and H2O laser-absorption measurements*, Combustion and Flame 208 (2019), pp. 313-326.
[215] A.R. Laich, E. Ninnemann, S. Neupane, R. Rahman, S. Barak, W.J. Pitz, S.S. Goldsborough, and S.S. Vasu, *High-pressure shock tube study of ethanol oxidation: Ignition delay time and CO time-history measurements*, Combustion and Flame 212 (2020), pp. 486-499.
[216] C. Xu, Y. Hu, X. Li, X. Zhou, and A. Zhong, *Comparative experimental study of ethanol-air premixed laminar combustion characteristics by laser induced spark and electric spark ignition*, Korean Journal of Chemical Engineering 34 (2017), pp. 574-579.
[217] A. Katoch, A. Millán-Merino, and S. Kumar, *Measurement of laminar burning velocity of ethanol-air mixtures at elevated temperatures*, Fuel 231 (2018), pp. 37-44.
[218] L. van Treek, M.L. Lavadera, L. Seidel, F. Mauss, and A.A. Konnov, *Experimental and modelling study of laminar burning velocity of aqueous ethanol*, Fuel 257 (2019), p. 116069.
[219] M.P. Dunphy, P.M. Patterson, and J.M. Simmie, *High-temperature oxidation of ethanol. Part 2.—Kinetic modelling*, Journal of the Chemical Society, Faraday Transactions 87 (1991), pp. 2549-2559.
[220] J. Li, A. Kazakov, and F.L. Dryer, *Ethanol pyrolysis experiments in a variable pressure flow reactor*, International Journal of Chemical Kinetics 33 (2001), pp. 859-867.
[221] ---, *Experimental and numerical studies of ethanol decomposition reactions*, The Journal of Physical Chemistry A 108 (2004), pp. 7671-7680.
[222] W.K. Metcalfe, S.M. Burke, S.S. Ahmed, and H.J. Curran, *A hierarchical and comparative kinetic modeling study of C1− C2 hydrocarbon and oxygenated fuels*, International Journal of Chemical Kinetics 45 (2013), pp. 638-675.
[223] H. Hashemi, J.M. Christensen, S. Gersen, H. Levinsky, S.J. Klippenstein, and P. Glarborg, *High-pressure oxidation of methane*, Combustion and Flame 172 (2016), pp. 349-364.
[224] A. Zyada, and O. Samimi-Abianeh, *Ethanol Kinetic Model Development and Validation at Wide Ranges of Mixture Temperatures, Pressures, and Equivalence Ratios*, Energy & Fuels 33 (2019), pp. 7791-7804.
[225] A. Millán-Merino, E. Fernández-Tarrazo, M. Sánchez-Sanz, and F.A. Williams, *A multipurpose reduced mechanism for ethanol combustion*, Combustion and Flame 193 (2018), pp. 112-122.
[226] S. Roy, and O. Askari, *A new detailed ethanol kinetic mechanism at engine-relevant conditions*, Energy & Fuels 34 (2020), pp. 3691-3708.
[227] P. Saxena, and F.A. Williams, *Numerical and experimental studies of ethanol flames*, Proceedings of the Combustion Institute 31 (2007), pp. 1149-1156.
[228] N. Leplat, P. Dagaut, C. Togbé, and J. Vandooren, *Numerical and experimental study of ethanol combustion and oxidation in laminar premixed flames and in jet-stirred reactor*, Combustion and Flame 158 (2011), pp. 705-725.

[229] M. Bertero, G. de la Puente, and U. Sedran, *Fuels from bio-oils: Bio-oil production from different residual sources, characterization and thermal conditioning*, Fuel 95 (2012), pp. 263-271.
[230] K. Onarheim, Y. Solantausta, and J. Lehto, *Process simulation development of fast pyrolysis of wood using aspen plus*, Energy & Fuels 29 (2015), pp. 205-217.
[231] E. Zervas, *Formation of organic acids from propane, isooctane and toluene/isooctane flames*, Fuel 84 (2005), pp. 691-700.
[232] G. Yin, Q. Gao, E. Hu, J. Xu, M. Zhou, and Z. Huang, *Experimental and kinetic study on laminar flame speeds of formic acid*, Combustion and Flame 220 (2020), pp. 73-81.
[233] K.N. Osipova, S.M. Sarathy, O.P. Korobeinichev, and A.G. Shmakov, *Laminar Burning Velocities of Formic Acid and Formic Acid/Hydrogen Flames: An Experimental and Modeling Study*, Energy & Fuels 35 (2021), pp. 1760-1767.
[234] W.A. Bone, and J. Gardner, *Comparative studies of the slow combustion of methane, methyl alcohol, formaldehyde, and formic acid*, Proceedings of the Royal Society of London. Series A-Mathematical and Physical Sciences 154 (1936), pp. 297-328.
[235] *Kinetic and mechanistic studies of the reaction of hydroxyl radicals with acetaldehyde over an extended temperature range,* Vol. 26, 1, Elsevier.
[236] J.-G. Chang, H.-T. Chen, S. Xu, and M.-C. Lin, *Computational study on the kinetics and mechanisms for the unimolecular decomposition of formic and oxalic acids*, The Journal of Physical Chemistry A 111 (2007), pp. 6789-6797.
[237] J.M. Anglada, *Complex mechanism of the gas phase reaction between formic acid and hydroxyl radical. Proton coupled electron transfer versus radical hydrogen abstraction mechanisms*, Journal of the American Chemical Society 126 (2004), pp. 9809-9820.
[238] H.-G. Yu, G. Poggi, J.S. Francisco, and J.T. Muckerman, *Energetics and molecular dynamics of the reaction of HOCO with HO 2 radicals*, The Journal of chemical physics 129 (2008), p. 214307.
[239] P. Marshall, and P. Glarborg, *Ab initio and kinetic modeling studies of formic acid oxidation*, Proceedings of the Combustion Institute 35 (2015), pp. 153-160.
[240] E.v. de Wilde, and A. Van Tiggelen, *Burning velocities in mixtures of methyl alcohol, formaldehyde or formic acid with oxygen*, Bulletin des Sociétés Chimiques Belges 77 (1968), pp. 67-75.
[241] S.M. Burke, W. Metcalfe, O. Herbinet, F. Battin-Leclerc, F.M. Haas, J. Santner, F.L. Dryer, and H.J. Curran, *An experimental and modeling study of propene oxidation. Part 1: Speciation measurements in jet-stirred and flow reactors*, Combustion and Flame 161 (2014), pp. 2765-2784.
[242] E. Zervas, X. Montagne, and J. Lahaye, *Influence of Fuel Composition on the Emission of Oxygenated Pollutants (Organic Acids, Alcohols and Carbonyl Compounds) from a SI Engine*, Tech. Chron. Sci. J 1 (2004), pp. 49-58.
[243] E. Zervas, X. Montagne, and J. Lahaye, *Emission of alcohols and carbonyl compounds from a spark ignition engine. Influence of fuel and air/fuel equivalence ratio*, Environmental science & technology 36 (2002), pp. 2414-2421.
[244] N. Leplat, and J. Vandooren, *Numerical and experimental study of the combustion of acetic acid in laminar premixed flames*, Combustion and flame 159 (2012), pp. 493-499.
[245] *C1/C2 chemistry in fuel-rich post-flame gases: detailed kinetic modelling,* Vol. 25, 1, Elsevier.

[246] I. Woods, and B. Haynes, *C1/C2 Chemistry in Fuel-Rich Post-Flame Gases I. Experimental Results and Pool Modelling*, Combustion science and technology 87 (1993), pp. 199-215.
[247] J. Mackie, and K. Doolan, *High-temperature kinetics of thermal decomposition of acetic acid and its products*, International journal of chemical kinetics 16 (1984), pp. 525-541.
[248] H. Gg. Wagner, and F. Zabel, *Zum thermischen Zerfall von Keten in der Gasphase*, Berichte der Bunsengesellschaft für physikalische Chemie 75 (1971), pp. 114-118.
[249] C. Cavallotti, M. Pelucchi, and A. Frassoldati, *Analysis of acetic acid gas phase reactivity: Rate constant estimation and kinetic simulations*, Proceedings of the Combustion Institute 37 (2019), pp. 539-546.
[250] X. Zhang, B. Mei, S. Ma, Y. Zhang, C. Cao, W. Li, L. Ye, and Y. Li, *Characterizing the fuel-specific combustion chemistry of acetic acid and propanoic acid: Laminar flame propagation and kinetic modeling studies*, Proceedings of the Combustion Institute 38 (2021), pp. 449-457.
[251] E. Ranzi, C. Cavallotti, A. Cuoci, A. Frassoldati, M. Pelucchi, and T. Faravelli, *New reaction classes in the kinetic modeling of low temperature oxidation of n-alkanes*, Combustion and Flame 162 (2015), pp. 1679-1691.
[252] G. Fontaras, G. Karavalakis, M. Kousoulidou, L. Ntziachristos, E. Bakeas, S. Stournas, and Z. Samaras, *Effects of low concentration biodiesel blends application on modern passenger cars. Part 2: impact on carbonyl compound emissions*, Environmental Pollution 158 (2010), pp. 2496-2503.
[253] M.Z. Jacobson, *Effects of ethanol (E85) versus gasoline vehicles on cancer and mortality in the United States*, Environmental Science & Technology 41 (2007), pp. 4150-4157.
[254] J.S. Gaffney, and N.A. Marley, *The impacts of combustion emissions on air quality and climate–From coal to biofuels and beyond*, Atmospheric Environment 43 (2009), pp. 23-36.
[255] K. Yasunaga, S. Kubo, H. Hoshikawa, T. Kamesawa, and Y. Hidaka, *Shock-tube and modeling study of acetaldehyde pyrolysis and oxidation*, International Journal of Chemical Kinetics 40 (2008), pp. 73-102.
[256] J. Ernst, K. Spindler, and H.G. Wagner, *Untersuchungen zum thermischen Zerfall von Acetaldehyd und Aceton*, Berichte der Bunsengesellschaft für physikalische Chemie 80 (1976), pp. 645-650.
[257] Y. Hidaka, S. Kubo, T. Hoshikawa, and H. Wakamatsu, *Shock-tube study of acetaldehyde pyrolysis*, in *Shock Waves*, Springer, 2005, pp. 603-608.
[258] T. Bentz, F. Striebel, and M. Olzmann, *Shock-Tube Study of the Thermal Decomposition of CH 3CHO and CH 3CHO+ H Reaction*, The Journal of Physical Chemistry A 112 (2008), pp. 6120-6124.
[259] *Chemical Kinetics of Acetaldehyde Pyrolysis and Oxidation*.
[260] R. Mével, K. Chatelain, G. Blanquart, and J. Shepherd, *An updated reaction model for the high-temperature pyrolysis and oxidation of acetaldehyde*, Fuel 217 (2018), pp. 226-239.
[261] X. Zhang, L. Ye, Y. Li, Y. Zhang, C. Cao, J. Yang, Z. Zhou, Z. Huang, and F. Qi, *Acetaldehyde oxidation at low and intermediate temperatures: An experimental and kinetic modeling investigation*, Combustion and Flame 191 (2018), pp. 431-441.

[262] N. Leplat, and J. Vandooren, *Experimental investigation and numerical simulation of the structure of CH3CHO/O2/Ar flames at different equivalence ratios*, Combustion science and technology 182 (2010), pp. 436-448.
[263] M. Christensen, M.T. Abebe, E.J. Nilsson, and A.A. Konnov, *Kinetics of premixed acetaldehyde+ air flames*, Proceedings of the Combustion Institute 35 (2015), pp. 499-506.
[264] M. Christensen, and A.A. Konnov, *Laminar burning velocity of diacetyl+ air flames. Further assessment of combustion chemistry of ketene*, Combustion and Flame 178 (2017), pp. 97-110.
[265] T. Tao, W. Sun, B. Yang, N. Hansen, K. Moshammer, and C.K. Law, *Investigation of the chemical structures of laminar premixed flames fueled by acetaldehyde*, Proceedings of the Combustion Institute 36 (2017), pp. 1287-1294.
[266] M. Halstead, A. Prothero, and C. Quinn, *A mathematical model of the cool-flame oxidation of acetaldehyde*, Proceedings of the Royal Society of London. A. Mathematical and Physical Sciences 322 (1971), pp. 377-403.
[267] P. Felton, B. Gray, and N. Shank, *Low temperature oxidation in a stirred flow reactor. II. Acetaldehyde (theory).[400 to 750/sup 0/K]*, Combust. Flame;(United States) 27 (1976).
[268] J. Cavanagh, R. Cox, and G. Olson, *Computer modeling of cool flames and ignition of acetaldehyde*, Combustion and Flame 82 (1990), pp. 15-39.
[269] *Spontaneous ignition of hydrocarbon and related fuels: A fundamental study of thermokinetic interactions,* Vol. 20, 1, Elsevier.
[270] R. Sivaramakrishnan, J.V. Michael, L.B. Harding, and S.J. Klippenstein, *Resolving some paradoxes in the thermal decomposition mechanism of acetaldehyde*, The Journal of Physical Chemistry A 119 (2015), pp. 7724-7733.
[271] *Kinetic modeling of the low temperature cool flames of acetaldehyde in a well stirred reactor*.
[272] P. Gray, J. Griffiths, S. Hasko, and P.-G. Lignola, *Oscillatory ignitions and cool flames accompanying the non-isothermal oxidation of acetaldehyde in a well stirred, flow reactor*, Proceedings of the Royal Society of London. A. Mathematical and Physical Sciences 374 (1981), pp. 313-339.
[273] H. Hashemi, J.M. Christensen, P. Marshall, and P. Glarborg, *Acetaldehyde oxidation at elevated pressure*, Proceedings of the Combustion Institute 38 (2021), pp. 269-278.
[274] K.P. Shrestha, B.R. Giri, M. Adil, L. Seidel, T. Zeuch, A. Farooq, and F. Mauss, *Detailed chemical kinetic study of acetaldehyde oxidation and its interaction with NO x*, Energy & Fuels 35 (2021), pp. 14963-14983.
[275] *Chemical Kinetics of Acetaldehyde Pyrolysis and Oxidation*.
[276] T. Tao, S. Kang, W. Sun, J. Wang, H. Liao, K. Moshammer, N. Hansen, C.K. Law, and B. Yang, *A further experimental and modeling study of acetaldehyde combustion kinetics*, Combustion and Flame 196 (2018), pp. 337-350.
[277] A.P. Kelley, and C.K. Law, *Nonlinear effects in the extraction of laminar flame speeds from expanding spherical flames*, Combustion and Flame 156 (2009), pp. 1844-1851.
[278] *The use of expanding spherical flames to determine burning velocities and stretch effects in hydrogen/air mixtures,* Vol. 23, 1, Elsevier.

[279] C.S. McEnally, L.D. Pfefferle, B. Atakan, and K. Kohse-Höinghaus, *Studies of aromatic hydrocarbon formation mechanisms in flames: Progress towards closing the fuel gap*, Progress in Energy and Combustion Science 32 (2006), pp. 247-294.
[280] L. De Goey, A. Van Maaren, and R. Quax, *Stabilization of adiabatic premixed laminar flames on a flat flame burner*, Combustion science and technology 92 (1993), pp. 201-207.
[281] F.N. Egolfopoulos, N. Hansen, Y. Ju, K. Kohse-Höinghaus, C.K. Law, and F. Qi, *Advances and challenges in laminar flame experiments and implications for combustion chemistry*, Progress in Energy and Combustion Science 43 (2014), pp. 36-67.
[282] C.-J. Sung, and H.J. Curran, *Using rapid compression machines for chemical kinetics studies*, Progress in Energy and Combustion Science 44 (2014), pp. 1-18.
[283] K. Bhaskaran, and P. Roth, *The shock tube as wave reactor for kinetic studies and material systems*, Progress in energy and combustion science 28 (2002), pp. 151-192.
[284] S.M. Burke, U. Burke, R. Mc Donagh, O. Mathieu, I. Osorio, C. Keesee, A. Morones, E.L. Petersen, W. Wang, and T.A. DeVerter, *An experimental and modeling study of propene oxidation. Part 2: Ignition delay time and flame speed measurements*, Combustion and Flame 162 (2015), pp. 296-314.
[285] J. Michael, and A. Lifshitz, *Handbook of Shock WaVes*, Ben-Dor, G (2001), pp. 77-105.
[286] J. Livengood, *Correlation of autoignition phenomena in internal combustion engines and rapid compression machines*, (1955).
[287] A. Lifshitz, K. Scheller, A. Burcat, and G.B. Skinner, *Shock-tube investigation of ignition in methane-oxygen-argon mixtures*, Combustion and Flame 16 (1971), pp. 311-321.
[288] G. Ben-Dor, O. Igra, and T. Elperin, *Handbook of shock waves, three volume set*, Elsevier, 2000.
[289] W.-C.R. Chan, M. Kelbon, and B.B. Krieger, *Modelling and experimental verification of physical and chemical processes during pyrolysis of a large biomass particle*, Fuel 64 (1985), pp. 1505-1513.
[290] R.S. Miller, and J. Bellan, *A generalized biomass pyrolysis model based on superimposed cellulose, hemicelluloseand liqnin kinetics*, Combustion science and technology 126 (1997), pp. 97-137.
[291] C. Di Blasi, *Modeling chemical and physical processes of wood and biomass pyrolysis*, Progress in energy and combustion science 34 (2008), pp. 47-90.
[292] A. Sharma, V. Pareek, and D. Zhang, *Biomass pyrolysis—A review of modelling, process parameters and catalytic studies*, Renewable and sustainable energy reviews 50 (2015), pp. 1081-1096.
[293] S. Xiu, and A. Shahbazi, *Bio-oil production and upgrading research: A review*, Renewable and Sustainable Energy Reviews 16 (2012), pp. 4406-4414.
[294] C. Dupont, L. Chen, J. Cances, J.-M. Commandre, A. Cuoci, S. Pierucci, and E. Ranzi, *Biomass pyrolysis: Kinetic modelling and experimental validation under high temperature and flash heating rate conditions*, Journal of Analytical and Applied Pyrolysis 85 (2009), pp. 260-267.
[295] M. Calonaci, R. Grana, E. Barker Hemings, G. Bozzano, M. Dente, and E. Ranzi, *Comprehensive kinetic modeling study of bio-oil formation from fast pyrolysis of biomass*, Energy & Fuels 24 (2010), pp. 5727-5734.
[296] J.F. Peters, S.W. Banks, A.V. Bridgwater, and J. Dufour, *A kinetic reaction model for biomass pyrolysis processes in Aspen Plus*, Applied energy 188 (2017), pp. 595-603.

[297] B.H. Caudle, M.B. Gorensek, and C.C. Chen, *A rigorous process modeling methodology for biomass fast pyrolysis with an entrained-flow reactor*, Journal of Advanced Manufacturing and Processing 2 (2020), p. e10031.
[298] D. Humbird, A. Trendewicz, R. Braun, and A. Dutta, *One-dimensional biomass fast pyrolysis model with reaction kinetics integrated in an aspen plus biorefinery process model*, ACS Sustainable Chemistry & Engineering 5 (2017), pp. 2463-2470.
[299] E. Ranzi, P.E.A. Debiagi, and A. Frassoldati, *Mathematical modeling of fast biomass pyrolysis and bio-oil formation. Note I: Kinetic mechanism of biomass pyrolysis*, ACS Sustainable Chemistry & Engineering 5 (2017), pp. 2867-2881.
[300] V.Y. Basevich, *Chemical kinetics in the combustion processes: A detailed kinetics mechanism and its implementation*, Progress in energy and combustion science 13 (1987), pp. 199-248.
[301] F. Battin-Leclerc, *Detailed chemical kinetic models for the low-temperature combustion of hydrocarbons with application to gasoline and diesel fuel surrogates*, Progress in Energy and Combustion Science 34 (2008), pp. 440-498.
[302] C.K. Westbrook, and F.L. Dryer, *Chemical kinetic modeling of hydrocarbon combustion*, Progress in energy and combustion science 10 (1984), pp. 1-57.
[303] R.J. Kee, M.E. Coltrin, and P. Glarborg, *Chemically reacting flow: theory and practice*, John Wiley & Sons, 2005.
[304] H. McDonald, *Combustion modeling in two and three dimensions—some numerical considerations*, Progress in Energy and Combustion Science 5 (1979), pp. 97-122.
[305] G. Pio, V. Palma, and E. Salzano, *Comparison and validation of detailed kinetic models for the oxidation of light alkenes*, Industrial & Engineering Chemistry Research 57 (2018), pp. 7130-7135.
[306] R.J. Kee, F.M. Rupley, and J.A. Miller, *The Chemkin thermodynamic data base*, Sandia National Labs., Livermore, CA (USA), 1990.
[307] C.F. Goldsmith, G.R. Magoon, and W.H. Green, *Database of small molecule thermochemistry for combustion*, The Journal of Physical Chemistry A 116 (2012), pp. 9033-9057.
[308] C.L. Yaws, *Yaws' critical property data for chemical engineers and chemists*, Knovel, 2012.
[309] C.F. Goldsmith, W.H. Green, and S.J. Klippenstein, *Role of O2+ QOOH in low-temperature ignition of propane. 1. Temperature and pressure dependent rate coefficients*, The Journal of Physical Chemistry A 116 (2012), pp. 3325-3346.
[310] R.H. West, J.W. Allen, and W.H. Green, *Automatic reaction mechanism generation with group additive kinetics*, ChemInform 43 (2012), p. no.
[311] C.W. Gao, J.W. Allen, W.H. Green, and R.H. West, *Reaction Mechanism Generator: Automatic construction of chemical kinetic mechanisms*, Computer Physics Communications 203 (2016), pp. 212-225.
[312] J. Song, *Building robust chemical reaction mechanisms: next generation of automatic model construction software*. Massachusetts Institute of Technology, 2004.
[313] R.G. Susnow, A.M. Dean, W.H. Green, P. Peczak, and L.J. Broadbelt, *Rate-based construction of kinetic models for complex systems*, The Journal of Physical Chemistry A 101 (1997), pp. 3731-3740.

[314] A.G. Dana, B. Buesser, S.S. Merchant, and W.H. Green, *Automated reaction mechanism generation including nitrogen as a heteroatom*, International Journal of Chemical Kinetics 50 (2018), pp. 243-258.
[315] G. Smith, Y. Tao, and H. Wang, *Foundational fuel chemistry model version 1.0 (FFCM-1)*, epub, accessed July 26 (2016), p. 2018.
[316] M.P. Burke, M. Chaos, Y. Ju, F.L. Dryer, and S.J. Klippenstein, *Comprehensive H2/O2 kinetic model for high-pressure combustion*, International Journal of Chemical Kinetics 44 (2012), pp. 444-474.
[317] X. Li, A.W. Jasper, J. Zádor, J.A. Miller, and S.J. Klippenstein, *Theoretical kinetics of O+ C2H4*, Proceedings of the Combustion Institute 36 (2017), pp. 219-227.
[318] N. Cohen, and S. Benson, *Estimation of heats of formation of organic compounds by additivity methods*, Chemical Reviews 93 (1993), pp. 2419-2438.
[319] S.W. Benson, and J.H. Buss, *Additivity rules for the estimation of molecular properties. Thermodynamic properties*, The Journal of Chemical Physics 29 (1958), pp. 546-572.
[320] F.S. Khanshan, and R.H. West, *Developing detailed kinetic models of syngas production from bio-oil gasification using Reaction Mechanism Generator (RMG)*, Fuel 163 (2016), pp. 25-33.
[321] P.L. Bhoorasingh, B.L. Slakman, F. Seyedzadeh Khanshan, J.Y. Cain, and R.H. West, *Automated transition state theory calculations for high-throughput kinetics*, The Journal of Physical Chemistry A 121 (2017), pp. 6896-6904.
[322] F.M. Wako, G. Pio, and E. Salzano, *Modeling Formic Acid Combustion*, Energy & Fuels (2022).
[323] G. Pio, X. Dong, E. Salzano, and W.H. Green, *Automatically generated model for light alkene combustion*, Combustion and Flame 241 (2022), p. 112080.
[324] M.J. Frisch, *Gaussian09*, http://www. gaussian. com/ (2009).
[325] A. Grinberg Dana, D. Ranasinghe, H. Wu, C. Grambow, X. Dong, M. Johnson, M. Goldman, M. Liu, and W. Green, *ARC-Automated Rate Calculator*, version.
[326] M. Puig-Arnavat, J.C. Bruno, and A. Coronas, *Review and analysis of biomass gasification models*, Renewable and sustainable energy reviews 14 (2010), pp. 2841-2851.
[327] A.G. Adeniyi, J.O. Ighalo, and F.A. Aderibigbe, *Modelling of integrated processes for the pyrolysis and steam reforming of rice husk (Oryza sativa)*, SN Applied Sciences 1 (2019), pp. 1-10.
[328] *Predictive pyrolysis process modelling in Aspen Plus*.
[329] M.B. Gorensek, R. Shukre, and C.-C. Chen, *Development of a thermophysical properties model for flowsheet simulation of biomass pyrolysis processes*, ACS Sustainable Chemistry & Engineering 7 (2019), pp. 9017-9027.
[330] F.A. Aly, and L.L. Lee, *Self-consistent equations for calculating the ideal gas heat capacity, enthalpy, and entropy*, Fluid Phase Equilibria 6 (1981), pp. 169-179.
[331] K.S. Pitzer, D.Z. Lippmann, R. Curl Jr, C.M. Huggins, and D.E. Petersen, *The volumetric and thermodynamic properties of fluids. II. Compressibility factor, vapor pressure and entropy of vaporization1*, Journal of the American Chemical Society 77 (1955), pp. 3433-3440.
[332] *Phase equilibria in a third-generation process simulator*, Deutsche Gesellschaft für Chemisches Apparatewesen Great Neck, NY.
[333] A. Plus, *V10. 0; Aspen Technology*, Inc.: Burlington, MA (2017).

[334] E. Situ, *Upgrading of Fast Pyrolysis Vapors*, US Department of Energy Bioenergy Technologies Office (2015).
[335] *A Simplified Approach to Aspen-Plus© Mass and Energy Balances for Preliminary Process Analysis and Economic Feasibility of Pyrolysis of Switchgrass to Bio-Oil*.
[336] A.A. Konnov, A. Mohammad, V.R. Kishore, N.I. Kim, C. Prathap, and S. Kumar, *A comprehensive review of measurements and data analysis of laminar burning velocities for various fuel+ air mixtures*, Progress in Energy and Combustion Science 68 (2018), pp. 197-267.
[337] P. Dagaut, F. Karsenty, G. Dayma, P. Diévart, K. Hadj-Ali, A. Mzé-Ahmed, M. Braun-Unkhoff, J. Herzler, T. Kathrotia, and T. Kick, *Experimental and detailed kinetic model for the oxidation of a Gas to Liquid (GtL) jet fuel*, Combustion and Flame 161 (2014), pp. 835-847.
[338] D. Goodwin, *An open-source, extensible software suite for CVD process simulation*, Chemical vapor deposition XVI and EUROCVD 14 (2003), pp. 2003-08.
[339] R.J. Kee, J.F. Grcar, M.D. Smooke, J.A. Miller, and E. Meeks, *PREMIX: a Fortran program for modeling steady laminar one-dimensional premixed flames*, Sandia National Laboratories Report (1985).
[340] M. Smooke, H. Rabitz, Y. Reuven, and F. Dryer, *Application of sensitivity analysis to premixed hydrogen-air flames*, Combustion science and technology 59 (1988), pp. 295-319.
[341] T. Faravelli, A. Frassoldati, A. Cuoci, M. Mehl, M. Pelucchi, A. Stagni, and E. Ranzi, *CRECK Modeling Lab*, creckmodeling. chem. polimi. it (accessed May 2019 2019) (2020).
[342] A. Konnov, *Implementation of the NCN pathway of prompt-NO formation in the detailed reaction mechanism*, Combustion and Flame 156 (2009), pp. 2093-2105.
[343] U. Diego, *Chemical-Kinetic Mechanisms for Combustion Applications*, San Diego Mechanism web page, Mechanical and Aerospace Engineering (Com-bustion Research), University of California at San Diego (http://combustion. ucsd. edu).
[344] K. Osipova, S.M. Sarathy, O. Korobeinichev, and A. Shmakov, *Chemical structure of atmospheric pressure premixed laminar formic acid/hydrogen flames*, Proceedings of the Combustion Institute 38 (2021), pp. 2379-2386.
[345] M.L. Lavadera, and A.A. Konnov, *Laminar burning velocities of methane+ formic acid+ air flames: Experimental and modeling study*, Combustion and Flame 225 (2021), pp. 65-73.
[346] G. Yin, J. Xu, E. Hu, Q. Gao, H. Zhan, and Z. Huang, *Experimental and kinetic study on the low temperature oxidation and pyrolysis of formic acid in a jet-stirred reactor*, Combustion and Flame 223 (2021), pp. 77-87.
[347] A. Trendewicz, R. Braun, A. Dutta, and J. Ziegler, *One dimensional steady-state circulating fluidized-bed reactor model for biomass fast pyrolysis*, Fuel 133 (2014), pp. 253-262.
[348] C. Ellens, and R. Brown, *Optimization of a free-fall reactor for the production of fast pyrolysis bio-oil*, Bioresource technology 103 (2012), pp. 374-380.
[349] C. Guizani, S. Valin, J. Billaud, M. Peyrot, and S. Salvador, *Biomass fast pyrolysis in a drop tube reactor for bio oil production: Experiments and modeling*, Fuel 207 (2017), pp. 71-84.

[350] A. Pattiya, S. Sukkasi, and V. Goodwin, *Fast pyrolysis of sugarcane and cassava residues in a free-fall reactor*, Energy 44 (2012), pp. 1067-1077.
[351] A. Shoaib, R. El-Adly, M. Hassanean, A. Youssry, and A. Bhran, *Developing a free-fall reactor for rice straw fast pyrolysis to produce bio-products*, Egyptian journal of petroleum 27 (2018), pp. 1305-1311.
[352] E. Ranzi, A. Frassoldati, R. Grana, A. Cuoci, T. Faravelli, A. Kelley, and C. Law, *Progress Energy Combust*, Sci 38 (2012), pp. 468-501.
[353] E. de Wilde, and A. van Tiggelen, *Burning velocities in mixtures of methyl alcohol, formaldehyde or formic acid with oxygen*, Bulletin des Sociétés Chimiques Belges 77 (1968), pp. 67-75.
[354] S. Maharjan, A.M. Elbaz, and W.L. Roberts, *Investigation on the formic acid evaporation and ignition of formic acid/octanol blend at elevated temperature and pressure*, Fuel 313 (2022), p. 122636.
[355] W. Tsang, *Chemical kinetic data base for combustion chemistry. Part 2. Methanol*, Journal of physical and chemical reference data 16 (1987), pp. 471-508.
[356] J. Troe, *The thermal dissociation/recombination reaction of hydrogen peroxide H2O2 (+ M)⇔ 2OH (+ M) III.: Analysis and representation of the temperature and pressure dependence over wide ranges*, Combustion and Flame 158 (2011), pp. 594-601.
[357] S.S. Matveev, D.V. Idrisov, S.G. Matveev, and A.A. Konnov, *Laminar burning velocities of surrogate components blended with ethanol*, Combustion and Flame 209 (2019), pp. 389-393.
[358] L.B. Harding, Y. Georgievskii, and S.J. Klippenstein, *Roaming radical kinetics in the decomposition of acetaldehyde*, The Journal of Physical Chemistry A 114 (2010), pp. 765-777.

List of Figures

List of Tables

Acronomys

IEA	International Energy Agency
RED	Renewable energy Directives
EISA	U.S. Energy Independence and Security Act
RFS	Renewable Fuels Standard Scheme
LVG	Levoglucosan
HAA	Hydroxy acetaldehyde
CELL	Cellulose
CELLA	Activated Cellulose
HCE	Hemicellulose
LIG-C	Carbon rich Lignin
LIG-H	Hydrogen rich Lignin
LIG-O	Oxygen rich Lignin
NTC	Negative temperature coefficient
RCM	Rapid Compression Machine
LISI	Laser-Induced Spark Ignition
SI	Spark Ignition
RMG	Reaction Mechanism Generator
CCUS	Carbon Capture Utilization and Storage
PES	Potential Energy Surface
SVUV-PIMS	Synchrotron Vacuum Ultraviolet Photoionization Mass Spectrometry
HFM	Heat Flux Method
IDT	Ignition Delay Times
$\mathbf{S_u}$	Laminar Burning Velocity
$\boldsymbol{\varphi}$	Equivalence ratio

DTR	Drop Tube Reactor
RPLUG	Plug Flow Reactor
RYIELD	Yield Reactor

Appendix

Table S1. Chemical components and their representations used in the biomass pyrolysis process model

Chemical compound	Component ID	Type	Formula
Cellulose	CELL	Solid	$C_6H_{10}O_5$
Hemicellulose	HCE	Solid	$C_5H_8O_4$
C-rich lignin	LIGC	Solid	$C_{15}H_{14}O_4$
O-rich lignin	LIGO	Solid	$C_{20}H_{22}O_{10}$
H-rich lignin	LIGH	Solid	$C_{22}H_{28}O_9$
Activated cellulose	CELLA	Solid	$C_6H_{10}O_5$
Hemicellulose intermediate 1	HCE1	Solid	$C_5H_8O_4$
Hemicellulose intermediate 2	HCE2	Solid	$C_5H_8O_4$
C-rich lignin intermediate	LIGCC	Solid	$C_{15}H_{14}O_4$
O/H-rich lignin intermediate	LIGOH	Solid	$C_{19}H_{22}O_8$
Secondary lignin intermediate	LIG	Solid	$C_{11}H_{12}O_4$
Ash	ASH	Solid	CaO
Moisture	H_2OL	Conventional	H_2O
	Pyrolysis products		
Sinapyl aldehyde	FE2MACR	Conventional	$C_{11}H_{12}O_4$
p-coumaryl alcohol	COUMARYL	Conventional	$C_9H_{10}O_2$
Anisole	ANISOLE	Conventional	C_7H_8O
Phenol	PHENOL	Conventional	C_6H_6O
Levoglucosan	LVG	Conventional	$C_6H_{10}O_5$
Xylose	XYLAN	Conventional	$C_5H_8O_4$
5-hydroxymethyl-furfural	HMFU	Conventional	$C_6H_6O_3$
Furfural	FURF	Conventional	$C_5H_4O_2$
3-hydroxypropanal	$C_3H_6O_2$	Conventional	$C_3H_6O_2$
n-propionaldehyde	ALD3	Conventional	C_3H_6O
Hydroxy acetaldehyde	HAA	Conventional	$C_2H_4O_2$
Ethanol	C_2H_5OH	Conventional	C_2H_5OH
Glyoxal	GLYOX	Conventional	$C_2H_2O_2$
Acetaldehyde	CH_3CHO	Conventional	CH_3CHO
Acetic acid	CH_3COOH	Conventional	CH_3COOH
Methanol	CH_3OH	Conventional	CH_3OH
Formaldehyde	CH_2O	Conventional	CH_2O
Formic acid	HCOOH	Conventional	HCOOH
Ethylene	C_2H_4	Conventional	C_2H_4
Methane	CH_4	Conventional	CH_4
Carbon dioxide	CO_2	Conventional	CO_2
Carbon monoxide	CO	Conventional	CO
Hydrogen	H_2	Conventional	H_2
Water	H_2O	Conventional	H_2O
	Non-biomass components		
Argon	AR	Conventional	AR
Nitrogen	N_2	Conventional	N_2
Oxygen	O_2	Conventional	O_2

Characterization of Pyrolysis and Oxidation processes of Biomaterials, Biomasses and Biofuels

Abstract

The urgent need for alternative solutions mitigating the impacts of human activities on the environment has strongly opened new challenges and opportunities for the energy supply chain, in view of the energy transition. Indeed, the automotive industry is going through a revolutionary moment in its quest to reduce its carbon footprint, with biofuels being one of the viable alternatives. The use of different classes of oxygenated biofuels, such as alcohols, carboxylic acids, aldehydes, and esters as fuel additives or standalone fuel components has attracted the attention of many researchers worldwide. Despite their beneficial effects, biofuel's combustion can also result in the production of undesirable pollutants such as aldehydes and organic acids. Hence, the use of these fuels requires a complete characterization of the phenomena that occur during their production and consumption. Industrial scale-up of biomass conversion is challenging owing to the complexity of its chemistry and transport phenomena involved in the process, thereby affecting yield distributions and product compositions. In this view, the role of solid-phase and gas-phase chemistry is paramount for a complete understanding of energy recovery processes, undesired pollutants formation and consumption, and in general for several industrial sectors. Thus, this study is devoted to a detailed analysis of physical-chemical phenomena characterizing biomass pyrolysis and biofuel oxidation aiming at the realization and implementation in real systems of a kinetic mechanism. The solid-phase kinetics is dedicated to how the pyrolysis kinetic mechanism is constructed and implemented in process simulation software (i.e. Aspen Plus) to be able to simulate pyrolysis process. The pyrolysis mechanism has been represented by 20 first order decomposition reactions. In the gas-phase, predictive chemical kinetic models have been constructed following two approaches; manually upgrading the existing mechanism (i.e. KiBo_MU) and automatically generating a new mechanism using RMG (i.e. KiBo_AG). The former comprises 141 species and 453 reactions, while the latter contains 631 species and 28329 reactions. The accuracy of the pyrolysis kinetic mechanism has been tested against the experimental pyrolyzed product distributions from different biomass sources while, the combustion kinetic models have been evaluated through the investigation of fundamental combustion parameters (i.e. laminar burning velocity, species profile and ignition delay times) under wide range of reaction conditions and fuel compositions. Formic acid, acetic acid, acetaldehyde, methanol

and ethanol were considered for validation of the combustion mechanisms. Under the investigated conditions, the kinetic mechanisms captured the experimental trends well and in particular, KiBo_MU and KiBo_AG showed better accuracy when compared to the well-validated existing kinetic models. The overall agreement between experimental measurements and numerical estimations allowed for the use of KiBo_MU and KiBo_AG kinetic models to unravel the chemistry of the investigated species.

Although the development and validation of detailed kinetic mechanisms suitable for the evaluation of the chemistry of biomass-based fuels represent the main deliverable of this project, the realized procedure integrating schematic classifications with methodologies for the identification of common decomposition pathways and intermediates represents an additional source of novelty in this study. Besides, the fundamental-oriented nature of the adopted approach has allowed for the identification of the most relevant reactions and species under operative conditions of interest in different industrial applications, paving the way for the reduction of the kinetic mechanism. Eventually, the resulting skeletal version of a detailed kinetic mechanism can be intended for its integration with more complex models accounting for the fluid dynamics to accurately reproduce the behaviour of real systems and reactors.